

Design method for multi-functional artificial reefs in a coastal environment

Integrate ecological and coastal protection functionalities for a 3D printed artificial reef

Merel E. N. Kroon

Cover: 3D printed reef being placed, pilot project Monaco
Picture courtesy: J. Lescinski (2015)

Design method for multi-functional artificial reefs in a coastal environment

Integrate ecological and coastal
protection functionalities for a 3D printed
artificial reef

Master thesis

by

Merel E. N. Kroon

to obtain the degree of Master of Science

at Delft University of Technology
and

at National University of Singapore

to be defended publicly on Tuesday April 19, 2016 at 09:00 AM.

Student number: 1533460 / A0119557

Project duration: May 2015 – April 2016

Supervisors:	Prof. dr. ir. W. S. J. Uijtewaal	Delft University of Technology, chair
	Ir. J. Van den Bos	Delft University of Technology
	Dr. V. Chua	National University of Singapore
	Dr. ir. A. van Dongeren	Deltares
	Ir. J. Lescinski	Royal Boskalis Westminster N.V.
	Prof. dr. ir. M. J. F. Stive	Delft University of Technology

An electronic version of this thesis is available at <http://repository.tudelft.nl/>.

*In der Beschränkung zeigt sich erst
der Meister*

— J.W. von Goethe

Preface

This research was conducted in partial fulfillment of the Masters degrees in Civil Engineering at Delft university of Technology and Hydraulic Engineering & Water Resource Management at National University of Singapore.

The realization of this thesis has been made possible by a great number of people. First of all, I would like to thank Boskalis for allowing me to work at Hydronamic for almost one year, working on my research. A great number of people have contributed by letting me use their precious time for knowledge sharing and help in modeling. I am grateful to be given the opportunity to work within an inspiring environment with bright and enthusiastic people. In particular I would like to thank Ir. Jamie Lescinski for the brainstorm sessions and supervision at Boskalis. I am very grateful to Ir. Jeroen van den Bos for the additional support at the office. Dr. ir. Ap van Dongeren and Dr. Vivien Chua, thank you for being part of my graduation committee and support. Additionally I would like to thank Prof. dr. ir. Marcel Stive, for his encouragement and trusting me to succeed. The largest logistical challenge of this research was the setup and measurements of the physical modeling campaign. This could not have been completed successfully without the staff of the hydraulic lab at DUT, in particular Sander de Vree, Jaap van Duin, Hans Tas and Frank Kalkman. They have provided me with a lot of practical knowledge and were always available when some muscle-power was required. Special thanks to Dr. ir. Marcel Zijlema who, although not officially involved in this research, helped me setting up my SWASH model. I am very grateful to Prof. dr. ir. Wim Uijttewaai for being the chair of my thesis committee, helping me to keep the 'bigger picture' in sight and for his constructive comments when structuring the report. Finally I would like to thank my study buddies for the countless lunches at the 6th floor and friends and family for providing support and help throughout my studies. It was quite the ride!

*Merel E. N. Kroon
Papendrecht, April 2016*

Executive Summary

A global consensus exists that coastal zones are under increasing pressure from both sea- and landward side. The combination of sea level rise (SLR) and continuing economic development along coastlines, causes a phenomenon addressed as 'Coastal Squeeze' [59]. Anthropogenic pressure by growing coastal communities stresses the need for a stable coastline. Protective measures to arm coastlines against SLR, interfere with the landward movement of habitat caused by the change in physical environment. Therefore these coastal protection structures imply a strain on the natural habitat mitigation, causing the marine ecosystem to be 'squeezed'. Aim of this thesis is to contribute to the adaptation and restoration of natural habitat while ensuring coastline stability. The technique by which this research was triggered is 3D printing reefs by using dredged material and an environmentally neutral binder. This innovative method to construct Artificial Reefs (AR) was initiated by Boskalis, a pilot project was developed and placed in a marine reserve in Monaco (Pictured on the cover of this report). In order to investigate the techniques potential, it is explored if its ecological design can be extended with a coastal protection function.

Integration of ecological and coastal protection functions in a multi functional AR will introduce tension between desired hydrodynamic conditions from an ecological point of view versus a coastal protection point of view. In addition, there is a growing need for design tools that quantify the integration of design criteria for these functions. The objective of the research is to establish a method to integrate ecological and coastal protection functionalities for a 3D printed reef. The outcome is expected to contribute to the development of an integrated, multi functional AR design.

The main research question that is answered is: "*How can an integrated design approach of ecological and coastal protection functionalities, for a 3D printed reef, be established?*" The methodology that is followed in meeting the objective and answering this research question is pictured in figure 1.

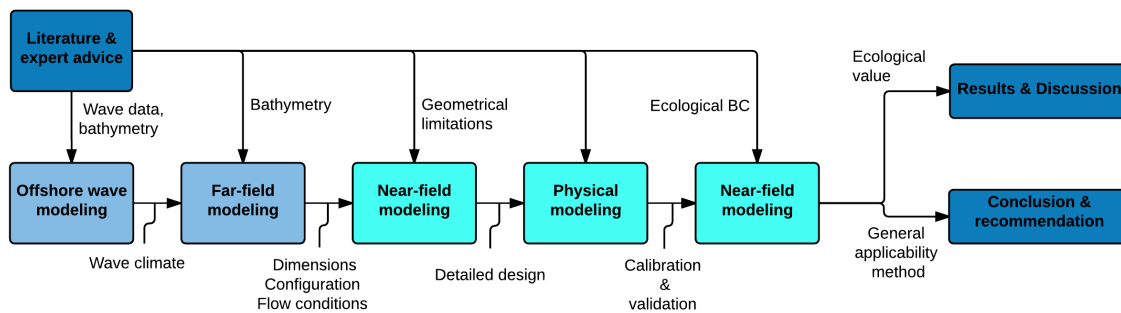


Figure 1: Methodology

Analysis is done in 2DV and the wave climate is simplified to monochromatic waves. Geographical focus lies on the Mediterranean, in particular the Italian coast. Natural rocky reefs occur there, but are depleted over the last centuries. This naturally ecological rich environment can be reinforced by placing artificial (3D printed) reefs.

The conducted literature study consists of the following components and results:

1. Scale considered in the research is meso scale, which is in the order of meters. This accounts for flow patterns, currents over the surface of the structure, habitat accessibility for fish.
2. A geometrical translation is made from known ecological thresholds for fish screens in inlets, to the reef situation. With this translation it is possible to define maximum resistible velocity u_{max} for the target species, which is juvenile Sea Bream. The defined empirical formula describes a relation between the length of the fish and it's maximum swimming capacity.

3. Physical parameters that will be used to link the ecological and coastal protection functions are wave transmission (C_t) and maximum horizontal velocity (u_{max}).
4. Bathymetric and hydrodynamic boundary conditions are defined for the case study site, which is located in the Lazio Region. The seabed has a gentle slope. Wave data is obtained from an offshore wave buoy in the vicinity of the study site.
5. Reef geometry: The underwater structure will consist of monolithic structures in a staggered grid. This is based on known feasible reef dimensions when the units are 3D printed. In order to create enough roughness to interact with the waves, they are applied in a field.
6. In total three numerical models are selected (see figure 1). For offshore to near-shore wave transformation, SWAN will be used in 2DH mode. To carry out the far-field modeling an XBeach model is applied, in 1DH. For the near-field, detailed modeling SWASH is used in 2DV.

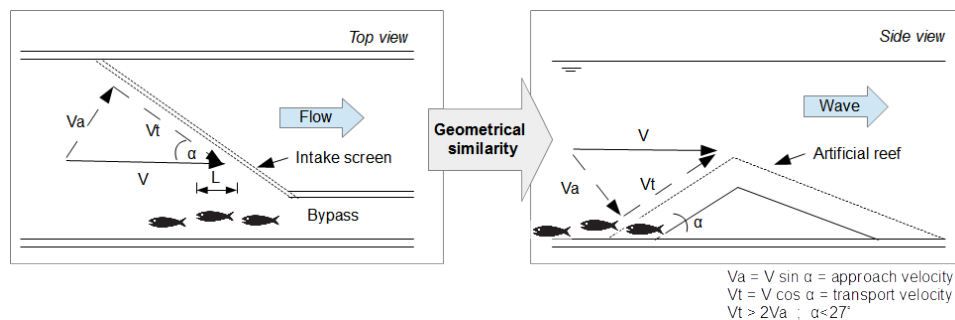


Figure 2: Geometrical translation of ecologically induced velocity threshold (Left image copied from Katopodis [41])

The SWAN model translates offshore wave data to input for the far-field model XBeach. A 2DH grid is setup that spans 40.000 km^2 . The output is generated on a point approximately 2000 m from the shore. An extreme value analysis is carried out (Peak over Threshold method) to acquire the 1/1000 year wave. The 1/1000 year wave has the following characteristics: $H_{rms}=5.23 \text{ m}$, $T_p=13.3 \text{ s}$ and depth is 32.5 meters. This wave condition is brought into the phase averaging computational model XBeach. Goals of the XBeach simulations are to determine the cross-shore location of the reef and translate waves to shallow water. The location of the reef is determined by running the model with 10 simplified reef geometries, at various depths between -2 and -5 meter. The wave damping ($1-C_t$) was divided by the cross sectional area of the reef, being a measure of effectiveness of the material in wave damping. The chosen location for the reef is the geometry with the highest damping per square meter material. The optimal cross sectional geometry is 10 meters wide, one meter high and located at a depth of 2 meter.

More detailed geometry of the structure is determined in the phase resolving model SWASH. SWASH is ran in two dimensional, non-hydrostatic mode. Geometry of the individual units is defined by modeling two consecutive reef units, 2 meter wide and 1 meter high. The angle of the face of the structure is altered in four scenarios, to determine if the slope of the face has significant influence on wave damping and maximum velocity. For both parameters there was no significant difference. Therefore the scenario with the largest lee side was chosen, arguing that the lee side offers highest potential for incorporating habitat. This results in an offshore angle of the structure of 50 degrees, and a lee side angle of about 30 degrees.

This reef structure is tested in the flume at Delft University of Technology. To mimic the 3D printed reefs, rock was glued to a steel profile in order to create the porous surface and an impermeable core. The rock size is predetermined, linking the target species size to pore size distribution following Buijs [12]. Measured quantities in the flume (in time) are water level η , u -velocity (away from the structure) and u, v, w -velocity above the structure. As an extension to these measurements one wave condition was also recorded using a Particle Image Velocimetry (PIV) setup. A dataset was created with seven transmission of the structure was very high for all wave conditions, between 96 and 100 percent. One monochromatic condition is selected with low reflection and low transmission. Specifications of this wave conditions are (prototype scale): Depth is 3.18 meter, wave height H is 0.72 meter and period T is 4 seconds.

The flume geometry and selected wave condition are brought back into SWASH, with the goal of validating the model. Physical characteristics of the reef are to be determined, by means of calibration with the

parameters roughness (Nikuradse roughness n_k) porosity (n) and the laminar (α) and turbulent (β) friction factors. Calibration of the parameters within their physically realistic boundaries did not return satisfactory results. While porosity n was expected to lie between 0.35 and 0.40, the highest mean correlation with measurements was obtained with $n=0.80$. The remaining calibration parameter values are $n_k=0.035$, $\beta=1.81$ and $\alpha = 1000$. The prototype scale calibrated SWASH model has a correlation with the water level measurements of $0.89 < r < 0.99$, with an average of $r = 0.96$. The velocity signals have a correlation of $0.92 < r < 0.99$, with an average of $r=0.96$.

The maximum velocities for the calibrated model are shown in figure 3.

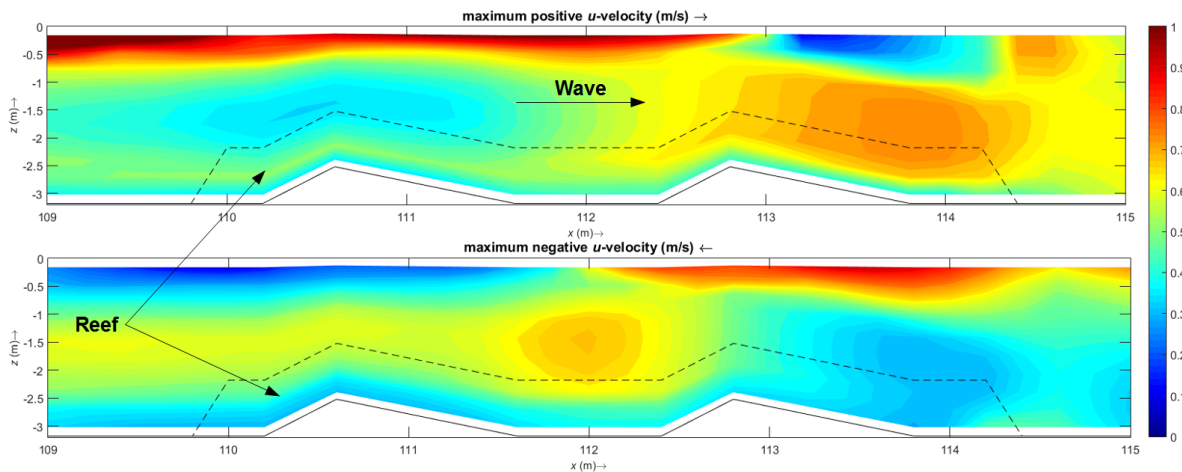


Figure 3: Maximum horizontal velocity for positive and negative x-direction

The ecological threshold for u_{max} can be calculated using the empirical 'fish screen' formula. The length of the target species (juvenile Sea Bream) is 20 cm. Since the front- and lee side of the structure have different angles, this imposes different values for u_{max} in positive and negative x-direction. When these values for maximum velocity are applied as limits to the SWASH model results, the following spatial boundaries for habitat (for this particular wave condition, target species and reef geometry) can be obtained:

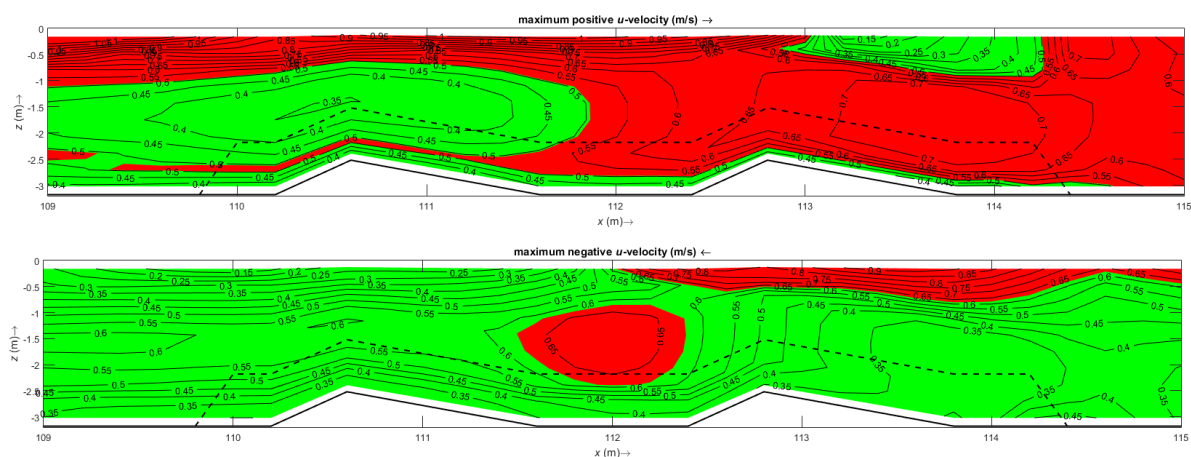


Figure 4: Maximum horizontal velocity for positive and negative x-direction, ecological threshold for $u_+ = 0.51$ m/s and $u_- = -0.66$ m/s indicated with color scheme (green = below threshold)

The figure above shows that an easy to interpreted, visual result is obtained. The numerical model is able to reproduce detailed hydrodynamic motion with high correlation. When this is combined with the defined empirical ecological threshold, a conclusion can be drawn regarding the 'accessibility' of the structure to a certain species. The parameters that were determined to be guiding for ecological and coastal perfor-

mance are transmission coefficient C_t and maximum horizontal velocity u_{max} . The model that should be used to integrate these parameters is SWASH, disregarding the inaccuracy that will be elaborated on below. The method does not show satisfying results for the case study, since most of the reef surface is unsuitable for creating habitat at some point in time. However, these results indicate that the method developed was proven functional, but with limited applicability as will become clear later. The tool can be used to optimize the cross section of a reef, using it to create favorable current patterns. For varying target species the habitat limitations can be different, which can be used to assess appropriate structure complexity consisting of several types of habitat in different locations along the cross section. Also the method can be used on existing breakwater designs to identify favorable locations for enhancement with habitat elements. This method has three degrees of freedom, which can be altered in order to apply it to another situation. These are fish length, wave climate and structure geometry.

As mentioned, there are a number of limitations to the developed method. These limitations are split into three categories: self-imposed, tool-induced and knowledge gap.

The self imposed limitations are that the model is set up in 2DV, which does not account for the full complexity of the system in 3D. Furthermore the wave condition is monochromatic, whereas in nature there will be a whole spectrum of waves interacting with the structure. The third self imposed limitation is that the model is only calibrated using one wave condition. Therefore the robustness of the calibration is unknown.

Tool-induced limitations are two-fold. The most significant is that an error was identified in SWASH when porosity is introduced in the domain. In the vicinity of the porous layer, the calculated vertical velocity is zero. Porosity is in SWASH included in the momentum balance in x- and y- directions, but not in z-direction. When coding the program it was assumed that this would be corrected automatically through the mass balance, which in this case turned out to be a wrongful assumption. Therefore conservation of mass and momentum is not guaranteed. Secondly an inaccuracy was found in the physical measurements, when using the EMS flow velocity meters to measure horizontal velocity. The disk-shaped instruments showed increasing underestimation of the velocity under the wave crest for higher waves. This was caused by the wake effect of the shape of the device. In future wave-measurements it is advised to use either sphere-shaped EMS instruments or 'sideways looking' disk-shaped instruments.

The last limitation is the knowledge-gap. In this research ecological value is determined using an 'engineering' approach; simplifying the system to a basic scenario and by looking at this simplified system assume that it is to an extent representative for the full system. Unfortunately, this is not how ecological systems work. It is stressed that evaluating a design for one target species does not warrant ecological success. However, alternative design tools for the integration of ecological and engineering design in the marine environment that capture ecological complexity are virtually non-existing. Therefore this attempt can contribute to the dialog between ecologists and engineers on integrating ecological value in coastal structures.

Main recommendation for industry:

- This concept can be used to analyze placing of habitat, when enhancing existing structures or designs with 3D printed or other ecologically driven elements
- Identify indispensable characteristics of the 3D printed reefs versus rubble mound or mounded structures, and try to incorporate these in an alternative production technique (molding, extrusion) to make it economically viable

Main recommendation for further research regarding this topic:

- Include ecologists in this field of coastal research to define design guidelines for ecological value by means of physical parameters, while taking into account ecological complexity as much as possible
- Bring the study for 3D printed reef structures into a 3D environment, to assess flow constrictions amongst the elements in a staggered field and study how this influences the velocity patterns over the surface. Subsequently eliminate other self imposed limitations
- In depth evaluation of the physical error in SWASH triggered by porosity, to ensure conservation of mass and momentum in the model

Contents

Preface	v
Executive Summary	vii
List of Symbols	xv
1 Introduction	1
1.1 Background	1
1.1.1 Motivation	1
1.1.2 Case	3
1.2 Problem description	4
1.3 Objectives.	5
1.4 Approach	5
1.4.1 Methodology.	5
1.4.2 Structure of report	8
2 Literature study	9
2.1 Natural rocky reefs	9
2.2 Artificial reefs	9
2.2.1 Functions	10
2.2.2 Design parameters	10
2.2.3 Reference projects	11
2.3 Reef ecology.	12
2.3.1 System analysis	12
2.3.2 Target species	13
2.4 Reef hydrodynamics	14
2.4.1 Roughness	14
2.4.2 Reef scale	14
2.4.3 Wave induced forcing	14
2.5 Low crested coastal defense structures (LCS)	15
2.5.1 Functions	15
2.5.2 Ecological impact LCS	17
2.5.3 LCS scale.	17
2.5.4 Dimensional requirements.	18
2.6 Ecological value determination	18
2.7 3D printed reef geometry	19
2.8 Scale integration	19
2.9 Consequence for research approach	19
2.10 Selection of models	21
3 Modeling	23
3.1 Offshore wave modeling	24
3.1.1 Input SWAN model	24
3.1.2 Output SWAN model.	25
3.1.3 Design conditions 1/1000 year	25
3.2 Far-field modeling	26
3.2.1 Work sequence.	26
3.2.2 Model setup	26
3.2.3 Critical parameters.	28
3.2.4 Intermediate results	28

3.3	Near-field modeling 1 - Design of laboratory setup	28
3.3.1	Work sequence.	28
3.3.2	Model setup	29
3.3.3	Intermediate results	30
3.4	Physical modeling	31
3.4.1	General concerns	31
3.4.2	Hydrodynamic input.	32
3.4.3	AR scale model.	33
3.4.4	Laboratory setup.	36
3.4.5	Planning	40
3.4.6	Intermediate results	41
3.5	Near-field modeling 2 - Validation of the model.	41
3.5.1	Boundary conditions.	41
3.5.2	Calibration parameters	42
3.5.3	Evaluation of calibration	44
3.6	Ecological thresholds	44
4	Results	47
4.1	Far-field modeling	47
4.2	Physical modeling	50
4.2.1	Water level measurements	50
4.2.2	Velocity measurements	52
4.3	Near field modeling.	54
4.3.1	Signal processing	55
4.3.2	Validation model scale - no structure	55
4.3.3	Calibration model scale - with structure	56
4.3.4	Validation prototype scale	59
4.4	Calibrated near-field model.	61
4.4.1	Final settings.	61
4.4.2	Correlation.	61
4.4.3	Maximum velocities	61
4.5	Ecological thresholds	62
4.6	Synthesis	62
4.6.1	Patchiness	63
4.6.2	Ecological value	64
5	Conclusions & Recommendations	65
5.1	Conclusions.	65
5.1.1	Parameters.	65
5.1.2	Method	66
5.1.3	3D printed AR	66
5.2	Case study Sant'Agostino	66
5.3	Method restrictions	67
5.3.1	Self imposed	67
5.3.2	Tool-induced	67
5.3.3	Knowledge gap.	67
5.4	Recommendations	68
5.4.1	Ecological design	68
5.4.2	Improvement of modeling	68
5.4.3	Recommendations for the industry	69
	List of Figures	71
	List of Tables	75
	Bibliography	77
A	Product development framework	81
B	SWAN input & Extreme value analysis	83

C	Target species	89
D	Rock grading & construction reef	91
E	Planning	97
F	Wave reflection	103
G	Fourier series of Vectrino signal	107
H	Bichromatic waves	111
I	Derivation stokes wave BC for SWASH	115
J	SWASH model setup	117
K	Results calibration SWASH	119
L	Velocity decomposition	123
M	PIV measurements	125

List of Symbols

a	Wave amplitude	[m]
B	Width structure	[m]
BL_c	Blockiness factor	[-]
C	Courant number	[-]
c	Celerity	[m/s]
c_f	Friction factor	[-]
C_t	Transmission coefficient	[-]
d	Grain diameter	[m]
D_{50}	Median sieve diameter of grading curve	[m]
D_{n50}	Median grain diameter of weight	[m]
f	Frequency	[s ⁻¹]
F	Coefficient of Rosin Rammler	[-]
$f(x, P_{80}, m, F)$	Pore size distribution	[m]
f_l	Laminar friction term	[-]
f_t	Turbulent friction term	[-]
g	Gravitational acceleration	[m/s ²]
H	Wave height	[m]
h	Waterdepth	[m]
H_{in}	Incoming wave height	[m]
H_{out} / H_t	Transmitted wave height	[m]
H_{rms}	Root mean square wave height	[m]
H_s	Significant wave height	[m]
k	Wave number	[rad/m]
K_c	Keulegan Carpenter number	[-]
k_t	Layer thickness coefficient	[-]
L	Wave length	[m]
L	Fish length	[mm]
L_0	Deep water wave length	[m]
m	Shape coefficient of Rosin Rammler	[-]
n	Porosity	[-]
n	Manning roughness coefficient	[s/m ^{1/3}]
n_k	Nikuradse roughness height	[m]
P_{80}	Slope coefficient Rosin Rammler	[-]
r	Pearson correlation coefficient	[-]
R^2	Coefficient of determination	[-]
R_c	Crest free-board	[m]
T	Wave period	[s]
T_{m01}	Mean period	[s]
T_p	Peak period	[s]
u	Velocity in x-direction	[m/s]
u'	Turbulent velocity	[m/s]
\bar{u}	Mean velocity	[m/s]
U_b	Wave energy flux at breaking point	[kg/s ⁻²]
U_w	Wave orbital velocity	[rad/s]
V	Filter velocity	[m/s]
v	Velocity in y-direction	[m/s]
V_a	Approach velocity	[m/s]
V_u	Velocity in u-direction	[m/s]
w	Velocity in z-direction	[m/s]

α	Angle of structure	[°]
α	Laminar friction factor	[-]
β	Turbulent friction factor	[-]
η	Free surface elevation	[m]
μ	Mean value	[-]
ω	Angular frequency	[rad/s]
Φ	Porosity	[-]
ρ	Density	[kg/m ³]
σ	Standard deviation	[-]
θ	Wave phase	[rad]

Abbreviations

AR	Artificial Reef
DELOS	Environmental Design of Low Crested Coastal Defense Structures
DUT	Delft University of Technology
LCS	Low Crested Structure
PIV	Particle Image Velocimetry
SLR	Sea Level Rise
1DH	One dimensional horizontal
2DH	Two dimensional horizontal (x,y plane)
2DV	Two dimensional vertical (x,z plane)

Introduction

Coastlines define the transition between land and water. The coastal zone serves as habitat to very many species of flora and fauna. As long as the earth exists, coastlines (and for that whole continents) have shifted and changed shape. This as such is not negative, since movement was driven by forces that caused the coastlines moving to a new, natural equilibrium. Only since the last centuries, this movement has been restrained due to human influence. A global consensus exists that coastal zones are experiencing increasing pressure from both sea- and landward side. The combination of sea level rise (SLR) and continuing economic development along coastlines, causes a phenomenon addressed as 'Coastal Squeeze' [59]. Sea level rise causes marine habitat to move landward, in order to keep up with the change in the physical environment. Anthropogenic pressure by growing coastal communities stresses the need for a stable coastline. Protective measures to arm coastlines against SLR, interfere with the landward movement of habitat. Therefore these coastal protection structures imply a strain on the natural habitat mitigation, causing the marine ecosystem to be 'squeezed'. Hopefully this research will contribute to the adaptation and restoration of natural habitat while ensuring coastline stability.

1.1. Background

First, a background will be sketched, from which the problem description and objectives of this research will be deduced. More in depth information on the subjects touched upon in the motivation will be explored in chapter 2.

1.1.1. Motivation

This research topic was born following recent innovations in the field of Artificial Reef (AR) design. The idea was first pitched in the Boskalis Innovation Challenge (BIC) and won first prize. Amongst others in the industry, Boskalis recognizes that a single function when developing a structure is no longer enough. Furthermore, limiting the negative environmental impacts of dredge disposal by binding this material is something that is generally seen as a positive development. The 3D printed reefs concept enables safe binding of dredged sediments into an ecology enhancing form, which has the potential to become a coastal structure, with further development. The concept is to create artificial reef units with high structural complexity, using a 3D printing technique. The printing materials (filler and binder) are environmentally neutral. However, the business case of this technique is not developed yet.

By investigating this technique's possibilities and eliminating its uncertainties, a new tool in the integration of ecological preservation while ensuring coastline stability may be at hand. In times where the integration of habitat restoration and economic development receive increasing attention, this opportunity is worth exploring. The general product development framework that will be used as guideline for development of the technique is visualized in figure 1.1.

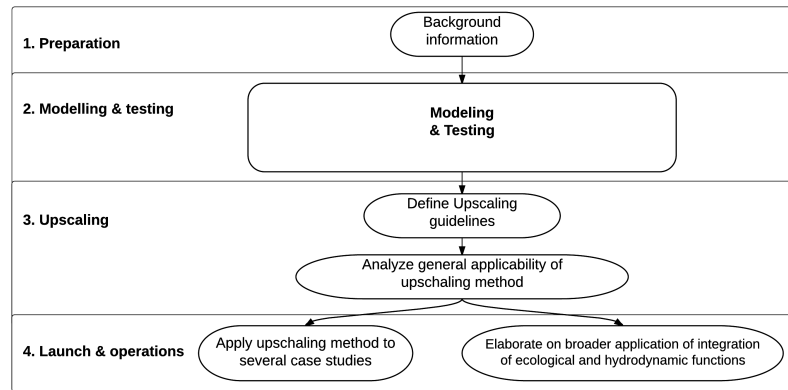


Figure 1.1: General product development framework for Artificial Reefs

The 3D printing production process was developed to meet the innovative objectives of the Larvotta AR pilot project in Monaco (see for more information Boskalis article by Hill [35]). The function of the reef is described to be both ecological and socio economic, in terms of habitat creation, ecological connectivity, fishery resources and amenities (diving and snorkling). The design is innovative in both ecological design as well as production technique and material.

Artificial reefs come in very many different forms. The origin of AR lie in the economic corner, being used as a tool to increase fishery resources [8]. The last decades the ecological value has increasingly been taken into account, resulting in placement of AR units in marine protected areas[46]. The main purpose of these reefs taken into consideration is to provide habitat and increase interconnectivity between ecological systems. There has been a lot of research on ecological effect of the material, placement and design of artificial reefs, by means of trial and error experiments [22]. The functions and design of AR is elaborated on later in chapter 2. For now it is emphasized that although various successful restorations of habitat using AR are reported, there is not one best practice regarding their design. This is due to the complexity of ecosystems, which makes it extremely difficult to capture the main design parameter for an AR.

For a long time hard structures were considered the way to go when a coastline showed signs of erosion. The basic driver of this approach is the assumption that introduction of hard substrate into an otherwise sandy environment offers the potential of wave energy dissipation. (Submerged) breakwaters, groins and sea dikes are common structures found all around the world. These structures limit wave energy reaching the sandy shoreline by causing a disturbance in the wave motion. This is reached by limiting depth, causing breaking of the waves, physically blocking the waves or reinforcing the shoreline so it becomes less vulnerable. However, these hard structures imply great changes in the natural environment. They can greatly influence the ecosystem, in ways that are not emphasized on beforehand. Another challenge encountered in this research is that available knowledge and data on submerged structures is fairly limited. The DELOS project ([33]) has made a huge effort in bundling available- and developing new knowledge on low crested coastal defense structures(LCS) and their role in the environment. This is almost exclusively focused on rubble mound structures. This is expected to have large geometrical differences from the AR units. Up until now LCS are considered a relatively poor surrogate of natural rocky shores [53]. One of the reasons for this is that LCS offer less complex habitats for species. A fix for this problem might be at hand with the 3D printing technique, since high structural complexity can be reached. Another issue identified by the DELOS project is that LCS experience higher rates of disturbance then a natural shore / rocky reef. This issue will be addressed in this thesis.

As mentioned, coastal zones around the world are under increasing pressure regarding ecological, social and economic factors. These are the three pillars that have to be included in order to pursue sustainable development. This is illustrated in figure 1.2. Integration of these -often conflicting- stakes has long been overlooked[66]. Currently, awareness for the need of sustainable development of the coastal zone is growing. Coastal management plans that take into account human safety, economic development and ecological integrity are being implemented [64].

Recognition that environmental sustainable development is crucial for long term well being is increasing. There is still a lot of knowledge to be gained in terms of harmonizing ecology and coastal protection. The concept of sustainability has been around for a while. The concept is implemented in concrete frameworks

and tools.

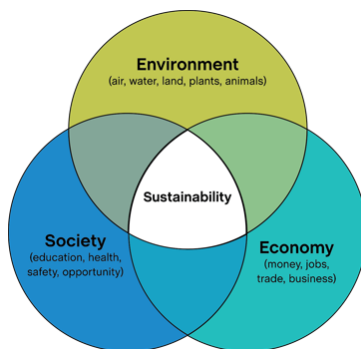


Figure 1.2: Three pillars of sustainable development, source: www.exhibitseed.org

The aim of this project is to contribute to integration of the environmental and social pillar. Ecological by providing habitat to certain species, Social by offering coastal protection to society. These two form the base of the design process. To make the 3D printed reef technique sustainable, the economic pillar has to be integrated with the other two as well. By up-scaling the fabrication in terms of production time and cost efficiency, the ecologically based design could be applied on a large scale. This makes it economically interesting and a potentially profitable new technique to enhance sustainable coastline protection and development. This benefits the business case, which has proved to be a challenge in many ecologically driven projects. The economic pillar is not further addressed in the scope of this research, but will be looked back upon in the recommendations.

In order to allow economic coastal development, society is in need of a stable coastline. An additional threat to coastline stability is the impact of climate change, which lead to sea level rise. The Mediterranean is pointed out as one of the areas that will experience the highest impact of change in the climates equilibrium [56]. The fore-casted increase of occurrence of extreme events as well as the rate of sea level rise, induces amongst many other threats, extra risk on coastline erosion and flood risk for the community. Combining this knowledge with the fact that most Mediterranean coasts are sandy, it is obvious that there is an urgent need for coastal protection.

1.1.2. Case

To narrow down the scope of this research, a case study location is defined at the Mediterranean coastline. A location along the Italian coastline that suffers from erosion was identified, namely Bay Sant d'Agostino. This site was picked when Boskalis started drafting a proposal on applying a 3D printed artificial reef in the near-shore at this site. The same parties were involved as in the earlier Monaco pilot project, which makes the conditions favorable to combine available knowledge from both projects. When this thesis research proceeded, the Sant d'Agostino project was postponed. The site is considered to be a good representation of the general Mediterranean near shore environment, therefore wave climate and bathymetric information of this location are continued to be used to apply the developed methods.

The bay of Sant'Agostino is located in the region of Lazio. It has experienced coastal erosion for a long time, several hard structures have been build in the vicinity, like groins and (submerged) breakwaters. The disadvantage of these structures is that when they are constructed on an (approximate) alongshore uniform coast, the sediment deficit that causes erosion, is mitigated downstream. This forces communities downstream of the sediment flow to take measures as well, as is the case at Sant'Agostino. The natural reef environment of the shallow Mediterranean coastal zones has been severely damaged to accommodate trawl fishing, which will be elaborated on in chapter 2. To restore the natural habitat, the need for some form of artificial reef is obvious. The location of this bay is squeezed between two Natura 2000 marine reserve-sites, see figure 1.3b. Therefore a high interest for environmental well-being is expected from governmental institutions.



(a) Location of the case site, source: maps.google.nl



(b) Natura 2000 marine reserve sites, source: natura2000.eea.europa.eu

Figure 1.3: Case study site Sant'Agostino, Italy

1.2. Problem description

To clarify the introduction above, the reasoning that leads to the need of an artificial reef or a breakwater from both ecological and coastal protection perspectives are individually mapped, up until the point where they conflict. The reasoning is found in table 1.1. This hypothesis is not to be interpreted as comprehensive in ecological or engineering functioning, it is meant to describe the processes that have led to this research's objective. The objective addresses a sub-set of functions that can lead to a successful multi functional structure.

Table 1.1: Problem description

	Ecology	Coastal Engineering
What	Artificial reefs can contribute to restore ecosystems that have a depleted count of hard substrate	Hard structures can serve as protection against wave attack
Why	A porous structure can serve as habitat for flora and fauna	Coastal protection is needed to minimize risk of flooding in coastal zones with sandy shorelines
Implication	Porosity and geometry of a reef influences ecological habitability Porosity and general shape of the reef influence hydrodynamic conditions	Geometry of the structure influences magnitude of wave damping Geometry of the structure has impact on hydrodynamic conditions
Translation	Hydrodynamic conditions can be linked to well-being of flora and fauna	Hydrodynamic conditions can be linked to wave attenuation
Problem	Integration of ecological and coastal protection function in a multi functional AR will introduce tension between desired hydrodynamic conditions from an ecological point of view versus a coastal protection point of view	

In addition to this physical description of the matter, there is a need for design tools that quantify the integration of design criteria for these functions. The DELOS project results suggest that the structural design of LCS can be altered to influence the abundance of species. Although ecological design is not straightforward due to the complexity of ecosystems, design criteria aim to integrate structures in the coastal system [53]. This tool development is to facilitate design of the structures, but also to serve as support in the dialog between coastal and ecological engineers.

The hypothesis has been projected on the described case study and the 3D printed reef technique, to frame the scope and make it manageable to address within one thesis.

1.3. Objectives

The main objective of this research is *to establish a method to integrate ecological and coastal protection functionalities for a 3D printed reef*. The outcome is expected to contribute to the development of an integrated, multi-functional artificial reef design. Goal of the total product development for the 3D printed reefs technique is to (re)colonize coastal waters in a planned manner, while stabilizing the coastline. Additionally the technique has to be proven sustainable, so in the future the business case will have to be justified. Therefore a minor objective of the study is defined: *Design of a product development framework*.

The main research question distilled from the above description of objectives is:

"How can an integrated design approach of ecological and coastal protection functionalities, for a 3D printed reef, be established?"

The following subquestions will serve as a guideline to come to a comprehensive answer to the main question. The aim is to address all these questions in the report.

- *Which ecological and hydrodynamic parameters should be analyzed?*
- *What method should be used to provide insight in both functions simultaneously?*
- *How can this method be used to contribute to the design of 3D printed reefs?*

The goal of this thesis is to help improve the effectiveness of AR as coastal protection system, while retaining ecological value. In the near-shore environment the AR's are expected to function like conventional coastal protection structures, but with the advantage that it generates less negative impact on the environment, or in the ideal case have a positive impact. In addition, based on the knowledge gained in this project, it can be demonstrated how these structures may represent an integrated solution that allows prevention of mitigation of the coastline while creating natural habitat. Furthermore, it will provide a method to quantitatively assess the ecological value of a structure.

1.4. Approach

1.4.1. Methodology

In this section the methods applied to come to a comprehensive approach is illustrated. These methods as a whole meet the objectives of this research.

First, the product development framework from figure 1.1 is extended to put this research in perspective. A subset of actions of the total framework is identified that is covered by the scope of this study. Secondly, a literature study is conducted in order to define the theoretical background and input for the modeling steps. Then, the modeling steps and their aims are introduced.

The product development of the AR units is expressed in a comprehensive framework. The goal is to translate the concept of a 3D printed, monolithic unit that has been prototyped in Monaco, to a mass-produced wave attenuating design which incorporates the same ecological value. This process is described by elaborating on the modeling steps on the product development framework, in figure 1.4. The framework has been defined by talking with experts on production techniques, material engineers, ecologists and project engineers. For the full description of the framework including suggestions for content of all steps, see Appendix A.

As stated in the objectives, the goal is to integrate the functions of an AR with those of Low crested coastal protection structures (LCS). It is not feasible to carry out the full product development, therefore a subset of actions is identified. Indicated in red are the components that will be addressed in this research. This smaller section of the framework is summarized in figure 1.5.

Next, the governing assumptions to limit the scope of this research and in particular modeling, are stated. Subsequently, the aims for the literature study are introduced. The first modeling process discussed is the far-field model setup, calibration and preliminary results. Then the first setup of the near field model is introduced, of which the results serve as input for the laboratory setup. Third modeling process is the design and setup of the laboratory tests. Guided by some preliminary results from the physical model, the second step in near-shore modeling is executed. Lastly the method that is used to couple hydrodynamic results to ecological value is elaborated on. All these steps are introduced in the next sections.

Governing assumptions This research will focus on the 2-dimensional, vertical environment. Also, the waves considered in this research are strictly monochromatic. This is to limit the amount of uncertainty imposed when the full complex system is assessed at once. Since the problem in essence is 3D, some substantial simplifications are inevitable. Other assumptions further on will be indicated as shown next.

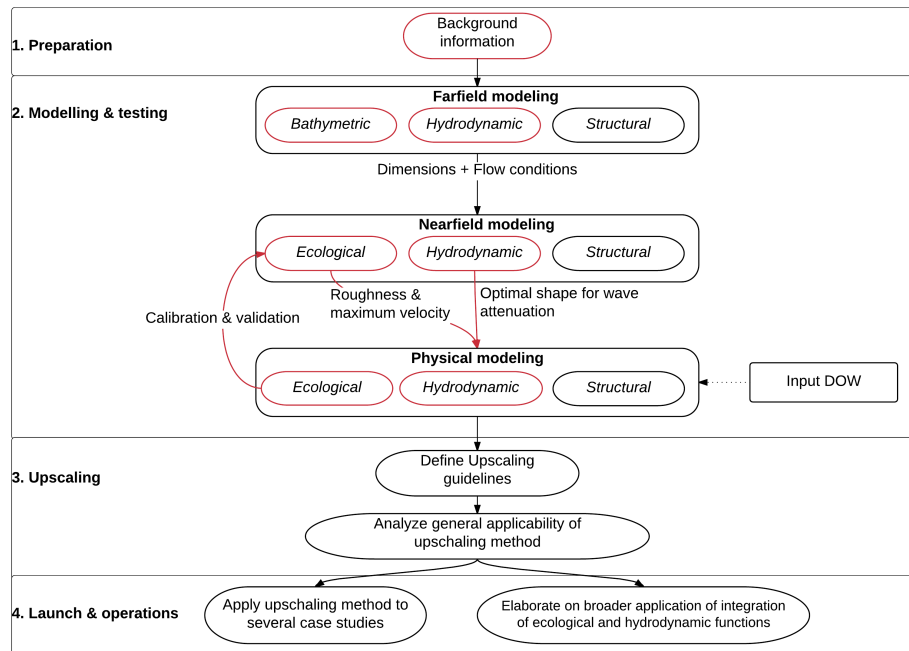


Figure 1.4: Framework for coastline defense AR product development

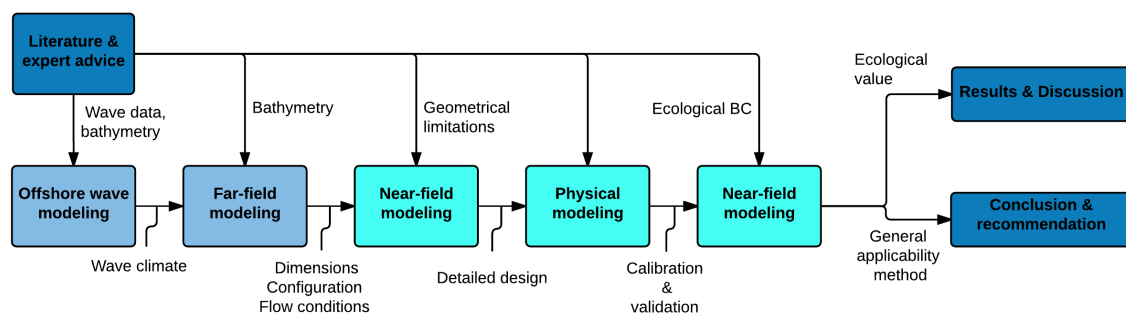


Figure 1.5: Methodology of this research

Assumptions to narrow down the scope are framed

Expected results from literature study In the literature study the boundary conditions and input for further analysis are explored. In depth research will be done to establish the functions of AR's and LCS. A parallel must be drawn between the two, and governing parameters are identified. It is decided which physical parameters will be used in giving expression to the objectives. Furthermore, the scale upon which the system is analyzed is explored. An ecological parameter has to be identified and thresholds of that parameter to which the effectiveness of a reef can be measured. The overall geometry of the reef and its assumptions are elaborated on. The choice of models that fit the above mentioned division in far- and near-field modeling is made based on if available hydrodynamic models are fit for purpose. The results from the literature study will serve as the base of further modeling and synthesis of the results.

Expected results from modeling To be able to quantitatively judge the performance of the reef units, a sequence of numerical models has to be selected. Numerical models can either be stochastic (phase aver-

aged) or deterministic (phase resolving) [44]. Stochastic models base their analysis on a probabilistic calculation, while deterministic models simulate hydrodynamic processes based on the conservation of mass and momentum [11]. The end result is emphasized to be a hydrodynamic model that accurately computes physical processes in a 2DV environment. Therefore the expectation is that at least the final model is phase resolving. This will be explained in section 2.10. The conditions have to be adaptable to the case study situation. The models will converge from large spatial scale to small and from simplified to complex geometry.

Modeling sequence Goal: to assess the preferred size and orientation of the artificial reefs (AR), and maximum horizontal velocity profiles linked to ecological thresholds. The dimensions are analyzed by looking at the wave damping calculated by the model. The interrelation and boundaries of the different models is indicated in 1.6.

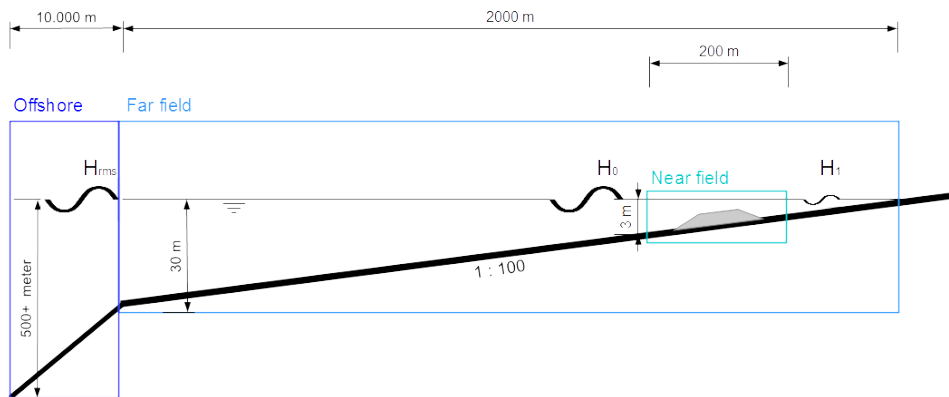


Figure 1.6: Differentiation of the domains of the four used models. Colors coincide with figure 1.5

The offshore wave model is applied to translate available wave data to input for the far-field model. This model is expected to be a phase averaged model. The output from this model is expected to be a wave spectrum. This will be analyzed by means of an extreme value analysis to result in a single wave condition (height and period) that is representative for the case study site conditions. The far-field model is 1DH (horizontal), the near-field model 2DV (vertical). They will be decoupled at the location in the larger domain where the structure starts interacting with the waves. This is done because the far-field model will not be able to accurately determine velocity profiles over depth when a structure is present, due to the decoupling of the continuity equations for every grid cell. It is phase averaged rather than phase resolving. The decision was made (see chapter 2) to model flow over the structure that is relevant to this research by solving in the vertical with a more detailed numerical model.

The numerical modeling goals are divided in two categories: Far-field and near-field. This was graphically explained in 1.6. Requirements of the different models are explained by means of their goals.

Goals far-field modeling The goal of the far-field modeling is to determine the location and large scale geometry of the field of structures in the cross-shore, plus translate wave height to shallower water. The benefit of using a phase averaged model is that computation time is limited compared to a phase resolving model. Therefore this was a large domain and time frame can be computed while calculation time is still manageable. In order to do this several scenarios will be modeled which are judged on their wave attenuating behavior. It does not need to solve for the reef elements individually, only the envelope around the reef. Far field effects are analyzed in the 1D cross-shore direction.

Far field modeling should therefore comprise:

- site specific wave conditions
- site specific bathymetry
- solve for wave damping (1DH)

Goals near-field modeling Goal of the near field modeling is to solve velocity fields in 2DV over the individual units, as well as varying geometry and porosity of the units. The expectation is that by varying geometry and porosity of the structures an optimal combination of the physical parameters identified in the

literature study can be found. Geometry will be varied mainly looking at angles of the seaward- and lee side of the structure. Because exact physical properties in time and space are a requisite a phase resolving model is needed. This implies heavier computations and thus potentially longer computational time. Boundary conditions will be extracted from the far field model, in order to reduce computational time by decreasing the length of the domain.

Near field modeling should comprise:

- Site specific wave conditions, in accordance to the far field model
- Ability to define roughness/porosity
- definition of detailed geometry
- Depth varying velocity and turbulence solver
- Tuning parameters that can be utilized to calibrate the model to physical modeling data

Goals physical modeling A physical modeling campaign will be setup to create a validation or calibration dataset for the detailed near-field model. Since the exact physical properties of the 3D printed surface of the reef structures is not known yet, validation of the model is necessary. Physical modeling should comprise:

- Reproduce wave conditions resulting from near-field model
- Physically realistic representation of the 3D printed surface of the reef
- Measurements with high accuracy of parameters that are identified as important

Synthesizing results In the results the final near-field model will be combined with the ecological thresholds. The added value of the total method to reef design and its limitations will be discussed. Also the outcome of the case study will be evaluated and the general applicability of the method is assessed.

1.4.2. Structure of report

To sum up the content of this thesis: In chapter 2 a literature study is conducted to place this research in proper perspective. The different fields of research that comprehend this study are discussed and some reference projects are introduced.

The next chapter, 3 consists of applied methods and materials. New concepts that are developed in the course of this study are introduced. In order to logically describe the sequence of models, some preliminary results are included when they contributed to the progress.

In chapter 4 the results of the different steps in methods are elucidated. This is followed by the synthesis. Here the results of combination of the coastal protection functionality and ecological thresholds are discussed.

Lastly, chapter 5 consists of the conclusions and recommendations. A reflection upon the objectives of the research is given, and the research questions are answered. Recommendations on further research, that emerged during this study, are stated.

The structure of the report and its content is visualized in figure 1.7.

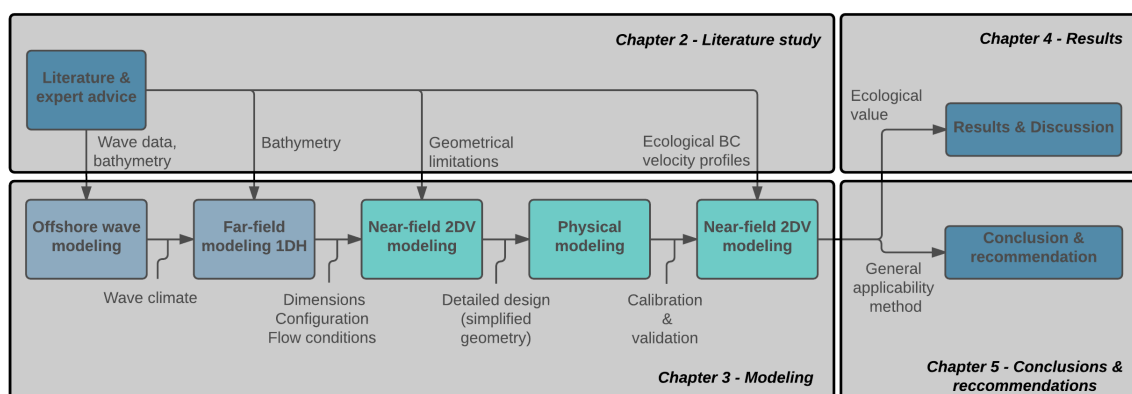


Figure 1.7: Structure of report

2

Literature study

In this chapter the existing knowledge on artificial reef development, near shore hydrodynamic processes and reference projects will be explored. To narrow down the geographical variability in ecological and coastal dynamics this study focuses on the Mediterranean. Parallels are drawn with conventional coastal protection works and existing artificial reefs. Relevant geographical information is elaborated on, like wave climate and ecological systems. Reef geometry is discussed, and the selection of numerical models is elaborated on.

This information will serve as base for further research in terms of model development and validation. In particular the following results are expected from the literature study:

- Identification of physical parameters to link ecological and coastal protection value
- A threshold definition for the ecological parameter
- Choice for numerical models
- Design limits on geometry of 3D printed reefs
- Definition of the scale at which the research will proceed
- Hydrodynamic and bathymetric boundary conditions for further modeling

2.1. Natural rocky reefs

Nearshore rocky reef environments are a key habitat with critical functional importance as a hub between eco systems Sala et al. [65]. As the name suggests, these habitats are found in the littoral zone. They consist of hard substrate, which forms the basis on which an ecosystem starting with algae and some coral species develop. This will be elaborated on in the next section.

The rocks building a rocky reef are deposited by glaciers. When these glaciers from the ice age melted, they left piles of rock, soil, and gravel. During the last centuries, many of these rocks have been removed to accommodate trawl fishing. This has caused a large change in the ecology, but also in the hydrodynamics. Since this proceeded on for many centuries, it is very difficult to establish a baseline for both ecology and hydrodynamics by which the health of the current system can be evaluated [65]. Rocky reefs have not been extensively studied in both ecological and hydrodynamic behaviour. Therefore a parallel is drawn with coral reefs, which have been widely studied worldwide by Gourlay and Colleter [29], Gourlay [30], Hearn [34], Lowe et al. [48], Monismith [52], Symonds et al. [71]. Rocky reef systems are different from coral reef systems. Although hydrodynamic properties might show some similarities (as is also assumed in 2.4) the origin and dynamics of the system itself are totally different. While coral reef systems appear and thrive only in certain environmental conditions [44], rocky reefs are created by seismic movement and not very vulnerable to change of the environment. The geographical location of the Mediterranean Sea implies that the reef environment that the AR will be mimicking is rocky reef rather than coral reefs, since coral reefs are predominantly found in tropical and subtropical waters.

2.2. Artificial reefs

The definition of artificial reef used by the European Artificial Reef Research Network (EARRN) is:[4] "A submerged structure placed on the substratum (seabed) deliberately, to mimic some characteristics of a natural reef".

In the Mediterranean these all consist of some sort of hard substrate introduced to an area where this was lacking [22].

2.2.1. Functions

The functions for which an artificial reef is intended substantially influence the design, location and support of the community [73]. The following functions of an AR are identified [73].

- Increase habitat (pro active)
- Enhance fishery resources
- Recreational diving opportunities
- Reduce user conflicts
- Restoration / rehabilitation / mitigation of habitat
- Socio economic benefits coastal community
- Scour protection
- Wave attenuation

The functions habitat creation and wave attenuation will be considered further on in this thesis. An overview of functions and parameters that play a role in artificial reef design is pictured in figure 2.10. Relevant parameters are elaborated on.

2.2.2. Design parameters

Various parameters that contribute to perform the functions of a reef are identified. These are divided into three categories, ecological/biological, material properties and physical/chemical. As will become evident in their description, the first category (eco/bio) can be influenced by the design of the reef structure. The latter category (phys/chem) is mainly determined by geographical location and therefore not elaborated on here. In general, studies examining environmental complexity and associated fauna find a positive correlation between structural complexity and species diversity and abundance [69]. Ecological / biological parameters that are found in literature are discussed, what they consist of and how they contribute to the ecosystem. Also a short comment is made on how the material influences the ecological environment.

Reef configuration Reef configuration is important to ensure a diversity in species. It can also be used to spatially divide different use (fishery, recreational diving, etc).

Reef vertical profile The vertical profile influences the species it attracts, and overall biomass it can support. AR with little vertical extend attract mainly demersal species, while high profile reefs provide habitat for pelagic fish [8].

Interstitial space This determines the degree and complexity of the community developing on the AR. Holes, walls and overhangs provide habitat requirements for various species, creating a diverse community. Juvenile fish seek shelter in cavities. Some species spawn in sheltered areas, while others lay eggs in holes and act territorial around the entrance during breeding season.

Total surface area In some cases total surface area is directly related to the amount of biomass an AR can support. The surface provides living ground for sessile and motile invertebrates, which in turn are important food sources for demersal fish species.

Circulation patterns in and around structure Current movement increases the reefs exposure to larval recruits which enhances the food supply. Furthermore Nakamura [55] discussed how pressure waves and ocean currents can influence fish. Chang [16] concluded that fish are attracted to locations that are shielded from strong currents, since they can save energy when resting in locations in current shadows. This concept will be used later on to judge ecological performance of the reef structures.

Roughness The surface roughness of the reef is important for plants and algae to be able to attach to the substrate. This can be integrated in the design and through material choice. Since this ecologically links to the micro reef scale, it is no further taken into account. This roughness should not be mistaken for the hydraulic roughness on reef scale, discussed in section 2.4.1.

Material Artificial reefs that have been introduced in marine environments have shown a very wide variety in effectiveness. Conclusion is that for a large part this is due to the choice of material. In Baine [4] a large variety of artificial reefs is studied with the widest range of materials, for example concrete, tires, plastic, ship wrecks, (steel) netting and train cars(!). This imposes a very large degree of freedom in the choice of AR material, but also imposes boundaries to the other design parameters.

Stability The structure should be stable over time, e.a. not roll over or slide down a slope. This can be achieved in various ways:

- Gravity based structure; center of gravity lies in the lower part of the structure, the base is wide and follows the bottom it is placed upon
- Fixed to the bottom; either with anchors keeping it in place, or by inserting pins into the sea bottom under the structure
- Scour protection; this is not exactly in the same line as former two points, but it has to be kept in mind that when flow patterns around the structure change, this might cause scour on the sea bed, which in time may harm structure stability

That the structure should stay intact and integer, is important to minimize disturbance by maintenance. It is proven that an artificial reef develops a more stable and flourishing ecosystem when left undisturbed [53].

visual attractiveness When one of the reefs objectives is to facilitate recreational diving activities, this is an objective that has to be kept in mind. Visual attractiveness is hard to express in numbers, but it is the overall consensus that an AR looking as close to a natural reef as possible is visually attractive.

In the modeling phase of this research material integrity and structural stability is assumed

Physical/chemical The following parameters are considered physical characteristics of the geographical location of the reef. Obviously, these parameters have great influence on the eco-system. Since these parameters are considered fixed they will no further be discussed here.

- Wave climate
- Tide
- Depth/ hydrostatic pressure
- Water temperature
- Light attenuation / turbidity
- Salinity
- Sedimentation

2.2.3. Reference projects

Some projects that are taken into consideration during this research are illustrated here. The reefballs are a very direct link to AR, while the other two are a little bit further off the topic. Findings of these are however very valuable in understanding the connection between structure and ecological value.

Reefballs The Reef BallTM is a proved efficient Artificial reef unit, molded out of concrete. It has been applied in over 60 countries worldwide. The design was originally developed to enhance habitat creation, but in later studies it was also applied for (beach) erosion control, adding to the coastal protection functionality. A large scale pilot project of the Reef BallTM as an underwater breakwater has been installed off the coast of the Dominican Republic and extensively studied [3]. The geometry and placement of these reef balls is used as an example for this research, see figure 2.1.



Figure 2.1: Reef balls, source www.reefball.org

Ecology-based bed protection The topic of this thesis is to evaluate the ecological value of regular rocky bed protection of an offshore wind turbine, in terms of cavity size, by Buijs [12]. This gives interesting insight what can be said about a structure ecologically, when looking at a design that is made from an engineering perspective, rather than an ecological view. This is exactly the opposite as what will be done in this thesis, but parameters considered are expected to show similarity. The resulting tool of this thesis is a formula to calculate pore size in rubble mound structures, in relation to specifications of the rock size distribution and shape. This equation and its parameters will be elaborated on in section 3.4.3.

multipurpose artificial underwater structure as a coral reef canopy This research is closely related to the study to be conducted. It consists of an ecological approach to a new technique to increase bed stability and provide habitat in an energetic, shallow water environment. The data set created in the laboratory is similar to that generated in this study, complementing each other. The well-defined ecological system definition of this is used in this study as well, already touched upon in section 2.3. This research by Danker Koliijn[44] was considered on micro-scale, since it focused on larval settlement. This is considered another tool in the toolbox that can help engineers integrating ecological value into the design of coastal structures.

2.3. Reef ecology

The Mediterranean has been depleted by intense exploitation over the last millennium, causing species to shift from large to small. Once there used to be seal, turtles, bluefin tuna, and so on. [65] Also Habitat destruction, pollution, introduced species and climate change have had a great impact on the Mediterranean. There are no pristine, undisturbed sites in the Mediterranean left that allow to set a baseline against which to compare the health of original rocky reef ecosystems, as also mentioned in section 2.1[65]. This section will elaborate on the ecological background against which the requirements of the AR can be defined. Since it will be combined with a wave attenuating function, the background will be sketched for shallow waters with high wave energy.

2.3.1. System analysis

There are two ways of analyzing the ecosystem: looking at the far-field ecological dispersion of species over the Mediterranean, or looking at the occurrence of species and its ecosystem in a specific location, which is considered near-field. Below a short introduction for both approaches, after that focus will lie on the near-field ecology.

On planning level several elements can be discerned in an ecological infrastructure[67]. This is pictured in 2.2

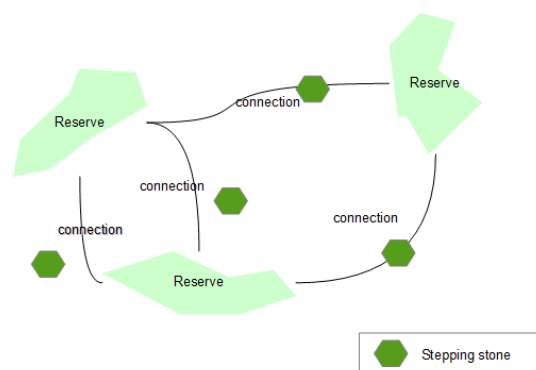


Figure 2.2: Ecological infrastructure (copied from Schiereck [67])

- Nature reserves. These are areas where species live in more or less ideal circumstances. The areas are large enough to ensure long term conservation of particular populations.
- Ecological connections. These connect nature reserves, and can serve certain species or be of more general use. When these connections malfunction or disappear, fragmentation of the ecosystem will follow, cutting of the different reserves.
- Stepping stones. When the distance between nature reserves is too large for species to cover by using an ecological connection, stepping stones can increase the dispersion of species. These are suitable as temporary habitat, but too small to ensure

that a system stays healthy on the long run (without dispersion of species).

In the scope of this research the artificial reefs will be considered as stepping stones. Further far-field ecological analysis is not carried out

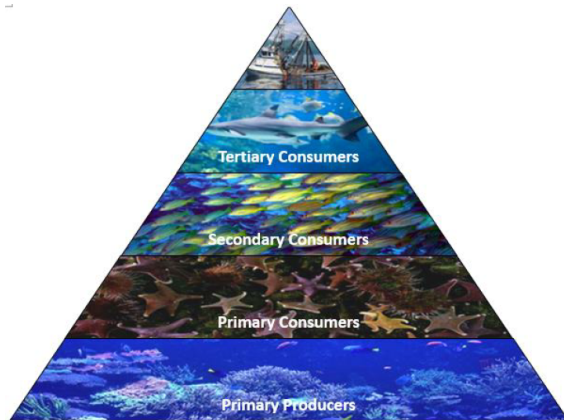


Figure 2.3: Food chain (as defined in Koliijn [44])

The reef-scale of an ecosystem is defined by the food chain. The food chain as described by Danker Koliijn Koliijn [44] is considered, see figure 2.3. The four categories of consumers are defined as follows. Also indicated is the reef scale at which these categories of species spread.

- **Primary producers:** Phytoplankton, algae and many species of seaweed. Habitat on micro-scale
- **Primary consumers:** Herbivores, zooplankton, larvae, sea urchins, crabs, herbivorous fish. Habitat on micro- to meso-scale
- **Secondary consumer:** Plankton feeders, corallivores, invertebrate feeders, piscivores. Habitat on meso- and macro scale
- **Tertiary consumers:** Carnivores (sharks, barracuda, seal). Habitat on macro-scale

2.3.2. Target species

This study aims to assess the functioning of an 3D printed Artificial reef in the near shore environment. To define quantifiable parameters, a target specie has to be composed. Since in this research the meso-scale of reefs is considered, the species habitat scale should agree. Following the foodchain in figure 2.3, this matches the primary or secondary consumers. These species should additionally be able to withstand a certain amount of wave induced forcing, i.e. being able to live in the near shore environment, and be associated with hard substrate.

By using the species database www.fishbase.org (freely accessible database, established, modified and checked by over 500 collaborators worldwide) a first selection of reef associated, Mediterranean, native species was made. This list was narrowed down by looking at the depth preferences and habitat definitions, as well as food source.

The list of potential target (fish) species that was distilled can be found in appendix C.

Targeted species

The first list of possible target species (in appendix C) was communicated to ecologist and professor Patrice Francour of University of Nice. After reconsidering chosen target species taking into account economic value, two fish species were appointed in consultation with professor Patrice Francour:

- Flatfish
- Juvenile sea bream

These two species are also valued for consumption, which makes it economically interesting if their population could be enhanced by introducing reefs.

flatfish Flatfish is a group of level one fish species. In the nearshore (<10 m depth) eastern Mediterranean this group consists of Flounder (avg 30 cm, max 60 cm), Sole (avg 30 cm, max 70 cm) and Juvenile Plaice (avg 30 cm). Flatfish live on a calm and sandy bottom, in the vicinity of hard substrate, since this is where their food source (crustaceans and mollusks) can be found. Since these fish do not live in the vicinity of rocky reefs, but in the sandy bottoms surrounding them, they will not be further considered.

Juvenile sea bream Adult sea breams live in open water. However, juvenile sea bream seek for shelter in the juvenile period of their lives. They find this in rocky reef environments and around other hard substrates.



Figure 2.4: Sea bream, source: www.fishdb.co.uk

They prefer shallower water since their natural predators inhabit the deeper coastal waters. In larval and juvenile stage they live in brackish water or lagoons, from 3 centimeters and up they migrate to shallow coastal zones, from 0-50 meters deep. They live over rocky bottom and sea grass meadows, which gives them shelter and feeding ground [18].

The size distribution of these fish from larval (0(mm)) to adult (30 cm) is fairly wide, therefore the approximate mean is taken as the governing length scale: 15-20 cm.

Target species is juvenile Sea Bream, 15-20 cm in length.

2.4. Reef hydrodynamics

A lot of research has been done on the hydrodynamic behavior of coral reefs. This has led to a reasonably detailed description of their behavior, which is far more detailed than the work that has been done on rocky reef environments. This can probably be explained by the fact that coral reefs are considered very vulnerable environments which need proper protection.

Reefs (being coral or rocky reefs) are geometrically very complex. This leads to interesting fluid mechanical problems, for example the behavior of unsteady flows over and through the structure [52]. One of the objectives of this literature study is to identify the scale at which this research is conducted. Therefore different scales are discussed here and later for coastal structures.

2.4.1. Roughness

Complex geometry implies a high roughness of reef structures. This in terms will induce quite high resistance to flow over and through their interior. An a priori determination of hydrodynamic roughness of (coral) reefs is not possible yet [52].

Therefore the roughness of the AR will be approximated by calculating the Manning roughness coefficient and later the Nikuradse roughness height. This is elaborated on in chapter 3.

2.4.2. Reef scale

There are different levels on which the hydrodynamic movement of flows can be considered, following Monismith [52]. The magnitude of currents and turbulence is very dependent on the presence of waves and the location of the reef in the watercolumn.

micro The micro scale is on the scale of (coral) colonies within the reef. AR should allow sufficient water circulation, to avoid stagnant water (diminishing of the productivity of the overall reef) and allowing for circulation that spreads sessile invertebrates. Also it should be kept in mind that when velocities get too high (turbulence) this can limit the possibility of settling of species/coral.

meso This is the scale of the boundary layer flow over reefs, which is characterized in length scales 1-10 M. This is the scale that initially will be targeted in this research, because this encloses the hydrodynamic, coastal protection functioning of an (artificial) reef.

macro This is the reef-scale, so the total system. The length scale is 100-1000 M.

2.4.3. Wave induced forcing

When reefs are located in deep water, wave induced forcing is limited. When moving into more shallow water, the movement over and within the reef can be linked to the permeability of the structure. Also, they can be connected to larger scale implications, like carrying nutrients that are valuable to ecological well being. Since this is the situation that is considered in this thesis, two types of reef-wave interaction are discussed, on two different scales. ope

Micro-scale: Keulegan Carpenter One way of looking at the wave-structure interaction is to analyze the mass-transfer through the structure. An experimental based parameter that describes this process is the Keulegan-Carpenter number as described in Monismith [52]:

$$K_c = \frac{U_W}{\omega S} \quad (2.1)$$

with:

- U_W = Wave orbital velocity
- ω = Frequency
- S = Cylinder spacing

When K_c is large, the flow is drag dominated and velocities inside the colony are much lower than in the free stream. When K_c is small, the velocities in the interior merely match exterior ones, and total mass transfer is enhanced over that of steady flows.

The cylinder spacing S resembles a model of a (coral) reef complexity, during the experiment arrays of cylinders were used to create a varying degree of porosity. This concept has been successfully applied by Danker Koliijn Koliijn [44] to assess ecological value for larvae settlement.

Meso-scale: Flow Patterns Waves in open water have a certain orbital velocity pattern, which becomes increasingly elliptical shaped when entering shallow water. When waves encounter a structure or a reef, the flow patterns are disturbed and varying patterns in the cross shore plane emerge. This has implications for accessibility of the structure for species and their food source. A quantifiable expression for this 'accessibility' has not been found in literature. In this research therefore a method to give expression to this accessibility is sought after.

The reef scale considered in this research is meso-scale

2.5. Low crested coastal defense structures (LCS)

The use of coastal defense structures is wide spread all over the world. The forecast is that they will become even more widespread in the coming 10-30 years as a response to stormier seas and economic development of the coastal zone[53]. The sub category of low crested structures has been extensively described by the DELOS research project [33]. The description of an LCS following DELOS is that they are shore parallel, low crested (crest below mean sea level) coastal defense structures. Because the AR units will perform the same functions as LCS, they will be closely looked into, in order to assess the similarities that can be used for the design method of the AR units.

2.5.1. Functions

The main function of an LCS, defending the coastline, is reached by a number of physical characteristics. Together they lead to a decrease of wave energy reaching the vulnerable sandy coast. These processes are elaborated on as being separate functions. In fact, they interact and reinforce or attenuate mutual processes.

Wave attenuation The wave damping ability of a LCS can be calculated by using the formula for Rubble mound low-crested, narrow structures of Briganti, [62] equation 2.2.

$$C_t = \frac{H_{out}}{H_{in}} = -0.4 \frac{R_c}{H_s} + 0.64 \left(\frac{B}{H_s} \right)^{-0.31} (1 - e^{-0.5\xi p}) \quad (2.2)$$

Where C_t is the coefficient of transmission. Other dimensional parameters can be found in figure 2.5, which resembles a conventional lcs.

This formula has been fitted to an extensive amount of data sets, but these are all within the limits of traditional LCS, with a gentle slope on the offshore side, a berm with significant width and a sloping lee side. This general geometry is pictured in 2.5. The structures considered in this research are beyond the limits of this empirical formula, resulting in physically unrealistic values of $C_t > 1$. This shows that the combination of dimensions is outside the validity of the formula. Therefore, for the assessment of the wave damping behavior the use of a physical or numerical model is necessary.

The coefficient of transmission (C_t or K_t in literature) concept will be used in this research, as coastal protection governing parameter.

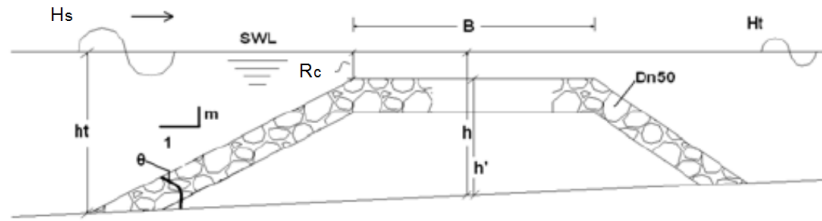


Figure 2.5: Low crested structure dimensions [62]

Wave refraction Refraction is the phenomenon of incoming wave rays aligning with the coastline when they enter shallow water. This is quantified by Snell's Law [70].

$$\frac{\sin\theta}{c} = \text{constant} \quad (2.3)$$

with θ = Angle between incoming wave ray and shore normal, c = shallow water wave celerity and h = water depth.

When incoming waves encounter a submerged structure, this can be modeled as a sudden decrease in depth h . Wave celerity c will increase, which induces a decrease in wave angle θ , forcing the wave rays to turn parallel to the shoreline.

Because this research is 2DV, only normally incident waves will be considered, so $\theta = 0$

Long-shore transport A submerged breakwater has a wave attenuating and refracting effect on incoming waves. These both influence the littoral (sediment) transport along the shore. This can be quantified by looking at the CERC formula for long-shore sediment transport;

$$I = K_c P \quad (2.4)$$

with I = Submerged weight of sediment, K_c = Empirical constant (0.77) and P = 'Long-shore energy flux factor' (of which the physical interpretation is unclear).

P can be expressed in two contributing factors, wave energy flux and the angle between the wave crest and coastline;

$$P = U_b \cos(\phi_b) \sin(\phi_b) \quad (2.5)$$

with U_b is the wave energy flux at breaking point 'b' and ϕ_b is the angle between wave crest and coast at breaking point.

The wave energy flux in 2.5 can be expressed as follows;

$$U_b = (Ec_g)_b = \frac{1}{8} \rho g H^2 \quad (2.6)$$

These formulas show that sediment transport is related to H^2 so a small wave height reduction results in significant decrease in long-shore sediment transport. Also as ϕ decreases when the wave refracts over the structure, this will also positively influence coastline stabilization regarding long-shore transport[70].

The fact that a decrease in wave height will thus prevent erosion by reducing longshore transport is noted. Since incoming wave angle is assumed to be zero, longshore transport will no further be discussed or taken into account.

Longshore transport is not taken into account since the problem is assessed in 2DV. It is noted that a reduction of wave height leads to a reduction of longshore transport.

Cross shore transport Cross shore transport is mainly governed by the incoming wave energy. In general high waves tend to carry sediment offshore, while lower waves carry them onshore. A milder wave climate will therefore restore the beach by carrying sediment landward [19]. In 2.5.1 it is explained how submerged breakwaters will damp out the larger waves, thus cause a milder wave climate. Therefore it will increase onshore sediment transport and decrease offshore directed cross shore transport. Something that has to be considered is the occurrence of a concentrated return current, when the structure prohibits the natural return flow. This is comparable to a rip current and may occur around the edges of the structure(s), and can carry sediment offshore.

Cross shore sediment transport is the governing transport phenomenon considered in this research. Since the exact dynamics and geometry of the system are unknown a priori, the cross shore transport is only assessed in a qualitative manner, by comparing wave damping to the current situation.

A decrease in significant wave height near the shore will lead to a decrease in offshore directed sediment transport.
The potential occurrence of rip-like currents carrying sediment offshore is neglected.

2.5.2. Ecological impact LCS

As already mentioned in the introduction, the DELOS project concluded that LCS can be regarded as poor surrogate for natural rocky shores [33]. A positive correlation exists between the structural complexity of an LCS and specie abundance. Also LCS are more prone to disturbance both physical (wave / current action) and anthropogenic (maintenance). In some cases it was reported that LCS accommodate invasive species. DELOS have identified several considerations to be taken into account in LCS design to minimize or mitigate ecological impact. General guidelines for engineering intervention in the design are defined by DELOS. These can be considered when trying to minimize ecological disturbance by an LCS [53]. First the already mentioned increasing structure complexity. This enhances settlement and abundance of species. Topographic features also provide shelter from wave action and predation. Another general guideline is placing it lower in the shore, for more submerged area and less wave impact. Increasing size and number of structures will provide higher interconnectivity of habitats (this will be elaborated on in the next section). However, the increased interconnectivity caused by LCS can also have a negative impact. It can cause invading species to connect to new habitat, potentially harming the existing equilibrium of species in this new environment. The longer a structure is in place, the more complex the eco system becomes. It is therefore important to design a structure for the longest lifetime feasible. Also it should be kept in mind to minimize maintenance. All these general guidelines need to be tailored to the specifics of the system considered, and its desired management goals [53].

This research tries to take it one step further and develop a method to add to the design toolbox that will allow the LCS to positively contribute to the environment.

2.5.3. LCS scale

The scales at which a LCS can be considered are divided in the same way as the reefs are done in section 2.4. In order to make a clear distinction between reefs and LCS, it will be defined by means of far-field, near-field and structure-scale.

far-field Long shore currents, tidal movement, undertow, sediment transport. These are all processes that are assessed on the far-field scale. The far field scale considers (in 2DV) the whole area from deep water (50 meters plus) to the shore. Order of magnitude is 100 to 1000+ meters.

Near-field The near-field scale is considered comparable to the meso-scale in reefs. This implicates that it covers currents and velocity patterns over the structure (in 2DV), as well as wave height before and after the structure. This is in the order 1-10 meters.

Structure scale At the structure-scale, the stability and integrity of the structure, and forcing by wave action that are connected. Also scour and turbulence are considered to be within this scale of the structure. Order of magnitude is < 1 m.

2.5.4. Dimensional requirements

A typical build up of a low crested structure is pictured in figure 2.5. The mentioned dimensions can be derived from analytical formulas, which are linked to required wave attenuation, micro- and macro stability and available building material. Many of the design formulas can be found in the Rock Manual [62].

Significant wave conditions One of the main design criteria for LCS is the significant wave height. This is established per location, and based on extreme wave conditions that can occur in that location. Waves naturally do not occur in a regular signal, with one wave height H and period T . Statistics is applied, which characterizes a wave field by means of statistical parameters. For each individual wave in a wave field, statistics can give the probability of occurrence of those forces [67]. Since it is impossible (and very uneconomic) to design a structure that will never fail, an acceptable risk of failure is calculated for the design. A common and accepted probability of failure is 1/1000 years. This is also the probability of failure that is used to derive the significant wave conditions section 3.1.3.

2.6. Ecological value determination

It proved to be a challenge finding quantitative measurement scales to predict ecological value of the reef. Where engineering academics focuses on formulas, thresholds and hard numbers, ecological science does not. Ecological systems are extremely sensitive to many factors. Keeping this in mind, an effort was made to develop a method to quantify reef properties in terms of ecological value. This was done by drawing parallels with a known structure for which ecological thresholds were used in design, namely fish screens. This introduces simplifications, which will be pointed out and reflected upon in the conclusions of this research.

In order to make a translation to ecological values the comparison is made with fish screens at intake facilities in channels, since research in this field has been done on the maximum velocities for fish species in order to prevent ecological clogging of filters. The theory of Katopodis [?] is used. A translation to the reef situation is made in figure 2.6. Since this theory was developed for constant flow rather than flow under a wave, only uni-directional velocities are taken into account, and not orbital velocities. This will cause an underestimation of approach velocity V_a , since this will be amplified by the w -velocity in z -direction under waves, due to the orbital motion. Since this research focuses on shallow water however, the orbital motion has largely transformed to a flat ellips. Therefore it is assumed this theory can be applied, but it has to be kept in mind that it underestimates V_a . The resulting patterns that occur are cross checked with the general notion mentioned in section 2.2.2, that fish are attracted to locations that are shielded from strong currents, since they can save energy when resting in locations in current shadows (Chang Chang [16]).

The maximum approach velocity is defined in equation 2.7 Katopodis [41].

$$V_a = 0.02L^{0.56} \quad (2.7)$$

with V_a is approach velocity (m/s), L is fish length (mm).

Translation to u -velocity:

$$u_{max} = V = \frac{V_a}{\sin \alpha} \quad (2.8)$$

The maximum horizontal velocity will be used later on in this research, as governing parameter to resemble ecological value of the structure.

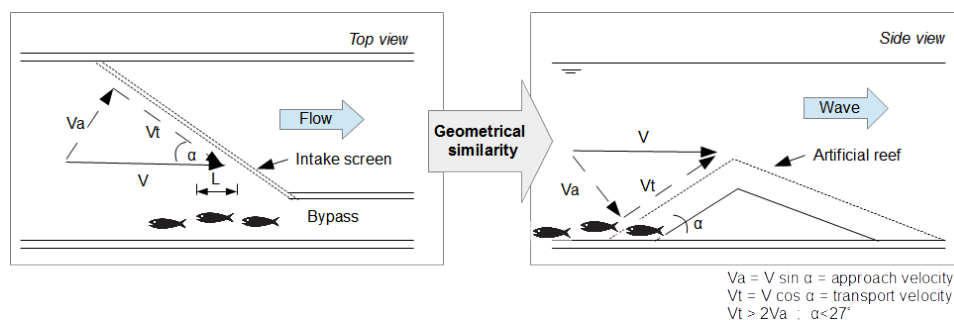


Figure 2.6: Geometrical translation of ecologically induced velocity threshold, left image copied from Katopodis [41].

2.7. 3D printed reef geometry

In essence, the geometry of the reef is open to interpretation on all aspects of its geometry. In order to limit possibilities and stay within the known feasibility limits of 3D printed reefs, some assumptions on its geometry will be done.



Figure 2.7: 3D printed unit for Monaco pilot project (deep water)

The 3D printed units are considered monolithic. This rules out mounded structures. This is in accordance to the application in Monaco. The Monaco reef geometry can be found in 2.7. Obviously this geometry is too fragile to be placed in a high energy, near shore environment. Assumptions on the reef unit dimensions in this study derived from the Monaco reef units are:

- Monolithic structure (stand alone)
- Maximum cross sectional area is $2 m^2$
- Core of the structure is impermeable

Since the reef units are applied as monolithic units, the geometry of the full reef-like structure is limited to a single layered geometry. The units are assumed to be placed in a 'staggered' grid like manner, to maximize surface coverage of the structures. An impression of this application is shown in 2.8. This has great similarity to the application of Reefballs, discussed in section 2.2.3.

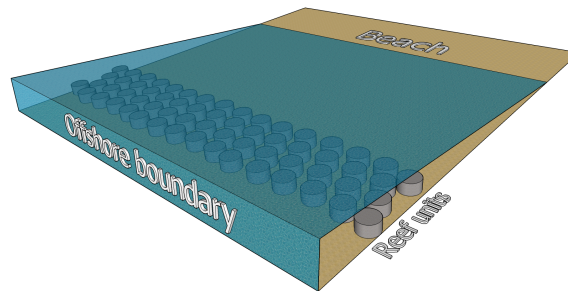


Figure 2.8: impression of staggered application of monolithic reef units

Reef units are monolithic, impermeable, $2m^2$ maximum cross section and applied in a staggered grid

2.8. Scale integration

The above mentioned scales for both reefs and LCS are compared. To narrow down the scope of the research it is decided that the scales considered are Near-field (LCS) and Meso-scale (reefs). These account for the same order of magnitude, which indicates it will be possible to assess the two functionalities at these scales in the same spatial resolution. This means it is very likely they can be assessed in the same model. A recap of the scales is shown in figure 2.9.

2.9. Consequence for research approach

Most commonly, when an artificial reef structure is developed the main function of the reef has been considered in the design, while the detailed ecological impact is roughly estimated rather than incorporated in the design. All identified factors that are involved in the design of an AR are gathered in the chart in figure 2.10. Also the coastal protection parameters are incorporated and possible design process input is included. These factors all contribute to the degree of functionality of the structure. Furthermore it is expressed that combination of high wave attenuation and high habitat complexity will be difficult to realize, which gives expression to the expected tension in incorporation of ecological and coastal protection functionalities, elaborated on in the problem description, section 1.2.

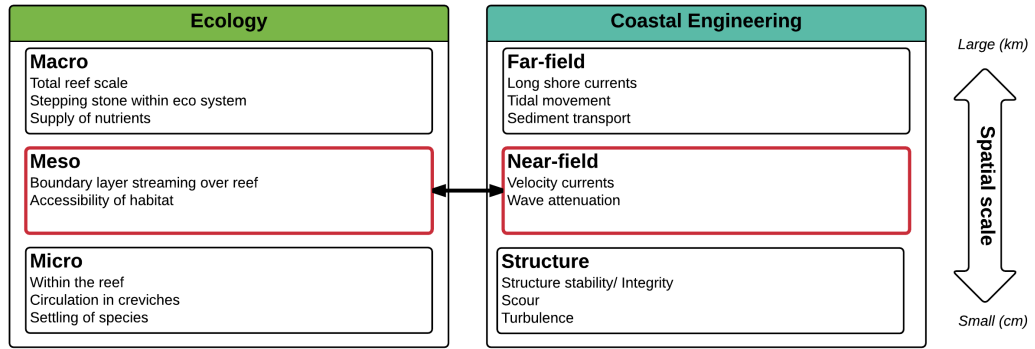


Figure 2.9: Ecological and hydrodynamic scales

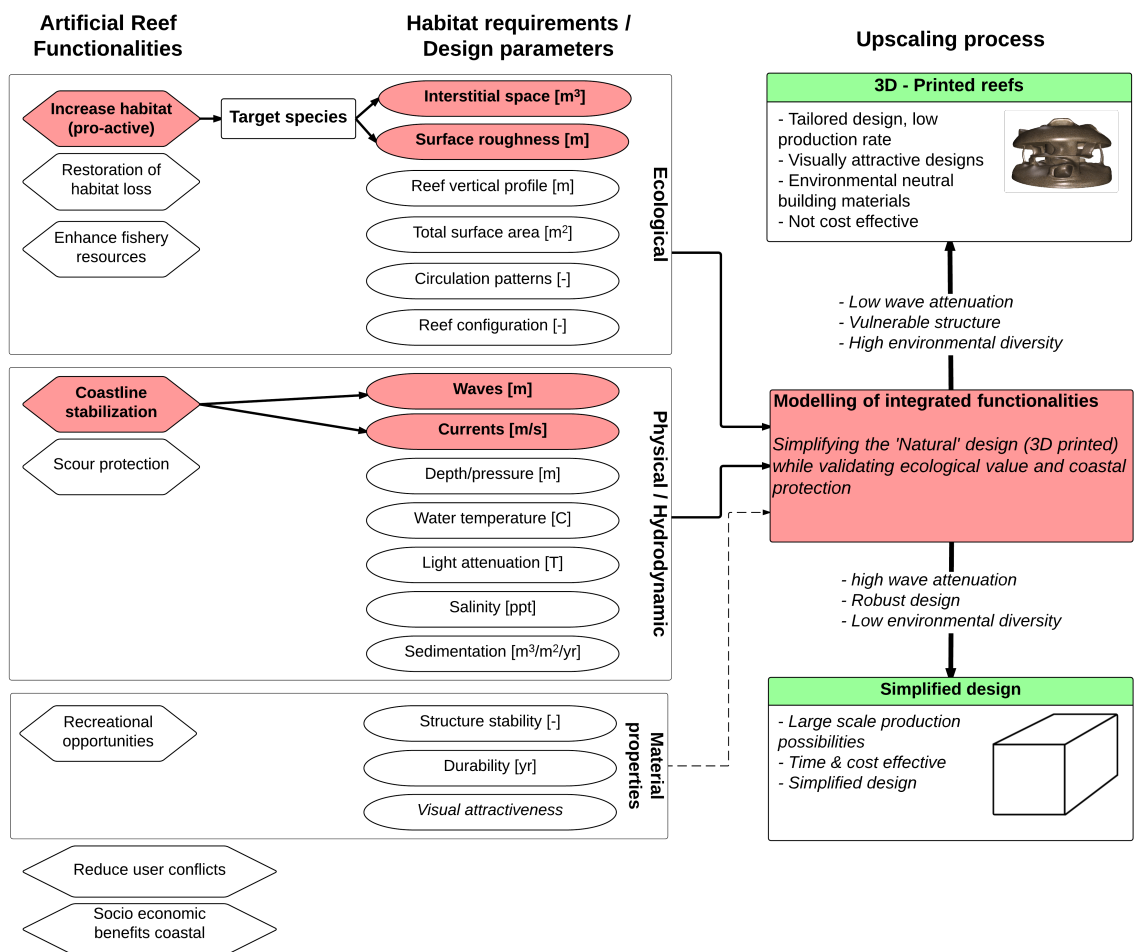


Figure 2.10: Focus in analyzing reef design during this study

In *red* the parameters of AR design that this thesis will focus on are indicated in figure 2.10. Others will not be addressed.

2.10. Selection of models

Since modeling in this research is modular, there are three situations for which the applicability of numerical models has to be considered, as stated in chapter 1. First a translation of offshore wave data has to be made to the depth at which the far-field model domain starts. Then the far-field 1DH model is selected, which contributes to translation of waves to near-shore conditions, as well as the position of the structure. The 2DV near-field model is the most sophisticated, since this has to solve for an extra dimension (vertical) and parameter (velocity). Several hydrodynamic models have been considered, keeping the above mentioned functional requirements in mind.

The offshore wave data comes in form of a wave spectrum. This is input for the wave model that translates from deep to shallow water. The wave model selected is SWAN. This is a wave propagation model, developed at Delft University of Technology (DUT), that computes random, short-crested wind-generated waves in coastal regions. The choice for SWAN was arbitrary, it is incorporated in the tool 'Worldwaves' for both deep and shallow waters, developed by Fugro. This is the shallow water waves tool used by Boskalis to compute wave conditions at project locations from MET-ocean datasets.

For far-field modelling XBeach is selected. It consists of the required functionalities while providing numerical stability and robustness [21]. XBeach is a public-domain model, co-developed by DUT.

For the near-field modelling, phase resolving model SWASH is selected. SWASH is a shock-capturing hydrodynamic model, which can model non-hydrostatic free surface flows. It is based on the non-linear shallow water conditions and also accounts for non-hydrostatic pressure. Shock-capturing models require large vertical resolution in order to solve the energy dissipation in the surf-zone due to breaking waves [77]. SWASH was launched in 2012 and is under continuous development in the department of environmental hydraulics of the DUT. This high vertical resolutions have the downside of being computationally expensive compared to XBeach, but this vertical detail is an asset when looking at ecological scale at velocity and turbulence. Therefore SWASH is used to solve near field hydrodynamics of the reef.

The reason why XBeach is used next to SWASH is somewhat trivial; this analysis could also have been done in SWASH 1D mode, however, the setup for the XBeach model had progressed before the decision of using SWASH as a near-field tool. Therefore the use of XBeach has continued for the far field computations. A benefit is that XBeach as a tool is more easily accessible than SWASH.

SWASH is a model that is under development. It has never been validated for a reef-like structure before. Therefore a dataset has to be found to validate the outcomes of SWASH. Because the 3D printed reefs are new, it is not yet known how the geometry behaves under wave orbital motion, how it influences the flow. Therefore it is decided a flume experiment has to be carried out. This will have to be done in a wave flume, with a 2DV representation of the printed reef. Extra attention has to be paid to the translation of 3D printed characteristics to the experiment setup, since it is unlikely a 3D printed scale model is available during the tests.

The spatial distribution of the modeling domains is visualized in figure 2.11.

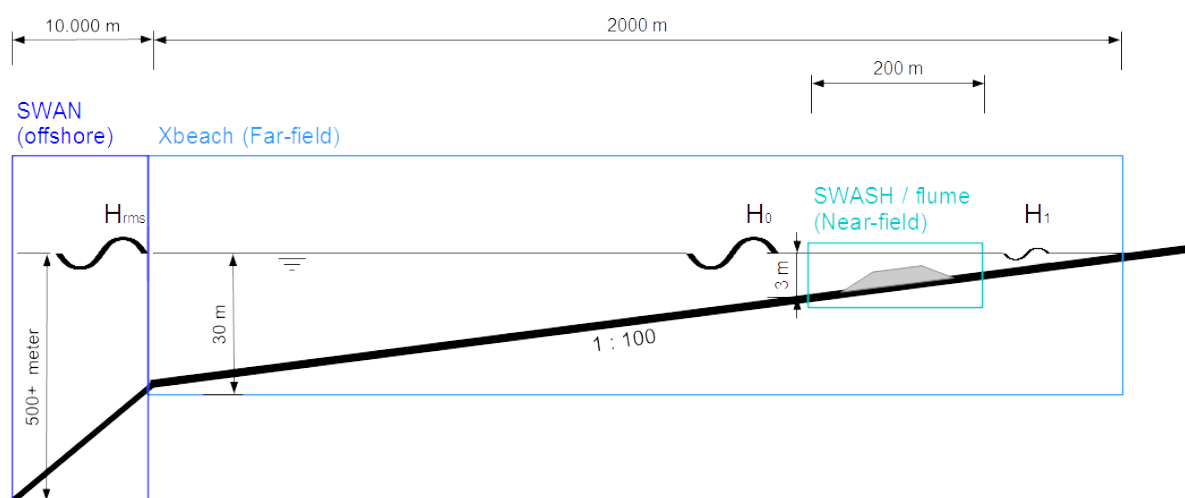


Figure 2.11: Spatial distribution of models used

3

Modeling

In this chapter the details of every modeling phase are explained. From the literature study knowledge will be carried into this part of the research, concerning:

- scale and dimensions of the spatial domain to be modeled
- Coastal protection and ecological parameters that will be assessed, transmission coefficient C_t and velocity u_{max} .
- Choice of the tools that will be used during this modeling phase
- Boundary conditions implied by the case study site

The choice of far-field and near-field models has been elaborated on in section 2.10. The position of modeling in the total research is pictured in figure 3.1. Spatial division of the models is pictured in figure 2.11.

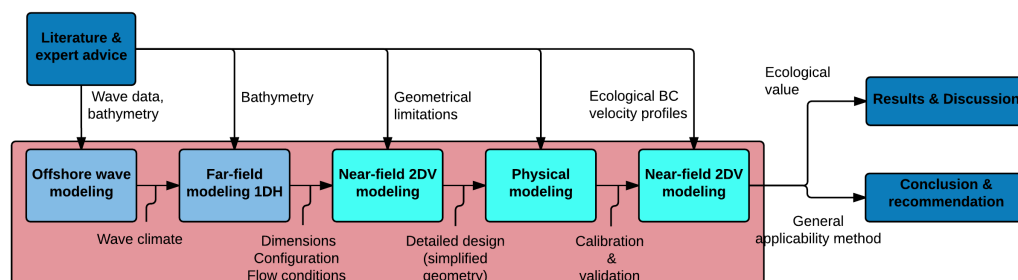


Figure 3.1: Place of modeling within research (red)

The goal of this modeling train is to get detailed insight in the behavior of an artificial reef, on the meso / near-field scale. By developing this model train, offshore wave data will eventually be translated to a detailed hydrodynamic model that can accurately solve wave attenuation (expressed by transmission coefficient C_t) and velocity patterns (ecological boundary u_{max}) simultaneously. This tool can then be assessed to be generally applicable. If so, it could provide to be a very valuable way of assessing ecological functioning of an underwater structure.

First the offshore wave data will be translated to input for the XBeach far-field model. This is done using shallow water waves model SWAN. The output of SWAN is still in spectral format, therefore an Extreme value analysis is carried out to extract one monochromatic wave condition. This is fed into XBeach, which translates the waves to the nearshore. In XBeach, an assessment is made for the location of the reef. This is judged by looking at wave attenuation per square meter structure. Then the first translation to near-field model SWASH is made, in order to determine the geometry of the structure that will be used in the physical model. The setup of the physical model is elaborated on. Here, a lot of practical issues have to be solved and design assumptions are made. The setup of the flume is subsequently modeled in SWASH, the obtained dataset is used to calibrate the SWASH model. The calibration process is worked out later in this chapter.

3.1. Offshore wave modeling

In order to translate offshore wave conditions to a near-shore significant wave, a series of steps has to be made. First input data will be gathered, by means of wave and bathymetric data. Second, a SWAN wave model is set up to translate the offshore wave conditions to a location that is suitable for further modeling. Lastly, the obtained wave data will undergo statistical analysis to end up with one significant wave condition, that will be used for further modeling.

Detailed offshore wave and wind climates and near-shore wave climate were gathered. The offshore wave data is obtained 25 km from the coast, where the depth is 500+ m.

3.1.1. Input SWAN model

Offshore wave climate A met/ocean (Meteorology/Ocean) database that is available within Boskalis which contains wave data on offshore locations worldwide. The nearest location at the case study site is located at 42° N 11° 50'E. This location is indicated in 3.2. The database consists of wave and wind information every 6 hours, from 1997 to 2013.

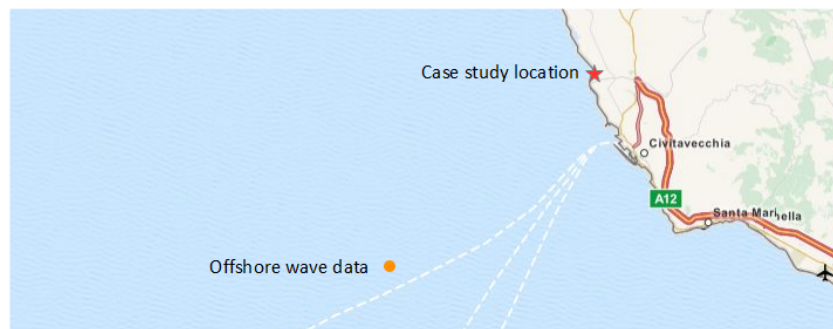


Figure 3.2: Location of wave data from met/ocean database, *caption from Boskalis.world at 06/08/2015*

Wave roses for this location can be found in Appendix B.

Bathymetry As can be seen in figure 3.3 the seabed around the site has a very gentle slope. The 5m contour line lies approximately 230 meters away from the coastline [40].

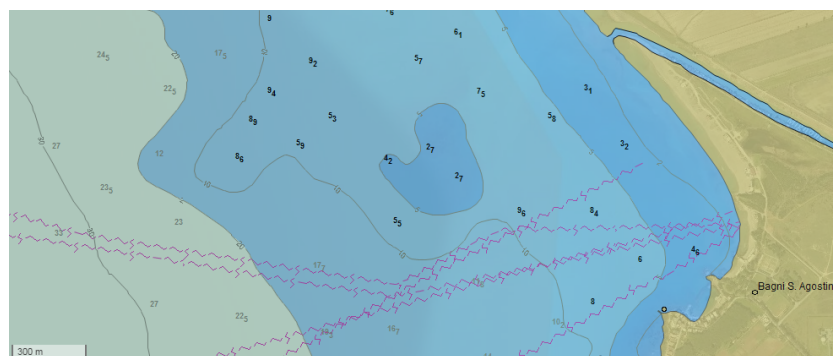


Figure 3.3: Bathymetry in the vicinity of the case site [40]

To have accurate wave calculations from deep to shallow water, the bathymetry is input for the wave model. The depth contours up to -500 m were digitalized from admiralty charts 1911 (Isola del Giglio to Isola d'Ischia) and 1999 (Livorno to Civitavecchia including Northern Corse) from the United Kingdom Geographic office [63], using GIS software. The resulting bathymetry used in the wave model is plotted in figure 3.4. Total length of the digitalized coastline is approximately 400 km. This is done to ensure total coverage of the 2DH SWAN model. In addition this provides the opportunity to show that the Italian west coast shows similar bathymetry for a large stretch of the coastline. Therefore analysis in this research can be considered to be more broadly applicable than just this particular site.

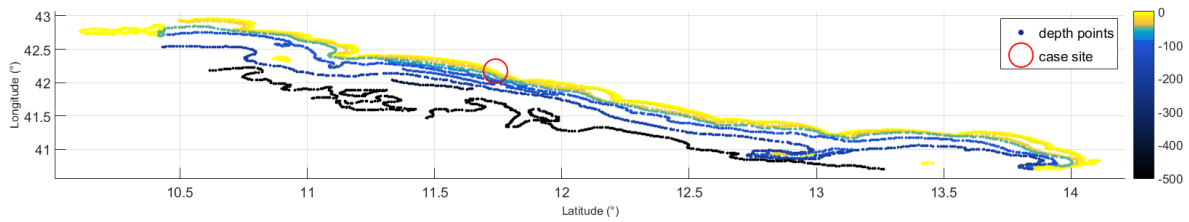


Figure 3.4: Bathymetry in vicinity of the case site, the red circle is the location of the case study site and colors indicate depth. Length of coastline is approx. 400 km

Sediment properties Sea bed specifications for the occurring sediment in the vicinity of the case site is available through samples taken in Civitavecchia, Italy, approximately 20 km from the case study site. The properties of the sediment are not considered in this research, therefore it is not elaborated on here either.

Scour and subsoil stability are not taken into account

3.1.2. Output SWAN model

In order to be able to use the offshore data for further hydrodynamic modeling, the wave conditions have to be translated to nearshore conditions. Output locations for nearshore wave data will have to be chosen carefully, close to the case study location but far enough to be outside the zone where waves start to deform and break, since this is not accounted for in SWAN. Setup for the Worldwaves model is discussed in Appendix B.

For the far-field model XBeach output point 6 will be used, which will serve as boundary condition for the far field numerical model, see figure 3.5. Point 6 for output was chosen from a set of output points, that were defined for SWAN to generate wave conditions. When SWAN was set up it was not decided if the near field model would be 2D or 3D. Therefore multiple output points were defined. Point 6 lies on a perpendicular line to shore, with a monotone sloping bottom. Therefore this point was chosen for output for the 1DH XBeach model.



Figure 3.5: SWAN output point for nearshore wave data

3.1.3. Design conditions 1/1000 year

For the data points indicated in figure 3.5 in the calculated near shore environment, a probabilistic analysis is carried out. The Peak over Threshold (PoT) method will be used to extrapolate the data set to a 1/1000 year significant wave H_s and its accompanying wave period T_p . Extreme value analysis (EVA) is performed, the results can be found in table 3.1. Elaboration on these results is found in Appendix B.

Table 3.1: Peak over Threshold results for location 6

Location	Depth (m)	$H_s(1/1000)$ (m)	$T_p(1/1000)$ (s)	R^2
6	32.5	7.4	13.3	0.994

The wave climate is strongly simplified to a stationary situation, with the analyzed $H_s = 7.4m$ and $T_p = 13.3s$ from location 6, with a 1/1000 yr probability of occurrence.

Xbeach input is not H_s and T_p , but H_{rms} and T_{m0} . The relation between H_{rms} and H_s is given in equation 3.1. Since this is considered a very narrow spectrum (stationary waves) it can be assumed that $T_{m0} \approx T_p = 13.3 s$ [70].

$$H_s \approx \sqrt{2}H_{rms} \quad (3.1)$$

Which gives $H_{rms} = 5.23m$.

3.2. Far-field modeling

3.2.1. Work sequence

First the boundary conditions of the simplified situation that will be modeled have to be established. The wave condition is derived from the extreme value analysis in the preceding section.

Secondly a parameter that can be used to assess the performance was defined. Wave damping will be expressed as wave transmission, which is quantified using the transmission coefficient $C_t = \frac{H_t}{H_i}$, as in equation 3.3.

The base case, without a structure, will be modeled, preparing settings that are numerically stable and resembling the required system's processes and amount of detail. The orientation and size of the AR is modeled, in several scenarios. The AR is simplified to the envelop that surrounds the unit, see section 3.2.2. To make up for the irregular shape a certain porosity and roughness could be added to the rectangular shape.

The optimal location then is assessed and carried on with in further modeling.

3.2.2. Model setup

Parameters that have been set to meet this models specific requirements are elaborated on in this section. The other parameters are ran in default mode.

Water depth LCS are applied in shallow water. At small depths the structure can interact with the waves to ensure damping, without having to use excessive amounts of material. The range at which they are applied lies generally between 5 and 2 meters, depending on the specific coastal and hydrodynamic conditions [33].

The wave-boundary conditions (as discussed in section 3.1.3) are applied on a depth of 32 m. The domain considered is depicted in 3.6. This bathymetry is based on the nearshore profile found in the Admiralty charts, see figure 3.4.

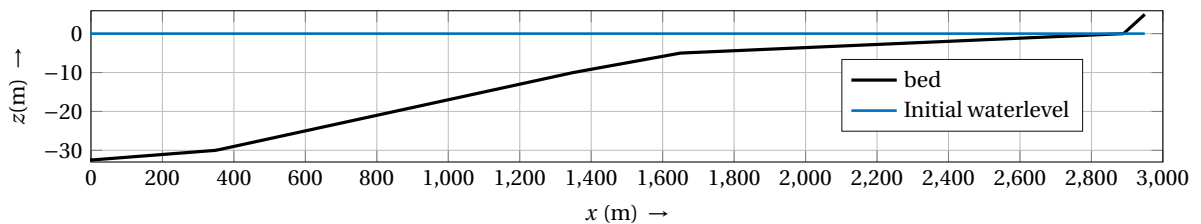


Figure 3.6: Bottom profile based on case study S't Agostino

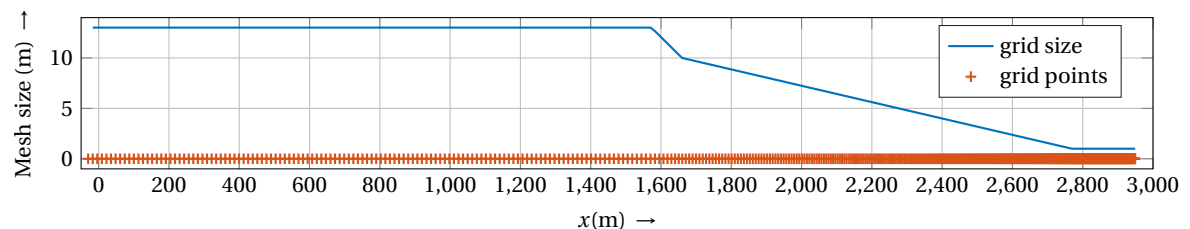


Figure 3.7: Interpolated grid spacing and depth, number of grid cells = 597

Grid setup The grid is set up to have ample detail where the structure will be embedded in the bathymetry. In order to limit computational time the grid spacing is interpolated from the offshore side of the bathymetry. This is shown in figure 3.7. The interpolation is necessary in order to stay within limits of the CFL (Courant, Friedrichs, Lewy) condition, see equation 3.2 [62].

$$C = \frac{u\Delta t}{\Delta x} < 1 \quad (3.2)$$

With C is the Courant number, u is velocity, Δt is time step and Δx is mesh size. XBeach automatically adjusts the time step to fulfill the CFL condition, but this functionality can not cope with instant large changes in Δx .

Geometry structure It is assumed that the individual reef units are applied in a staggered grid, so that they together form a reef-like field, as described in section 2.7. This is to create a sufficiently large length scale to interact with relevant wave lengths. In the cross-shore plane, the circumference of this grid of structures is from here on referenced to as 'structure envelope', or in short 'envelope'. This is explained in figure 3.9.

A set of 10 envelopes is evaluated, see figure 3.8. This is to get a first understanding of the behavior of waves and currents over and around various geometry. Obviously, this envelope overestimates the area of the structure by factor 2. Therefore the quantitative results will not be representative, but are considered a valid comparison parameter between the reef envelopes.

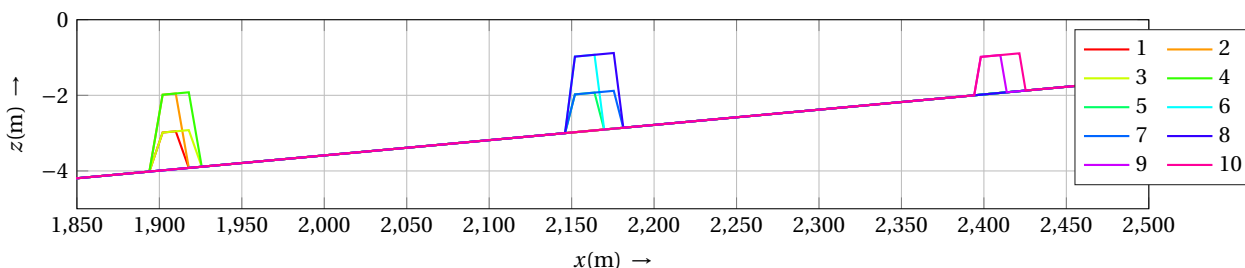


Figure 3.8: 10 reef envelopes analyzed in XBeach

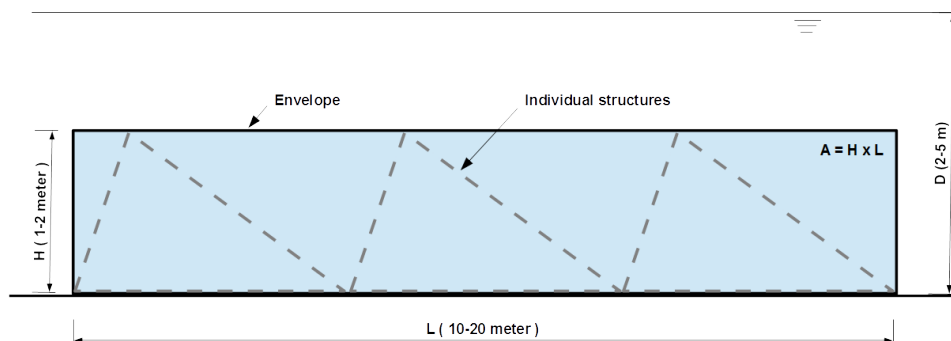


Figure 3.9: Concept of 'structure envelope' with relevant dimensions

Wave conditions The XBeach computations transform the deep water waves that were calculated in the EVA to near field shallow water wave conditions. These will be used as input for the near field simulations in SWASH as well as input for the wave paddle in the Hydraulics lab.

A matrix of wave heights and periods is developed, creating six wave condition scenarios. The wave heights are 25 percent above and below the Hrms from the Extreme Value analysis, and next to the Tp (1/1000) of 13.3 seconds, a second shorter period is analyzed, of 8 seconds. From the results of the extreme value analysis it can be concluded that this is the approximate mean value for Tp. The 6 wave conditions are summed up in table 3.2.

These scenarios are analyzed in XBeach stationary mode, output that is recorded is wave height at the boundary of the physical testing area and wave set-up. Results can be found in chapter 4.

Table 3.2: Wave condition scenarios in deep water

Hydrodynamic settings There are three options for wave resolving in XBeach:

- Stationary
- Surfbeat (in-stationary)
- Non hydrostatic

H_{rms} (m)	T_p (s)	
	8	13.3
4	1	2
5.23	3	4
6.6	5	6

In stationary mode wave propagation, directional spreading, shoaling, refraction, bottom dissipation, wave breaking and roller dissipation are included, but the wave groups (long waves) and infra-gravity motions are

neglected [36]. This mode is suitable for moderate wave conditions, with small incidence of waves. It is less computationally expensive than the other two options, but it does not solve for long waves, which are important in the coastal erosion process [62]. However, these are not included in this research but will be a recommendation to integrate in the analysis in a later stage. Specifics of the stationary mode and the other two modes are described in the Xbeach Manual, Hoonhout [36].

3.2.3. Critical parameters

The performance of each scenario is judged by two features, being wave transmission and area of cross section (minimize material use).

Wave transmission is calculated using equation 3.3[62]. This has been elaborated on in section 2.5.

$$C_t = \frac{H_t}{H_i} \quad (3.3)$$

with

- C_t = transmission coefficient
- H_i = Incoming wave height, in front of offshore toe of structure
- H_t = Transmitted wave height, < 5 meters behind structure

In order to get here, time series of wave height will be analyzed in the grid points before and after the structure envelopes. This is indicated in figure 3.10.

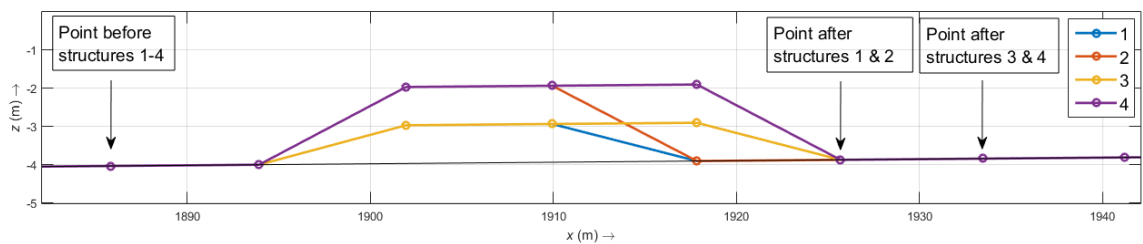


Figure 3.10: Example of points for which wave height is analyzed (zoom of structure envelopes 1-4)

The area of the structure is used as indication of the amount of material used in the reef. Because 3D printing material is very costly, much more than alternative building materials like rock or concrete, it is of additional importance to minimize the cross section of the structure.

The cross sectional areas of the 10 reef envelopes in figure 3.8 are summed up in table 3.3.

3.2.4. Intermediate results

The reef envelope that performed most favorable looking at the combination of wave damping and used material (= cross sectional area) is structure 9. This means the depth at which the structure is installed will be approximately 2 meter, with a height of 1 meter and a length of 10 meters. The wave height that is extracted from the xbeach results at the depth of 2.2 meter is $H_s=0.7$ m and a period of 13.3 s. This is elaborated on in chapter 4. These values will be used for the near field model.

Table 3.3: Dimensions of 10 reef envelopes

Reef envelope	H (m)	L(m)	A (m ²)
1	1	10	10
2	2	10	20
3	1	20	20
4	2	20	40
5	1	10	10
6	2	10	20
7	1	20	20
8	2	20	40
9	1	10	10
10	1	20	20

3.3. Near-field modeling 1 - Design of laboratory setup

3.3.1. Work sequence

For this analysis the SWASH model is used, a hydrodynamic model that solves in 2DV and the full wave motion (phase resolving). First a translation of the far-field XBeach model to the near-field SWASH model will be

made by means of bathymetry and wave boundary conditions. A more detailed assessment of the AR shape and its influence on wave attenuation and velocity profiles will be made.

This will give an approximation of the desired unit geometry, in the 2DV plane. This will be used as input for a physical model.

3.3.2. Model setup

Bathymetry The SWASH domain covers a small part of the XBeach domain, as indicated in figure 3.11. Results from the far field analysis determined depth at which the structure has to be placed is two meter (see 3.2.4).

The domain that is modeled in swash has to agree with the dimensions of the flume, in the scale model. The scale is decided to be 1:6, therefore the maximum length of the swash domain is 32 m (effective flume length) $\times 6 = 192$ m. It is shown in 3.12. In consultation with SWASH expert M. Zijlema it was determined that the structure should be placed on two thirds of the computational domain, to rule out boundary effects from the offshore boundary affecting the structure.

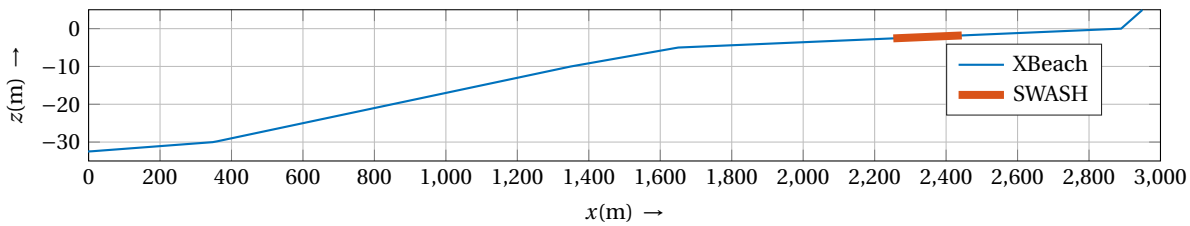


Figure 3.11: XBeach and SWASH domains

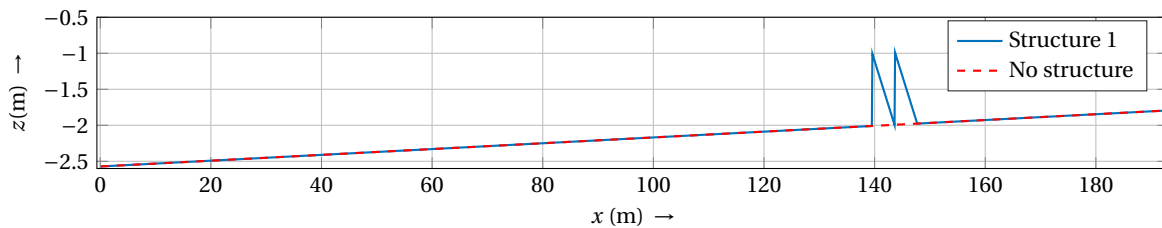


Figure 3.12: Zoom of domain considered in SWASH and physical tests

roughness of structure The spatially varying roughness of the structure and bed is expressed using Manning's roughness coefficient [62].

For the bed the roughness is approximated by a Mannings coefficient of $n = 0.02$, which is common for a sandy smooth bottom. Since manning roughness for the AR type structure is not defined, it will be approximated. The formula to compute Mannings roughness coefficient for non-standard structures is defined by equation 3.4, the values for the factors are given in table 3.4.

$$n = (n_0 + n_1 + n_2 + n_3 + n_4)m_5 \quad (3.4)$$

The approximation of the structures roughness coefficient is $n = 0.0675 \pm 0.0025 \approx 0.07 \text{ s/m}^{1/3}$. This manning friction is transformed to the dimensionless friction factor c_f by equation 3.5 from Hoonhout [36].

$$c_f = \sqrt{\frac{gn^2}{h^{1/12}}} \quad (3.5)$$

Since waterdepth $h = 2.2 \text{ m}$ is constant, $c_f = 0.21$.

Wave conditions

For this SWASH model setup the wave condition used was limited to the significant wave condition deducted from XBeach results, being $H_s = 0.7 \text{ m}$, and $T_p = 13.3 \text{ s}$.

Table 3.4: Values for factors in Mannings roughness coefficient

Channel conditions		Components of n	
Material involved	Earth	n_0	0.020
	Rock cut		0.025
	Fine gravel		0.024
	Coarse gravel		0.028
Degree of irregularity	Smooth	n_1	0.000
	Minor		0.005
	Moderate		0.010
	Severe		0.020
Variations of channel cross section	Gradual	n_2	0.000
	Alternating occasionally		0.005
	Alternating frequently		0.010-0.015
relative effect of obstructions	Negligible	n_3	0.000
	Minor		0.010-0.015
	Appreciable		0.020-0.030
	Severe		0.040-0.060
Vegetation	Low	n_4	0.005- 0.010
	Medium		0.010-0.025
	High		0.025-0.050
	Very high		0.050-0.100
Degree of meandering	Minor	m_5	1.000
	Appreciable		1.150
	Severe		1.300

Reef geometry The reef envelope that was selected in the far field computations has dimensions $L \times H = 10 \times 1$ meter, at a depth of 2 meters. Therefore structure height is set to 1 meter. Assumed in chapter 2 is that area cross sectional area should stay under $2m^2$. In further analysis focus will lie on the velocities around the structure rather than wave attenuation. This is because wave attenuation of submerged structures has been modeled a lot already, while velocities have not received quite so much attention in literature. Therefore, and in order to limit resources used in the physical testing setup, from here on only two reef units will be modeled. It was chosen to use two since this does create the interaction of reflection flow from the second unit with the first unit. Also it is assumed that successive reef units will encounter milder velocities due to dissipation of wave energy over the first units.

In SWASH a quick assessment is made to value the influence of the shape of the 2DV structure on wave attenuation, for four different geometries, see figure 3.13.

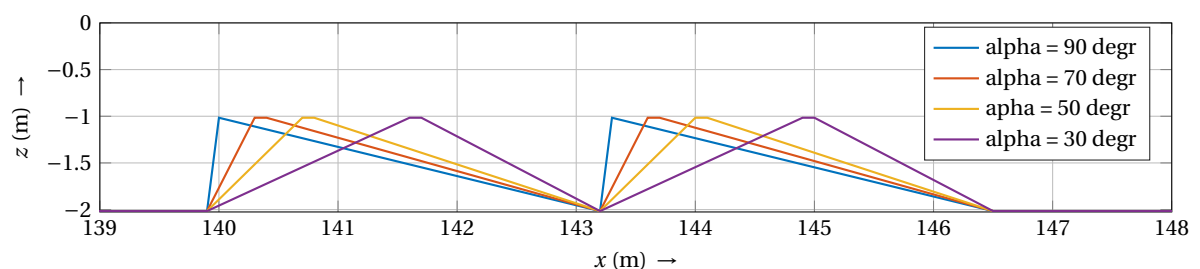


Figure 3.13: 4 structures analyzed for varying angle of structure face

3.3.3. Intermediate results

Critical parameters assessed in this short analysis are wave transmission and maximum velocity above the first structure. Because this analysis is meant to generate design input for the physical model, the most important results will be stated here.

Wave transmission In figure 3.14 the influence of structures 1-4 on the water level fluctuation is plotted. As can be seen the water level shows some deformation of the monochromatic wave signal, but this is almost

identical for all 4 structures.

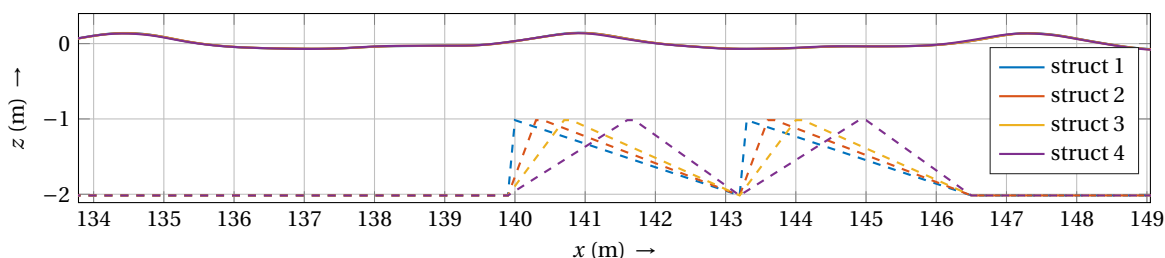


Figure 3.14: Influence on structures 1-4 on water level is negligible

The influence on wave-height of the angle of these structures was negligible, so none of these geometries could be ruled out based on wave attenuation.

Maximum velocity The maximum velocities over depth for the middle of the structures on the lee side has been evaluated, this is shown in 3.15. The velocities for different structures does not show significant amplification or attenuation of flow velocity. In later analysis with the SWASH model these type of velocity structures will be evaluated more in depth.

Because both velocity and wave attenuation did not give conclusive results on the preferred geometry of the structure, a judgment call is made that a larger area on the lee side is preferred for habitat creation, while not having a vertical plane on the sea ward side, to limit scour and reflection.

Therefore structure number 3, with an angle of 50 degrees on the sea side and approximately 30 degrees on the lee side is selected.

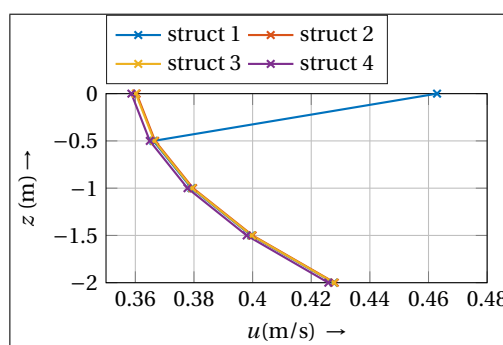


Figure 3.15: Maximum velocity profile for 4 structures, in 5 sigma layers

3.4. Physical modeling

The physical model is an essential element in this methodology, as also depicted in figure 1.5.

This laboratory measurement campaign consists of simplified Artificial reef (AR) units with a porous upper layer (see section 3.4.3), which is designed for the environment of the gentle sloping, Mediterranean near-shore environment.

NOTE: From the start of the physical tests it became clear that mechanical limitations of the wave paddle caused the selected wave conditions to be out of bounds. therefore it was decided to go to deeper water but within the range of the considered scenarios in XBeach, shown in 3.8. Depths are now 3.18 and 3.50 meters, compared to 2.0 and 2.2 as first proposed, in 4.2. This adjustment is elaborated on in section 3.4.2.

3.4.1. General concerns

Foreshore modeling of the bathymetry can be ignored if all of the following conditions are fulfilled, following Frostick et al. [26]:

- $\tan\alpha < 1:250 - 1:1000$
- $h/L_0 > 0.045$
- $H_s/h < 0.3$

These conditions are applicable to geometry considered, thus no bathymetry will be included in the physical tests.

Scaling Since the measurements can not be conducted in the field, they will be scaled down in order to fit the flume at the hydraulic laboratory. Following the Users Guide to Physical modeling and experimentation, [26], for this research Froude scaling will be applied.

The Froude criterion is a parameter that expresses the influences of gravity and inertia in a hydraulic environment, i.e. the relationship between inertia acting on a fluid particle and the weight of the particle. The Froud scaling rules are given by equation 3.6.

$$\sqrt{\frac{\text{Inertial forces}}{\text{gravity force}}} = \sqrt{\frac{\rho L^2 V^2}{\rho L^3 g}} = \frac{V}{\sqrt{gL}} \quad (3.6)$$

Froude scaling means the Froud number is to be equal in model scale and prototype scale, resembled in equation 3.7. The scale ratios, which form the Froude model criterion is given in 3.8.

$$\left(\frac{V}{\sqrt{gL}}\right)_\rho = \left(\frac{V}{\sqrt{gL}}\right)_M \quad (3.7)$$

$$\frac{N_v}{\sqrt{N_g N_L}} = 1, N_T = \sqrt{\frac{N_L}{N_g}} \quad (3.8)$$

Froude scaling ensures that gravity forces are correctly scaled. Since surface waves are gravity driven, it will enforce that wave resistance and other forces are correctly translated. The following typically used scaling relationships for the Froude law can be derived, in terms of the length scale factor n_L , see table 3.5.

Table 3.5: Froude scaling laws

Wave height (m)	$n_H = n_L$
Time (s)	$n_T = n_L^{0.5}$
Velocity (m/s)	$n_u = n_L^{0.5}$
Acceleration (m/s ²)	$n_a = 1$
Mass (kg)	$n_M = n_\rho * n_L^3$
Pressure(kN/m ²)	$n_P = n_\rho * n_L$
Force (kN)	$n_F = n_\rho * n_L^3$
Discharge (l/s/m)	$n_q = n_L^{1.5}$

In similar testing with regard to rubble mound breakwaters, the difference in density of salt and fresh water are accounted for by preserving the value of a 'stability parameter', between prototype and model. Most of the time this results in a higher weight of the armour. In this research this will not be considered, since the 'armour' is glued to the structure and stability is therefore not a concern.

The scale ratio has to be as small as possible, in order to limit scaling effects. Because earlier research (Kolijn [44]) experience showed to have difficulties generating certain wave climates with the same flume and wave paddle, using scale 1:5, the scale ratio for this physical experiment is 1:6, or N=6.

3.4.2. Hydrodynamic input

Wave conditions As can be seen from table 4.1 in chapter 4, actually only two distinct wave conditions can be identified. Especially seen the degree of accuracy that can be reached in the flume, it was decided to define two wave conditions from the above table. Governing parameter that determines wave height and setup is obviously the wave period. The two scenario's with highest setup are selected, being Scenario 5 and 6 from table 4.1.

For calibration purposes two more wave climates are generated, namely the wave height for the '0 meter-setup' for the same wave periods, 8 and 13.3 seconds. These wave heights are extracted from the same XBeach runs as scenario 5 and 6, but at the position where the water depth (including setup) is 2 meters.

For validation purposes two more wave periods will be analyzed, assuming that this again will return the highest possible wave height for this period. In order to maintain similarity to the dataset created by Danker Kolijn [44], the wave periods are chosen so that they are within the range of periods used in Kolijn's dataset. These are 6 and 10 seconds. These six wave conditions are summed up in table 3.6.

Table 3.6: Monochromatic wave conditions used in this physical measurement campaign

Wave condition	Prototype conditions			Scaled conditions			Comments
	H (m)	T (s)	WL (m)	H (m)	T (s)	WL (m)	
1	0.58	8.00	2.27	0.10	3.27	0.38	max setup T=8
2	0.72	13.30	2.56	0.12	5.43	0.43	max setup T=13.3
3	0.52	8.00	2.00	0.09	3.27	0.33	no setup T=8
4	0.58	13.30	2.00	0.10	5.43	0.33	no setup T=13.3
5	0.48	6.00	2.00	0.08	2.45	0.33	T=6
6	0.54	10.00	2.00	0.09	4.08	0.33	T=10

NOTE: As will become clear in the next section, these wave conditions are re-defined and wave conditions in table 3.7 are used. It is however considered valuable to keep the argumentation on the original wave climates considered in this report for documenting purposes.

Wave paddle input Wave input will be generated using the Delft/AUKE software. The wave theory used in the conversion from wave parameters to paddle input is second order stokes theory. This has proven to be a flaw in the design of this research, since the wave conditions selected by numerical modeling as described in 3.2, summed up in table 3.6, are not within the limits of second order stokes wave theory. The limits of this theory and the proposed wave climates are plotted in 3.16a.

It was not attempted to eliminate the software limitations, since scheduled time at the laboratory was limited. A new set of wave conditions was proposed, as mentioned in the introduction of this chapter. The new wave conditions are stated in table 3.7, these are within the limits of the second order Stokes waves (see figure 3.16b), well spread amongst the theories' domain and within the range of XBeach and SWASH computations that have preceded the physical testing.

Table 3.7: New wave conditions

Wave condition	Prototype conditions			Scaled conditions		
	H (m)	T (s)	WL (m)	H (m)	T (s)	WL (m)
1	0.18	13.3	3.5	0.03	5.43	0.58
2	0.48	8.00	3.50	0.08	3.27	0.58
3	0.30	10.00	3.50	0.05	4.08	0.58
4	0.72	6.00	3.18	0.12	2.45	0.53
5	0.72	4.00	3.18	0.12	1.63	0.53

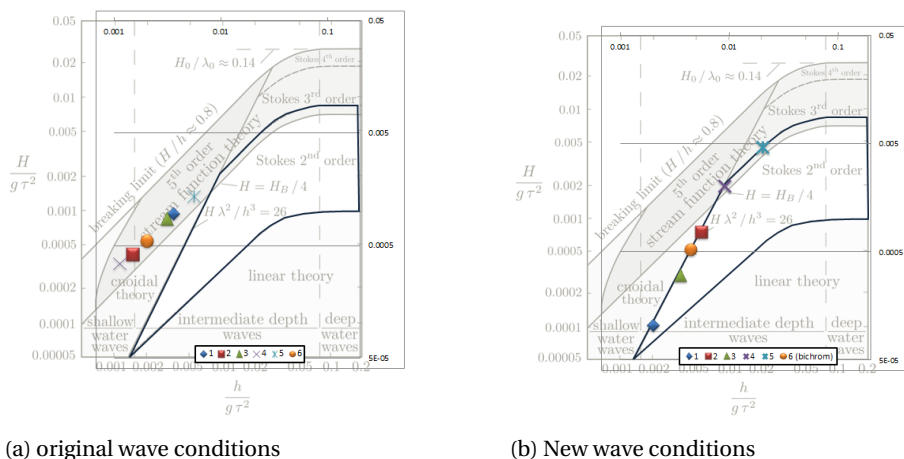


Figure 3.16: Change in wave conditions plotted against wave theories (Le Mehaute ([23]))

Water depth The wave conditions are tested for 2 different depths in total. The water level was adjusted to 3.18 and 3.5 meter above the bed, in order to eliminate paddle difficulties.

The water-levels are summed up in table 3.7.

3.4.3. AR scale model

General concerns Since the 3D printed units are expected to have a solid core, the core is considered impermeable. To resemble the ecologically motivated design with its cavities and pores, as can be seen in the Monaco pilot project design (see figure 2.7) a porous media is added that is assumed to impose comparable roughness and therefore damping behavior. This is described in the section 'Porous layer'.

In SWASH an assessment was made on the dimensions of the reef, considering the limitations on its geometry stated in section 3.2.2. Since the flume experiment is not focused on wave attenuation but on the velocity structure in combination with combining ecological habitat, structure 3 (see figure 3.13) is chosen

to be modeled, based on gentler slope on the front, while preserving enough surface space on the lee side to potentially develop habitat. The construction method is elaborated on in the next two sections.

Porous layer The surface of a reef is expected to provide habitat to various species, as defined in chapter 2. In order to do so, interstitial space (cavities) are very valuable (see also the research of Buijs [12]). Furthermore, when looking at the wave damping function of an LCS, a rough structure is much more efficient in dissipating energy than a smooth surface. The 3D printed prototype (as can be observed on the cover page of this report) consists of various types and dimensions of habitat. The habitat element that will be simulated in this experiment is interstitial space. This is created by gluing rock to a frame, to create pores in between the rock that have a meaningful geometry for ecology.

Ecological length-scale Fish species that are targeted in this simplified design is the juvenile sea bream, or Dorade. For more information on the species see section 2.3.2. Since no preference of pore size relative to the Sea Bream fish size has been established, the assumption is made (following the thesis assumption of Wieger Buijs, [12]) that median pore diameter (D_{p50}) is equal to the upper limit of the fish size, so 0.2 m.

Translation to rock size distribution A method has to be found that can ascribe meaningful physical properties to the ecological length scale and 3D printed surface described above. In the 3D printing technique, the porous surface of the structure can be adjusted to whatever vertical and horizontal variations desirable. This will provide an optimal habitat customized to its proposed environment. Downside is that up until now, there are no known hydrodynamic properties assigned to this type of surface, making it impossible to model. Therefore two assumptions are made:

1. the surface has a uniform pore distribution over the full structure
2. translated to a known porous medium, which is scalable and can be modeled with adequate accuracy

In his thesis, Wieger Buijs has developed a relation between grading curves of rock classes and their pore size distribution. Since this allows integration of ecological length scale and on top of that gives a scalable outcome (stone size distribution) this method is used to determine the rock class, that will cover the surface of the structure.

The pore size distribution (f) as described in Buijs [12] follows from 3.9.

$$f(x, P_{80}, m, F) = 1 - e^{\ln(0.2) * (\frac{x-F}{P_{80}})^m} \quad (3.9)$$

with:

$$P_{80} = (-2.13 * \Phi * \frac{D85}{D15} + 13.2) * \frac{D50}{25} \quad (3.10)$$

$$m = (-0.533 * \Phi * \frac{D85}{D15} + 2.29) \quad (3.11)$$

$$F = (27.5 * \Phi - 3.35) * \frac{D50}{25} \quad (3.12)$$

where the parameters are:

- P_{80} = Slope coefficient Rosin Rammler [-]
- m = Shape coefficient of Rosin Rammler [-]
- F = Coefficient of Rosin Rammler [-]

These dimensionless factors give expression to the particle size and shape distribution [12]. By iteration of above formulas, using a narrow grading with $D85/D15=1.5$, the following pore size distribution curve, resembled by f , was established as shown in figure 3.17.

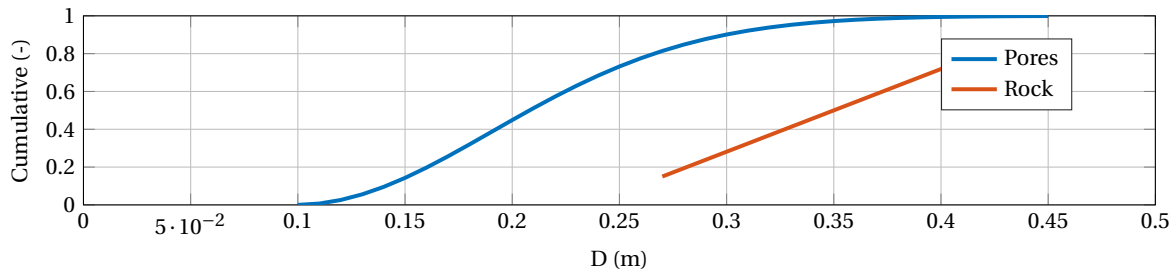


Figure 3.17: Pore and rock size distribution, with a median pore size of 20 cm

The rock D_{n50} that will be applied in the physical testing are geometrically scaled in table 3.9.

$$D_{n50} = 0.84D_{50} \tag{3.13}$$

Table 3.8: Rock grading in accordance to a median pore-size of 0.2 meter

Distribution (%)	Size (m)
D15	0.27
D50	0.35
D85	0.43

Thickness of rock layer In armour layer calculations the thickness is $2 * k_t * D_{N50}$ for random placed stones [62]. k_t depends on the packing density, which is in turn dependent on the rock shape, amount of layers, placement, and the survey method (highest point vs. spherical foot staff). The assumed properties of the rock used are;

- Layer and placement type: Double standard
- Survey method: Highest point survey method
- Blockiness: Blocky rock, so $BL_c = 0.65$

This gives a k_t factor of 0.96. This is rounded to 1, so thickness of the layer is $2D_{N50}$.

Rock specification In order to model the 3D printed surface rock will be glued to the metal frame. The rock specifications were only evaluated for dimensions, specific weight does not play a role since it will be glued. Also an effort was made to select a rock type that has the most uniform roughness. This led to the selection of a split type rock over natural pebbles. The rock-class that was used is specified as 'Basalt split 40 - 75 mm', which encloses the desired rock diameter as described in table 3.9, being 58 mm. The specific weight is assumed to be $\rho = 3011 \text{ kg/m}^3$.

Table 3.9: Scaled rock grading characteristics

	D (m)	D_n (m)	M (kg)
15%	0.045	0.038	0.143
50%	0.058	0.049	0.312
85%	0.072	0.060	0.578

The smallest segment was removed, partly by the sieve it was washed in (sieve size approximately 30 mm), partly by hand, pictured in figure 3.18a.

After this a sample of approximately 25% of the batch was analyzed by means of a grading test. In this test 156 samples were weighed. The cumulative mass distribution is shown in 3.19a, the mean and nominal diameter are pictured in 3.20.



(a) Smallest rocks removed



(b) Sample to be analyzed

Figure 3.18: Rock sample handling

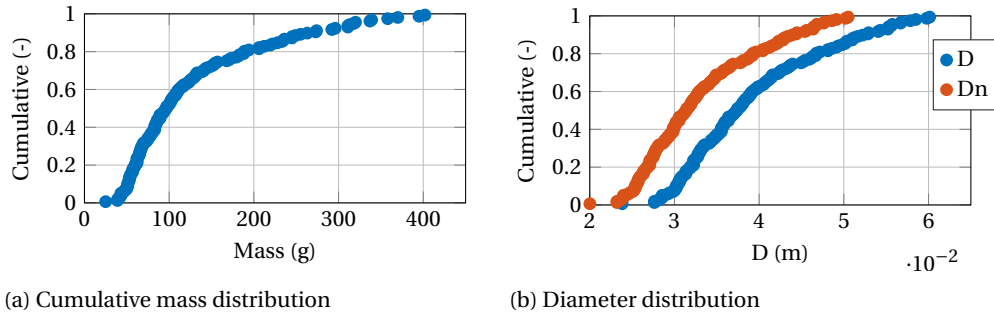


Figure 3.19: Characteristics of rock sample (N=156)

Table 3.10: Rock grading characteristics

Percentile	D (m)	Dn (m)	M (kg)
15%	0.031	0.026	0.055
50%	0.038	0.032	0.097
85%	0.05	0.042	0.228

The distribution of resulting rock size deviates from the desired size, the actual grading table determined by the grading test is given in table 3.10. This is translated to prototype-scale rock size and pore distribution, figure 3.20 shows the results.

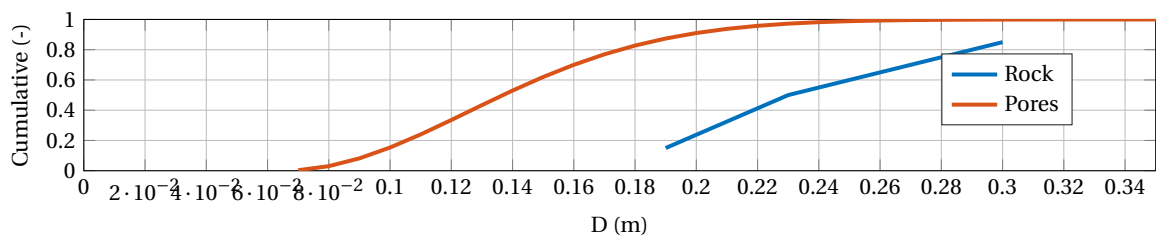


Figure 3.20: Pore size distribution prototype scale

The prototype median pore size is unintentionally reduced from the required 20 cm to 14 cm. The grading test data for these calculations can be found in appendix D.

Table 3.11: Rock grading according to grading test - Prototype scale

Distribution (%)	Size (m)
D15	0.19
D50	0.23
D85	0.30

Reef unit dimensions The outer boundaries of the reef structures, so enclosing the layer of rock, should match dimensions of structure 3 in 3.13. The thickness of the rock layer ($2 \cdot Dn_{50} = 7$ cm) is subtracted from the outer dimensions. This gives the dimensions of the impermeable core, which is constructed from steel plating. See figure 3.21 for the exact dimensions.

3.4.4. Laboratory setup

This section outlines the physical modeling procedure. The features of the facility that will be used are described, the measurements are stated with their relations to the objectives of this study and finally a schedule for the measurements is suggested.

Facility The testing was done in the Fluid Mechanics laboratory at the DUT. The flume used is the largest wave flume available, pictured in 3.22. This is done so scaling discrepancies between dimensions and fluid viscosity are limited. The scaling procedure is already touched upon in 3.4.1.

The flume is 38 meters long, with an effective length of 32 meters.

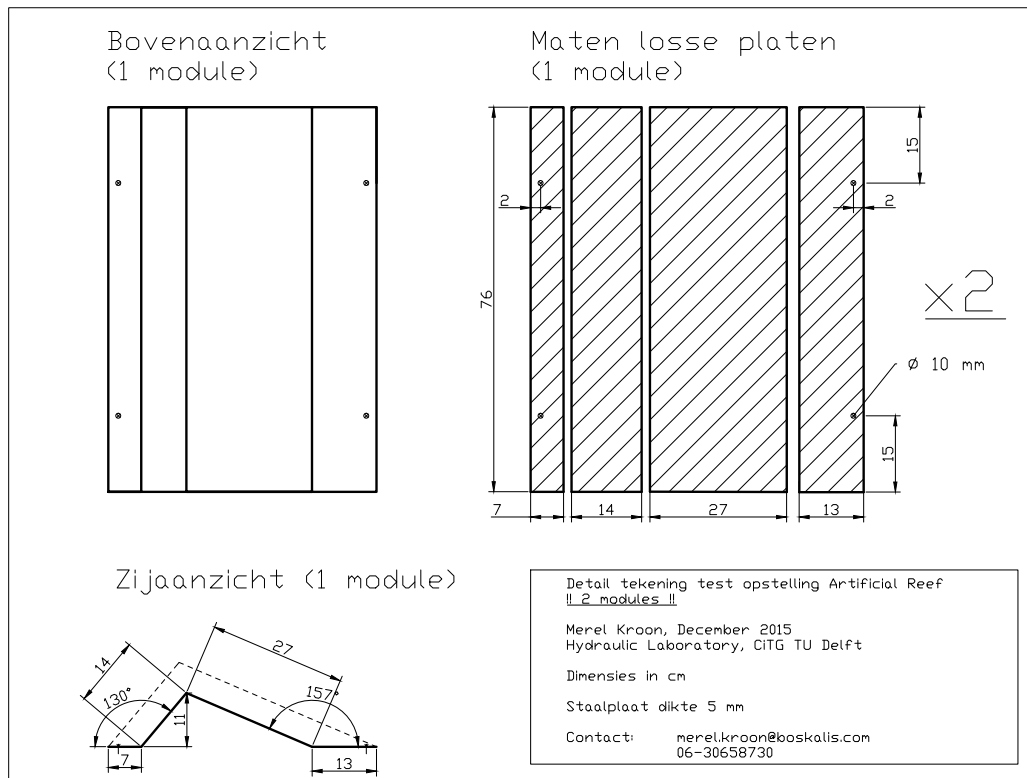


Figure 3.21: Geometry of steel frame (dimensions in cm)

The flume is equipped with a wave paddle, which is powered by a hydraulic system and controlled digitally. The software that defines wave paddle movement is programmed with second order Stokes wave theory, as mentioned before. Furthermore it is calculated using a simple mass balance: The water depth and required wave height and period have to be defined. Subsequently the Delft/AUKE program calculates the required movement of the paddle to generate the required mass to be moved at what pace.

At the end of the flume, the last six meters, a wave damper is installed. This consists of a rock layer with ascending height. This damper was already present in the flume, dimensions were optimized for earlier experiments. The average reflection of waves, that was thus not damped but reflected by the damper, was said to be 10 percent. This has to be validated by calculating reflection for these particular wave conditions. The method to do so is discussed in appendix F, and will be used in chapter 4 to calculate both flume and structure induced reflection.

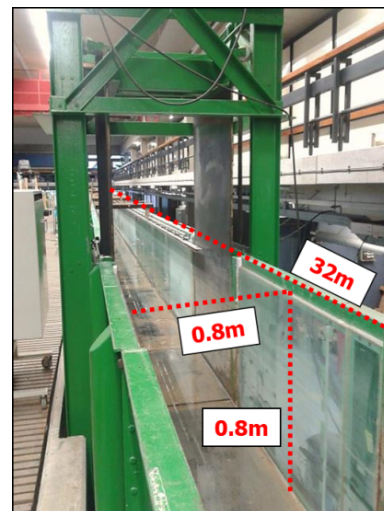


Figure 3.22: Flume dimensions (Picture(44))

Flume setup In the plan below the flume setup is pictured in figure 3.23. The structure is placed in the middle of the flume. This is to give the waves coming from the paddle enough room to develop, while keeping distance from the damper to minimize reflection effects on measured time series. In figure 3.24 the reef structures in the flume, before and after filling the flume are shown.

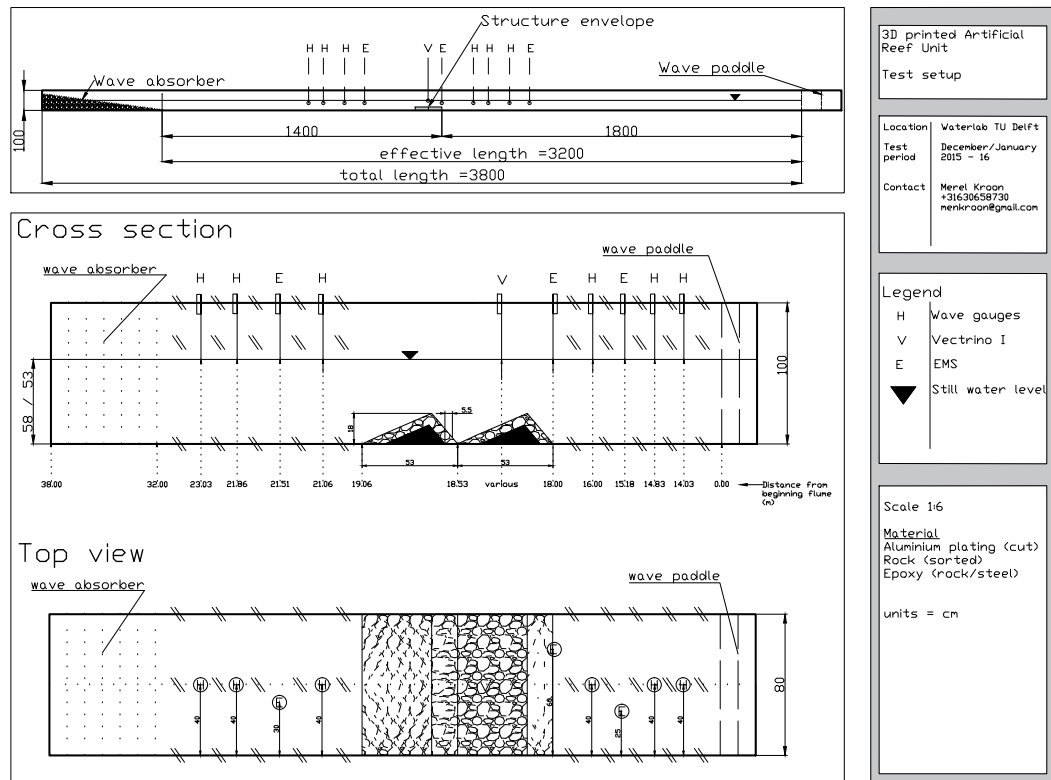


Figure 3.23: Overview of test setup



(a) Before filling



(b) With wave, EMS2 and Vectrino are visible

Figure 3.24: Reef structures in flume

Measurements and instruments As can be seen in figure 3.23, the flume has 10 instruments installed: 6 wave gauges, 3 EMS velocity meters and 1 Vectrino velocity profiler.

From the physical measurement campaign, the following parameters and processes have been examined and used to calibrate and validate the SWASH model:

- Wave height
- Orbital velocity away from the structure
- Velocity profiles over structure

Vectrino profiler Vectrino working is based on the Doppler effect of sound waves that hit particles in moving water. The transmitter emits sound waves which are scattered by fine particles in the flow and detected by three receivers oriented in such a way that they register the signal from a well-defined volume. With

three receivers the full three-dimensional velocity vector is measured in a volume of typically 0.25cm^3 located 5 centimeter from the probe [57]. The vectrino consists of the elements pictured in 3.26.

The velocity measurements over the reef to accurately describe the velocity fields over the reef are indicated in 3.25. Since the experiment is considered 2DV, only two of three directions of velocity are used: u -velocity and w -velocity, which are consecutive in the longitudinal direction of the flume and vertical directed.

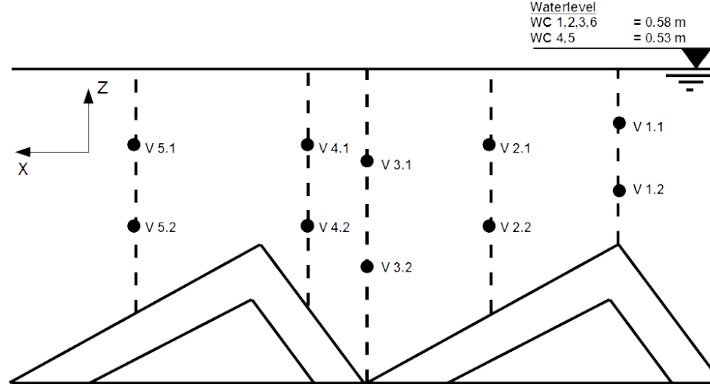


Figure 3.25: Overview of Vectrino measurements setup

The Vectrino measurements are the most important, since the velocity profile acquired from these measurements is used to determine if calibration of the SWASH model is successful. In order to create a tool that can be used for estimation of ecological value of a low crested barrier, this is the critical parameter.

The vectrino has a sampling rate of 25Hz. It is a very sensitive instrument. High sampling rate and high sensitivity result in a raw measurement signal that is prone to disturbance. The velocity that the Vectrino measures is therefore split up in three components:

$$u_{total} = \bar{u} + u' + u_{noise} \quad (3.14)$$

Where u_{total} is the raw measurement signal, \bar{u} is the mean velocity signal, u' is turbulence and u_{noise} indicates both high and low frequency disturbance by various sources of error. The mean velocity signal is what is used in further analysis, therefore the other terms are from here considered disturbance. Velocity decomposition is done by means of a fast Fourier transformation of the measured signal, as in equation 3.15. The Fourier transformation can be automatically carried out by the curve fitting tool in Matlab. More information on the decomposition of the velocity signal can be found in appendix L.

$$y = a_0 + \sum (a_i \cos(iwx) + b_i \sin(iwx)) \quad (3.15)$$

The goodness of fit is expressed by the Root Mean Square Error (RMSE);

$$RMSE = \sqrt{MSE} = \sqrt{\frac{SSE}{\nu}} \quad (3.16)$$

with:

$$SSE = \sum_{i=1}^n w_i (y_i - \hat{y}_i)^2 \quad (3.17)$$

SSE is the Sum of Squares due to Error. A value closer to zero indicates that the fit has a smaller random error component. ν is an indication for the number of independent pieces of information involved in calculating the sum of squares. Just as the SSE the $RMSE$ indicates a fit that is more useful when the value (with no dimension) is closer to zero. The amount of desired terms can be specified. The algorithm computing the best fit, also gives information on the goodness of the fit in terms of Root Mean Square Error. The amount of terms is increased until the $RMSE$ does not significantly (order 0.0001) change anymore.

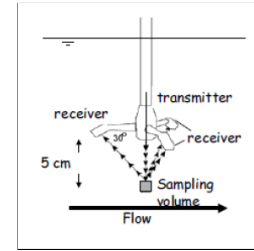


Figure 3.26: Vectrino (W Uijtewaal, 2013)

GHM wave gauges 6 GHM wave gauges are installed, in 2 sequences of 3 probes.

The GHM probes consist of two parallel stainless steel bars, with a small box connected at the bottom. This box contains conduction sensors. The rods act as the electrodes of an electric conduction meter. The analogue output signal is linearly proportional to the water level between the bars and represents the instantaneous water level. The probe can sample with a frequency of 0-10 Hz [44].

The GHM have to be manually calibrated to determine the linear conversion scale. The calibration was done before starting the measurements and at the end of the measurement campaign, to average out change of instrument behavior in the mean time. Results of the two calibrations is shown in figure 3.27. As can be concluded, the range of inaccuracy of the measurements differs between the GHM devices. The largest deviation is measured in GHM3. The largest error it could introduce is under 1 percent, therefore it is neglected and the mean value is used for conversion of the signal.

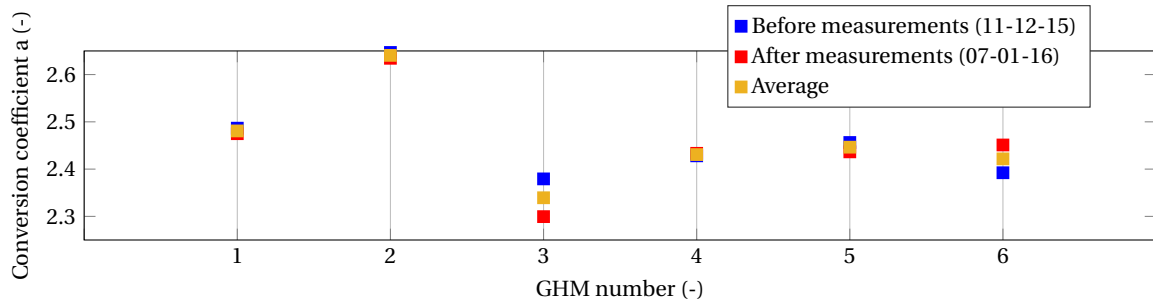


Figure 3.27: Calibration of GHM 1-6, linear conversion coefficient

In order to split the incoming and reflected waves, three probes have to be placed at a certain spacing. The method used to decompose the signal is developed by Zelt and Skjelbreia (1992). It is described by N points, measured at time $t=n\Delta t$ and $n = 1, 2, \dots, N$. The waves can be described by N spectral terms, being a sum of incident and reflected waves. Data registered by wave gauge p is represented by:

$$\eta(x_p, t) = \sum_{N-1}^{j=1} (a_{i,j} E^{-ik_j x_v} + a_{r,j} e^{-ik_j x_v}) e^{i\omega_j t} \quad (3.18)$$

$a_{i,j}$ and $a_{r,j}$ are complex numbers containing the phase shift of the incident and reflected wave. Standard Fourier analysis of $\eta(x_p, t)$ gives [44]:

$$\eta(x_p, t) = \sum_{N-1}^{j=1} A_{j,p} e^{i\omega_j t} \quad (3.19)$$

Equations 3.18 and 3.19 can be combined, creating a system of linear equations (equal to the number of probes) and two unknown complex values, $a_{i,j}$ and $a_{r,j}$, for each spectral component j . Since this research is only looking at monochromatic waves, $j=1$.

Using this theory, which is elaborated on by Lin & Huang, the distance between the 3 GHM on each side is determined, see table 3.12.

Table 3.12: Distance between probes, following Lin & Huang theory

GHM Nr	1:2	2:3
Distance (m)	1.17	0.80

EMS Flow meter Three electromagnetic flow velocity meters are installed, located before, at the toe and after the structure. The principle of the EMS is that the measured voltage between two electrodes, located in the probe, is linearly proportional to velocity.

The EMS are installed in order to serve as calibration dataset for far-field velocity magnitudes, away from the structure.

3.4.5. Planning

The laboratory tests were carried out in the period of November 30th 2015 until January 15, 2016. The schedule can be found in appendix E.

3.4.6. Intermediate results

Post processing is done for velocity measurements, to filter out turbulence and noise from the mean velocity signal. Also the reflection caused by the flume and the structure are calculated. Some of the results of the physical tests are used to setup the SWASH model, therefore they will be shortly stated here. In chapter 4 an elaboration on the results is given.

Governing wave condition In order to start setting up the SWASH model, one wave climate is selected from the tested 7 wave climates in the laboratory tests. The wave condition is selected based on:

- Low reflection from back of flume
- Noticeable influence on wave height by structure

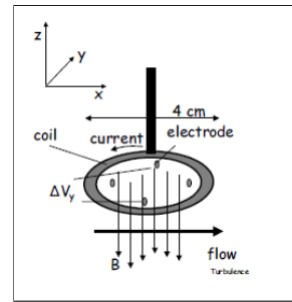


Figure 3.28: EMS (W. Uijtewaal, 2013)

Based on these selection criteria, looking at the reflection (see table 4.6), waveheight decrease (see figure 4.10), wave condition 5 was selected to be the governing wave condition for now on. Other wave conditions can be used to validate the robustness of the calibrated model later on.

3.5. Near-field modeling 2 - Validation of the model

Goals of the physical tests is to generate data that can be used to calibrate and validate the SWASH model setup. The obtained results from the physical model will be translated to SWASH input, in order to calibrate the numerical model. After the calibration is completed it will be translated to a prototype scale SWASH model, which will be linked to ecological performance of the reef. A typical input file for the SWASH model is printed in Appendix J.

The calibration and verification of the SWASH setup will be carried out following figure 3.29. This is the last step in the overall modeling, pictured in figure 3.1 at the start of this chapter.

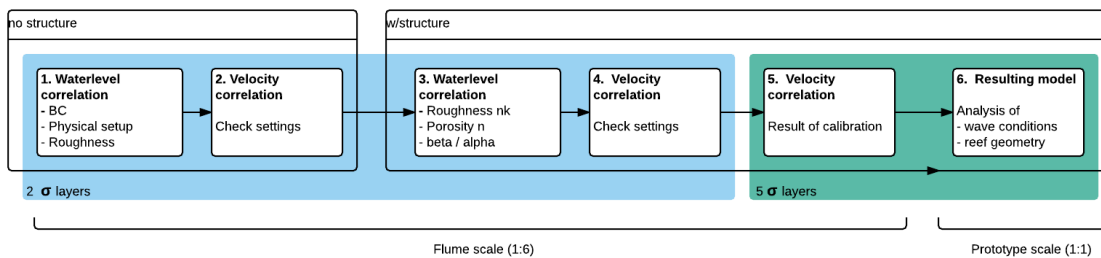


Figure 3.29: Steps in calibration process towards resulting model

In the first calibration step, the SWASH domain will be set up at flume scale rather than prototype scale, in order to minimize errors induced by scaling effects. When the calibration proofs to be effective, the SWASH model will be upscaled to prototype proportions.

3.5.1. Boundary conditions

Wave input The model will be set up for wave condition 5, see the measured and theoretical signal in figure 4.8.

Input of wave signal The second order Stokes waves will be expressed as an boundary condition to SWASH. For regular waves it is possible to specify the height and period, and let SWASH generate the signal. Alternatively, a time series can be used. Because the goal of this model is to mimic flume conditions, the latter is applied in order to minimize discrepancies. There are two possible time series boundary condition types which can be used, water level and velocity. A water level boundary is the simplest form, where in point $x,y(0,0)$ the water level is imposed and by means of the mass and momentum balance, SWASH calculates the η and v, u velocities. For the velocity boundary condition, the velocity signal in u -direction has to be specified for each sigma-layer. Since the water level boundary proved to be insufficient because of dispersion of

higher harmonics (see appendix I) a velocity boundary condition was applied. The detailed derivation of the boundary conditions from Stokes theory can be found in appendix I.

3.5.2. Calibration parameters

First order parameters As a first order calibration (based on water level measurements), the parameters roughness and porosity can be used. These are to be kept within physically reasonable limits, between 35 and 45 percent for porosity and Nikuradse roughness (assumed proportional to d_50 , following Yen, 1991[76]) height between 0.02 and 0.05 m. The roughness of the domain (flume) outside the structure is $7.5 \cdot 10^{-3}$. As mentioned in 3.2.9, this will be done with a model consisting of 2 σ -layers. Porosity in SWASH is included in the momentum balance. This is defined as dividing the terms in the momentum equation by porosity n . In this way momentum propagation through the porous layer is decreased. This is visible in the momentum equation 3.2.2.

Detailed parameters When numerically modeled water levels match the measured water levels, the detailed calibration will be done in 2DV with 5 sigma layers in the vertical, looking at mean velocity signals and turbulence measured with the Vectrino instrument.

SWASH uses a staggered grid for water level and velocity. This means that water level is computed on the grid-cell boundaries, while velocity is calculated for the center of each cell. For multiple layers the velocity profile will thus be computed in the midst of these layers, which is in accordance with the figure I.2 in appendix I. The measurements with the Vectrino are recorded at 1/3 and 2/3 in the water column. In order to minimize discrepancy between the location of this measurements and the output of SWASH the vectrino position is compared to the velocity output locations (v_n) for SWASH, being $v_n = \frac{1}{2N} + \frac{n-1}{N}$ with $n=1:N$ and N =number of layers. In figure 3.30 the position of vectrino measurements and SWASH output location for N layers is compared. The amount of 5 sigma-layers is chosen because these output locations are close (0.033 z/h) while computational time is acceptable. Furthermore the 5 layered model (and every other configuration with an uneven amount of sigma layers) produces velocity output at the midst of the watercolumn, which can be used to assess the exact correlation of the EMS measurements.

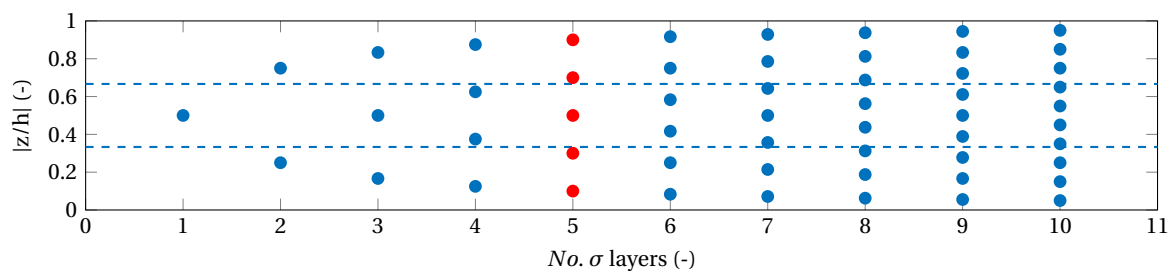


Figure 3.30: location of output locations v_n for SWASH, with the position of vectrino measurements in dotted line

Permeability rock layer The permeability of the rock layer (ease of flow through the pores) can be described by the Forchheimer equation.

The parameters that will be used for this second step in the calibration process are α and β . α indicates laminar friction loss, and β indicates turbulent friction loss. By Burcharth and Andersen Burcharth and Andersen [13] it is shown that for breakwaters with a core material of $d=0.03$ m and coarser, the contribution of the laminar flow is negligible and the hydraulic gradient I can be expressed as in equation 3.20 .

$$I = \beta' \frac{1-n}{n^3} \frac{V^2}{gd} \quad (3.20)$$

Here n represents porosity; V is the filter velocity.

Permeability tests for a variety of samples were carried out at the TUD laboratory by I. Verdegaal Verdegaal [74] and B. Mellink Mellink [51]. The results of these tests are used as an indicator for the value of β that will be implemented in SWASH. A quantitative comparison of the results is given in 3.13.

As a reminder the specifications of the physical test is stated in the first row of table 3.13.

Table 3.13: Values for turbulent friction factor β from literature

Specification	d_{50} (mm)	d_{85}/d_{15}	β	Source
Current model	38	1.5	?	-
Gravel	22.4 - 31.5		2.5	Verdegaal [74] Mellink [51]
Irregular rock		1.3-1.4	2.5-2.9	Shih [13]
		1.6	4.1 - 11	Dudgeon [13]
Equant rock		1.2	3.6	Williams [13]

In SWASH the Forchheimer relation is included in the porous momentum equations by two friction terms f_l and f_t . These equations are:

$$\frac{\delta \eta}{\delta t} = \frac{\delta(\frac{d}{n})}{\delta x} \quad (3.21)$$

$$\frac{1}{n} \frac{\delta u}{\delta t} + \frac{u}{n} \frac{\delta u}{\delta x} + g \frac{\delta \eta}{\delta x} + \dots + f_l u + f_t u |u| = 0 \quad (3.22)$$

The turbulent friction factor is defines as:

$$f_t = \beta \frac{1-n}{n^3} \frac{1}{d} \quad (3.23)$$

n is the porosity, ranging from 0(impermeable) to 1(water), d is the grain size.

The laminar friction factor is stated for a complete overview, but is not expected to have significant influence:

$$f_l = \alpha_E \frac{(1-n)^3}{n^2} \frac{\nu}{d^2} \quad (3.24)$$

Default values are $\alpha = 1000$ and $\beta = 2.8$. As mentioned, β will be used for calibration, values will range between 2.4 - 4.0, as is derived from the results in table 3.13. However, SWASH has limitations on the values of β being $1.8 < \beta < 3.6$. Therefore these threshold will be used in the calibration of the model.

Initial setup The flume geometry is implemented by applying a constant depth (dependent on the wave conditions, either 0.53 or 0.58 m). The wave damper in the back of the flume, pictured in figure 3.23, is represented by a sponge layer of the same length, 6 meter. The sponge layer accounts for total dissipation of wave energy, when the length is sufficient. Since reflection for most wave conditions in the flume is negligible, see table 4.5 the sponge layer is an accurate representation of the wave damper. For wave condition 1, where reflection is in the order of 20% however, it is important to realize that the attenuation is exaggerated in SWASH.

Other physical parameters of the model are summed up in table 3.14. An example of the input file is given in appendix J.

Table 3.14: Specifications of SWASH setup

Property	value	comments
dx	0.05 cm	>60 gridpoints per wavelength
σ -layers	2	Will be increased when structure is present
Boundary conditions	x,y=(761,0)	Radiation boundary to reinforce sponge layer
	Layer 1, x=0	Velocity time series
	Layer 2, x=0	Velocity time series
Friction bottom	$7.5 \cdot 10^{-3}$	Nikuradse roughness height
	Logarithmic wall law	Distinct between rough and smooth bed
Turbulence closure model	k- ϵ model	turbulent mixing is accounted for
Pressure gradient	Non-hydrostatic	Central Difference scheme
Space discretization	u/v -momentum equations	Central Difference scheme
	Water depth in velocity points	Central Difference scheme
Time integration	Explicit	Courant boundaries 0.2 - 0.5

A short elaboration on important or non-default settings :

Non hydrostatic pressure gradient scheme The central difference scheme is chosen over the default Keller-Box scheme, because the velocity in z -direction (w) is computed in the midst of the layer rather than on the layer boundary. This is meant for applications where vertical structures are important, like flows over steep and rapidly varying bottoms. Also this means w is computed in the same location as the velocity in x -direction (u) which gives more reliable output for comparison with the measured signals in two directions later on. This is illustrated in figure 3.31.

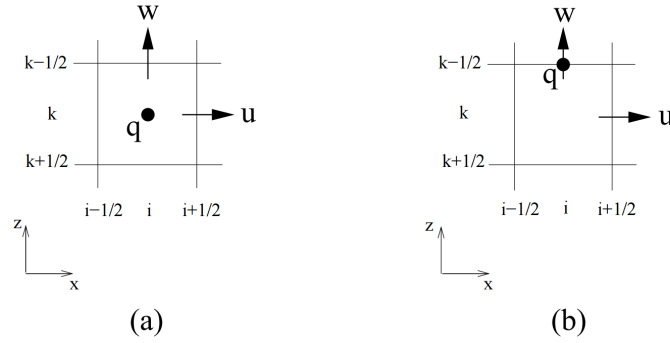


Figure 3.31: Arrangement of unknowns in a staggered grid: (a) standard layout (central difference scheme) and (b) Keller-box scheme. u is horizontal velocity, w is vertical velocity and q is non-hydrostatic pressure. Copied from Zijlema [77]

Turbulence closure model If interested in the vertical flow structure, the advise is to apply the standard $k-\epsilon$ turbulence closure model to account for vertical mixing in the water column (Zijlema [77]).

3.5.3. Evaluation of calibration

The correlation will be judged by two means: correlation coefficient of measured wave height and velocity compared to computed values, and correct representation of transmission and reflection by the structure.

The correlation of the water level computed by SWASH and measured in the flume is expressed using the Pearson correlation coefficient r , using a linear least squares regression for two vectors at a time, A and B. The statistic derivation is in 3.25.

$$r = \begin{pmatrix} \rho(A, A) & \rho(A, B) \\ \rho(B, A) & \rho(B, B) \end{pmatrix}$$

$$\rho(A, B) = \frac{1}{N-1} \sum_{i=1}^N \left(\frac{A_i - \mu_A}{\sigma_A} \right) \left(\frac{B_i - \mu_B}{\sigma_B} \right) \quad (3.25)$$

With σ is the standard deviation and μ is the mean value of the vector. Obviously, the correlation of A with A and B with B, so these values in the matrix are 1. The other two values represent r .

The theory of Goda and Suzuki that is used for determination of the reflection in both the flume and SWASH is described in F. Transmission is calculated using equation 3.3.

3.6. Ecological thresholds

In chapter 2 the target fish size is determined to be 15-20 cm. Since now the approximate orientation and geometry of the reef is known, as well as the order of magnitude of velocities, the equation 2.7 is expressed in a table. This table shows that the maximum velocity is positively correlated with the fish length. The steeper the structure, the lower the maximum velocity. This is in line with expectations that for a flat bed the maximum velocity is infinite, since then there is no structure as obstruction. In figure 3.32 the formula is expressed in a graph for various combinations of fish length and structure angle.

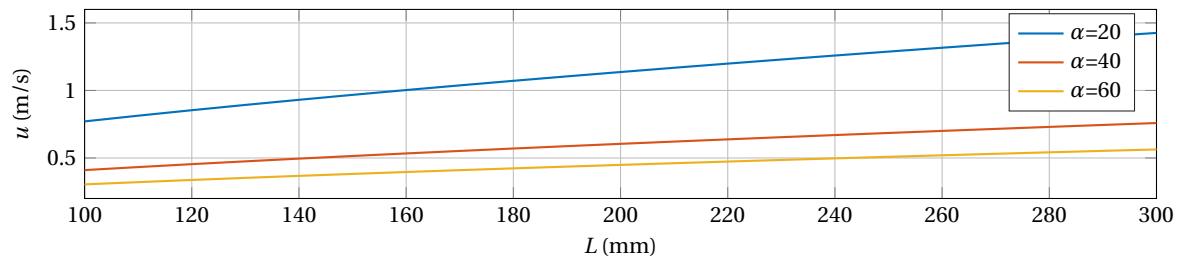


Figure 3.32: Maximum u -velocity for various fish length L and angle of structure α

This thresholds will be combined with the hydrodynamic modeling at the end of chapter 4. The synthesis of these two elements will lead to the desired integrated model.

4

Results

In this chapter the results of the modeling are presented and discussed. Part of these results have been used to link the subsequent models. Therefore some intermediate results have already been given in chapter 3.

The position of this chapter in the full methodology is indicated in figure 4.1. This chapter follows the same order as the modeling chapter, except that the offshore modeling and first near-field modeling is skipped since these results are only discussed in sections 3.1 and 3.3; they were intended solely as input for the next modeling step. Therefore first the far-field modeling results are discussed. Next the physical model results and some remarkable findings are discussed, and lastly the calibration and validation of the near-field model. Then the ecological threshold applied to the case study is presented. Finally results for both hydrodynamic modeling and ecological value are combined and discussed in the synthesis.

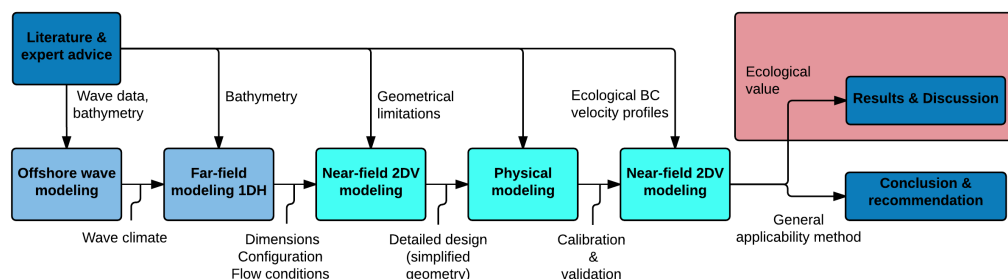


Figure 4.1: Place of results and discussion within research (red)

4.1. Far-field modeling

The results of far-field modeling consist of the final setup of the model, as well as the wave scenarios considered. One of the wave scenarios is used to determine the location of the reef-envelope.

As explained in 3.2.3, six wave conditions are analyzed in XBeach (see table 3.2 on page 27).

The transformation of the wave height is plotted in figures 4.3. First the bathymetry of the domain is plotted as reference. The remaining wave height is extracted at a depth of approximately 2 meter, since this lies within the possible range of reef position. The results of the wave height and wave induced setup at this depth are stated in table 4.1.

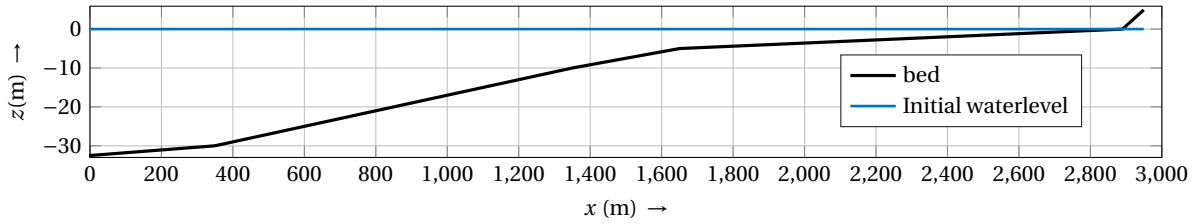
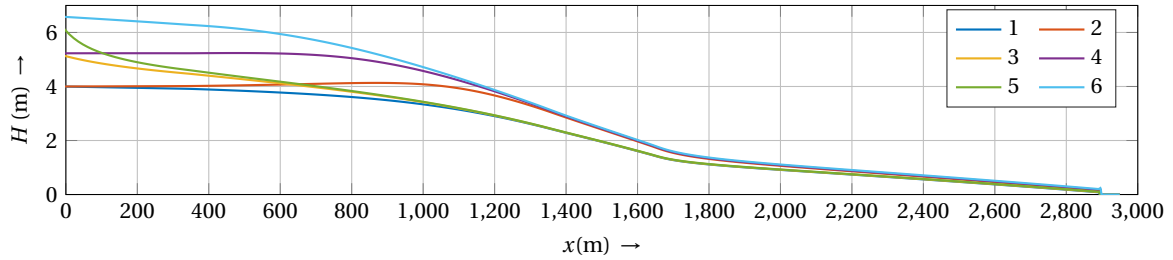


Figure 4.2: Bottom profile

Figure 4.3: H_{rms} for 6 scenariosTable 4.1: Deep water wave climates and their shallow water conditions at $z = -2.0$ m

Scenario	H_{rms} deep water (m)	T_{m01} (s)	H_{rms} shallow water (m)	Setup (m)
1	4	8	0.57	0.20
2	4	13.3	0.67	0.36
3	5.23	8	0.58	0.23
4	5.23	13.3	0.70	0.46
5	6.6	8	0.58	0.27
6	6.6	13.3	0.72	0.55

The resulting shallow water wave conditions can roughly be divided in two distinct wave conditions, namely:

- 1 $T=8$ s $H=0.6$ (Scenario 1,3,5)
- 2 $T=13.3$ $H=0.7$ (Scenario 2,4,6)

From these results two conclusions are drawn. First is that the wave period is governing for the wave height at shallow water. Furthermore a higher period results in higher setup. Here however the initial wave height also plays a role.

Next, the results will be discussed for the selection of the reef location. This will be done for the 'first' wave condition, because shorter waves show more significant interaction with structures.

Structure envelope selection Ten structure envelopes are analyzed. These geometries are pictured again in the picture below. The wave attenuation by structure envelopes 1-10 is analyzed in XBeach stationary mode, and shown in 4.5. In figure 4.6 the results of an analysis of the wave attenuation divided by the cross sectional area of structures 1 through 10 is shown. This is a measure of the effectiveness of the structure expressed per amount of needed construction material.

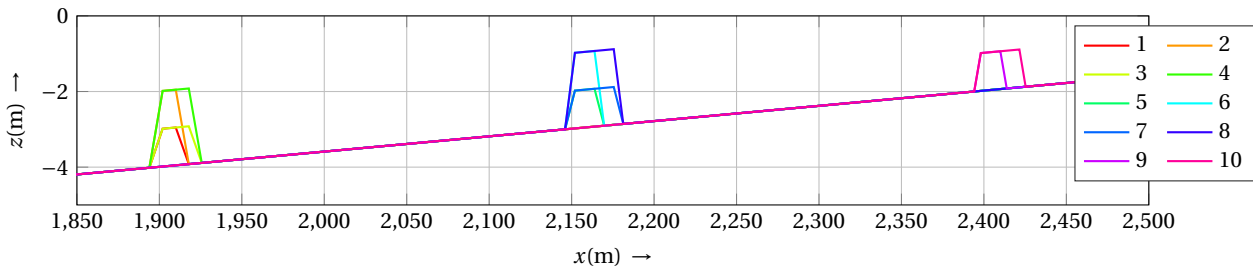


Figure 4.4: 10 reef envelopes analyzed in XBeach

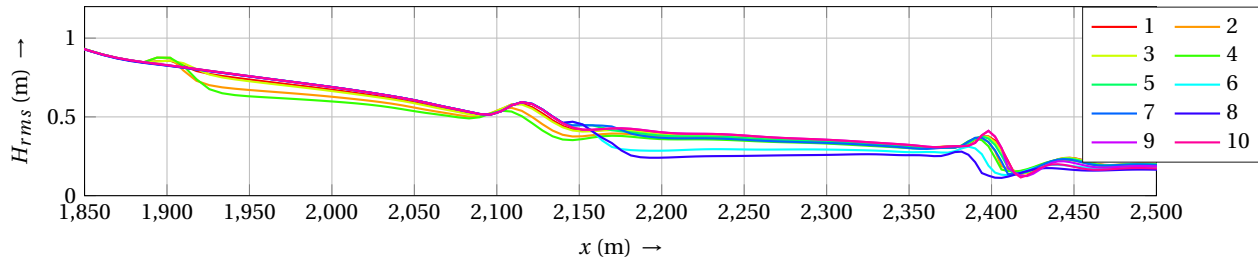


Figure 4.5: Wave-height decrease over structure envelopes 1-10

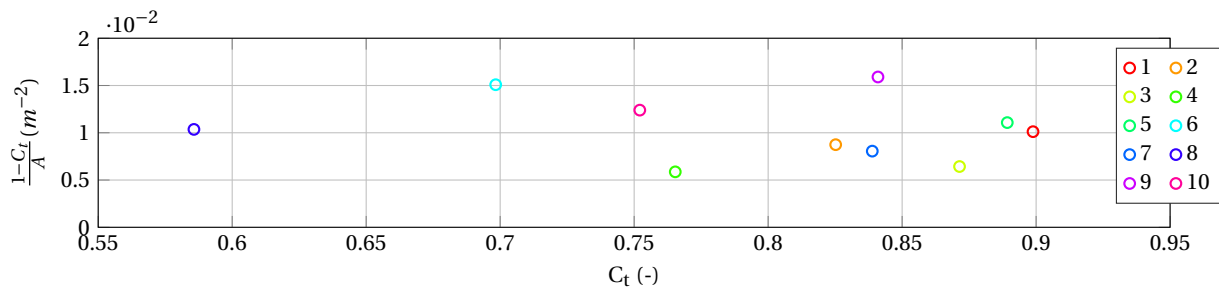


Figure 4.6: Transmission of waves per square meter cross sectional area of structures 1-10 (wave scenario 4)

The results are also shown in table 4.2. Parameters of the structures are H for height, B for width, D for depth and A for area of structure envelope.

Table 4.2: Analysis of wave transmission for structure envelopes 1-10

#	H (m)	B (m)	D (m)	A (m ²)	H _{in} (m)	H _{out} (m)	C _t (-)	$\frac{(1-C_t)}{A}$ (m ⁻²)
0	0	0	0		0.844	-	-	-
1	1	10	-4	10	0.844	0.756	0.896	0.010
2	2	10	-4	20	0.844	0.695	0.824	0.009
3	1	20	-4	20	0.844	0.733	0.868	0.007
4	2	20	-4	40	0.844	0.644	0.763	0.006
5	1	10	-3	10	0.491	0.437	0.891	0.011
6	2	10	-3	20	0.491	0.346	0.704	0.015
7	1	20	-3	20	0.491	0.412	0.840	0.008
8	2	20	-3	40	0.491	0.290	0.590	0.010
9	1	10	-2	10	0.280	0.237	0.849	0.015
10	1	20	-2	20	0.280	0.212	0.760	0.012

From table 4.2 it is concluded that reef envelope nine is the most effective in attenuating waves. This is visually confirmed by figure 4.6. Therefore the location and geometry of this reef will be considered in further analysis, being at 2 meters depth and approximately 1 meter high.

4.2. Physical modeling

The physical modeling campaign is executed to create a dataset with which the near-field numerical model can be validated. In order to do so, the focus lies on wave height and velocity measurements. Secondary effects caused by the flume, like reflection, are calculated. The results of wave height change for the 5 monochromatic wave conditions, and the velocity signal decomposition of these 5 are shown. Then one wave condition is chosen based on minimal reflection and maximum wave attenuation, that will be used for validation of the near-field model. Also two bichromatic wave conditions are tested, to expand the obtained dataset. Results of these two bichromatic wave conditions can be found in H., and will no further be discussed here. The considered wave conditions are repeated in table 4.3 for reference.

Table 4.3: Wave conditions for physical model

	Actual conditions			Scaled conditions		
	H (m)	T (s)	WL (m)	H (m)	T (s)	WL (m)
WC1	0.18	13.3	3.5	0.03	5.43	0.58
WC2	0.48	8.00	3.50	0.08	3.27	0.58
WC3	0.30	10.00	3.50	0.05	4.08	0.58
WC4	0.72	6.00	3.18	0.12	2.45	0.53
WC5	0.72	4.00	3.18	0.12	1.63	0.53

4.2.1. Water level measurements

Relation to theoretical wave The measured wave signals in GHM 1 (first wave gauge) for the 5 monochromatic wave conditions are plotted in figure 4.7.

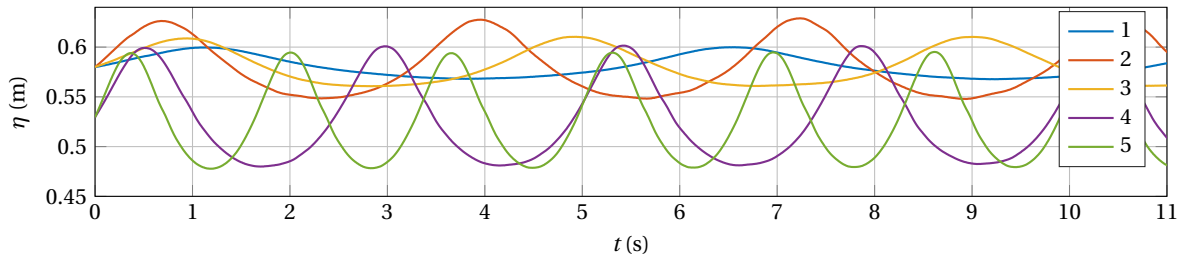


Figure 4.7: Measured wave signal of wave climates 1 to 5

GHM1 is located 14.08 meters from the wave paddle. It is observed that this is enough distance for the waves that come off the paddle to develop in their stable state. To check if this is indeed a valid observation, the measured waves in GHM1 are compared to the theoretical, 2nd order Stokes waves. The similarity between the measured and theoretical second order waves was very high, see the example in figure 4.8.

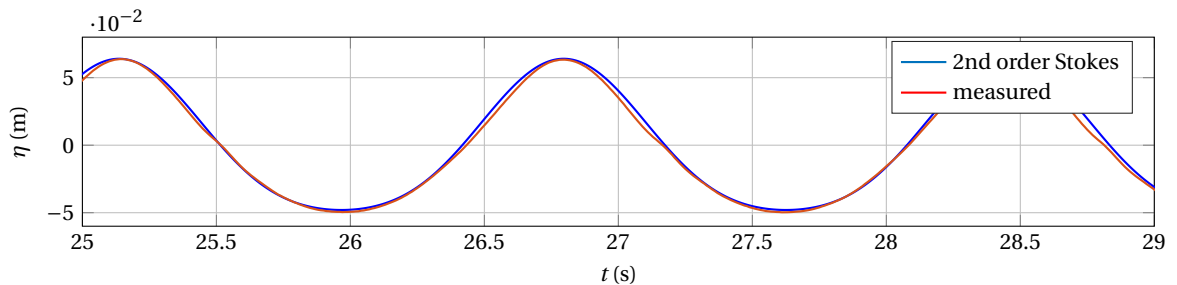


Figure 4.8: Comparison of theoretical Stokes wave vs. measured signal for wave condition 5

Reflection Although the wave flume is equipped with a wave damper consisting of rock in a mild slope at the back, some reflection is expected from the back of the flume. Since this returning wave will interfere with the original wave signal, it is important to know the magnitude of the reflection coefficient. From previous research the rough estimate of reflection of this particular wave damper is 20% [44].

For the simulated five wave conditions reflection is determined. This is done in runs without the reef present, to rule out any other wave-structure interactions other than that with the end of the flume.

The reflection is determined by using the Refreg program that is included in the script-package at the flume. The used method is defined by Suzuki and Goda [28]. This is elaborated on in appendix F. The reflection coefficient and wave amplitudes (measured) are summed up in table 4.4.

Table 4.4: Reflection of wave conditions

WC	d (m)	T (s)	L (m)	a_{in} (m)	a_{ref} (m)	refl.coeff (-)
1	0.58	5.421	12.759	0.015	0.003	0.217
2	0.58	3.267	7.509	0.038	0.001	0.031
3	0.58	4.080	9.504	0.024	0.002	0.085
4	0.53	2.451	5.257	0.057	0.001	0.021
5	0.53	1.651	3.273	0.057	0.002	0.036

This table shows, with exception of wave condition 1, a lower reflection of <8%. For wave condition 2-5 reflection can therefore neglected in further wave data analysis. For wave climate 1 it should be considered, since here a reflection of 20% occurs.

The following tables 4.5 and 4.6 are a more elaborate insight in the reflection of the flume and how this changes in the presence of the reef structure. Table 4.5 shows the reflection in front of the structure, so a large increase in reflection caused by the structure can be noted. Table 4.6 does not show such a significant in- or decrease of reflection, which is expected since this is behind the structure and the wave damper at the back of the flume is still in place.

Table 4.5: Reflection with and without reef, before structure (GHM3)

WC	d (m)	T (s)	L (m)	without reef			with reef			change refl.(%)
				a_{in} (m)	a_{refl} (m)	refl. (-)	a_{in} (m)	a_{refl} (m)	refl. (-)	
1	0.58	5.42	12.76	0.015	0.003	0.22	0.015	0.003	0.20	94.1%
2	0.58	3.27	7.51	0.038	0.001	0.03	0.038	0.004	0.10	316.5%
3	0.58	4.08	9.50	0.024	0.002	0.09	0.024	0.003	0.12	145.7%
4	0.53	2.45	5.26	0.057	0.001	0.02	0.057	0.007	0.12	574.5%
5	0.53	1.65	3.27	0.057	0.002	0.04	0.057	0.005	0.09	254.1%

Table 4.6: Reflection with and without reef, after structure (GHM4)

WC	d (m)	T (s)	L (m)	without reef			with reef			change refl.(%)
				a_{in} (m)	a_{refl} (m)	refl. (-)	a_{in} (m)	a_{refl} (m)	refl. (-)	
1	0.58	5.41	12.75	0.015	0.004	0.24	0.015	0.004	0.25	105.8%
2	0.58	3.26	7.49	0.037	0.002	0.05	0.037	0.002	0.06	111.2%
3	0.58	4.07	9.47	0.024	0.002	0.09	0.024	0.003	0.11	123.5%
4	0.53	2.45	5.03	0.057	0.002	0.03	0.054	0.002	0.04	126.5%
5	0.53	1.65	3.27	0.056	0.002	0.03	0.055	0.001	0.03	78.0%

Wave transmission The example in figure 4.9 is drawn to illustrate that although the magnitude is different, the relative change of the wave height has the same trend for both the mean and maximum wave height, analyzed from time series of 40 seconds. The maximum wave height was calculated by subtracting the minimum value from the maximum value in this particular time series, while the mean wave height was obtained by means of signal analysis.

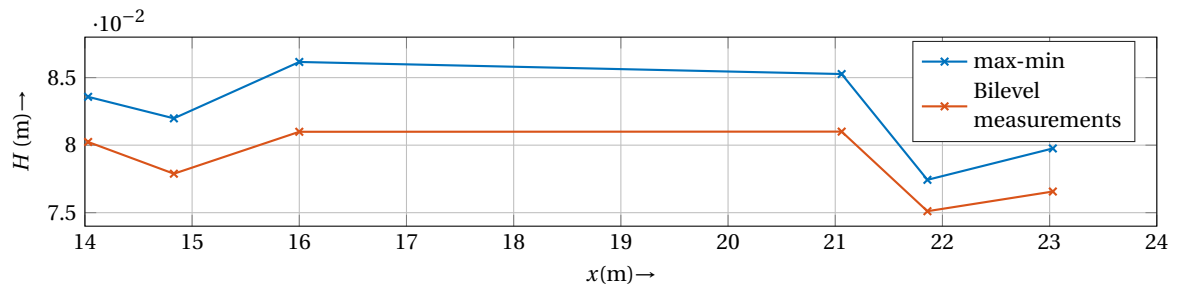


Figure 4.9: Example maximum and mean wave heights in GHM 1 to 6

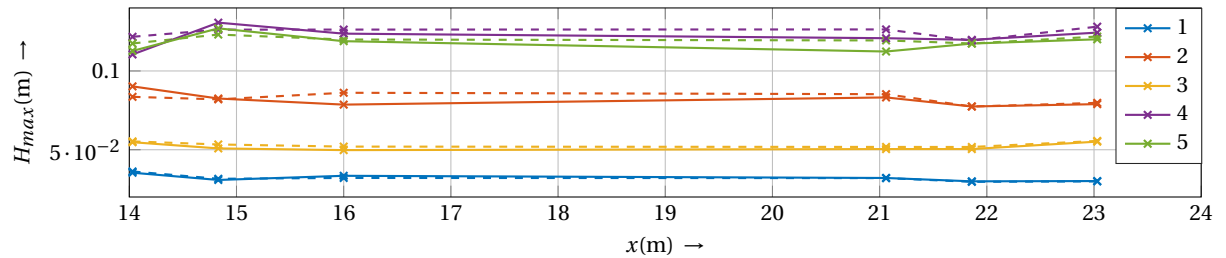


Figure 4.10: Maximum wave height for wave conditions 1-5, along the flume, with (solid) and without (dotted) structure

Table 4.7: Transmission coefficient C_t (H_{out}/H_{in})

Wave condition	C_t
1	1.01%
2	0.96%
3	1.00%
4	0.93%
5	0.97%

The transmission of the structure per wave condition is shown in table 4.7. This is calculated using the a_{in} values of the tables 4.5 and 4.6, with ref. Table 4.5 (before the structure) provides de H_{in} and table 4.6 the H_{out} . As can be seen, the transmission for all wave conditions is very high. For wave condition 1 the transmitted wave is even higher than the incoming wave, which is theoretically impossible. An explanation for this phenomena could be instrument inaccuracy. Another option is that the wave passing the structure does feel depth decreasing, therefore 'shoaling' occurs where the wave becomes higher and shorter. Since the distance between the structure and the wave gauge is very short compared to the wave length (2 meter versus 12 meter) it could occur that the wave has not settled back to the actual depth yet.

This theory is not explored or elaborated on. Wave conditions 2,4 and 5 do show attenuation of the wave. In table 4.5 it can be seen that the waves from wave condition 4 are reflected by the structure much more than wave condition 5. These high rates of reflection can lead to higher order harmonics occurring in the near-field model. The inflow boundary where waves are generated, is not equipped with an automatic reflection compensation (like the flume is). Therefore the validation of the near-field model will be carried out with wave condition 5. There is noticeable wave attenuation, but reflection is lowest of the three wave conditions which are attenuated.

4.2.2. Velocity measurements

The velocity is measured by means of 3 EMS and 1 Vectrino, as elaborated on in chapter 3.

Signal processing The EMS measurements are (after linear scaling by factor 10) ready to be analyzed. The Vectrino measurements however are in need of some post processing.

out lier correction The analog Vectrino data is captured in the same dataset as the wave gauge data, therefore the time-stamp is equal which automatically couples water level movement and velocity signal. However, the Vectrino is a very sensitive instrument, therefore some noise occurred in the signal. This can be caused by, amongst others, a deficit of particles to reflect the acoustic signal back to the receiver. An example of such an error can be seen in the signal in figure 4.11. These errors can be taken out manually, when analyzing the signal with the curve fitting tool in Matlab. It was observed that errors are generally larger when the velocities to be measured are low. Therefore examples are given for wave condition 1, which is a long and low wave, resulting in lowest orbital velocities. Outliers (as in figure 4.11) can manually be identified and left out of the fit, shown in 4.12.

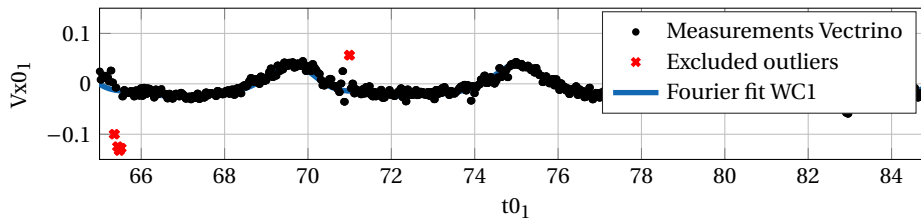


Figure 4.12: Outlier cancellation: manual selection (example for wave condition 1)

Velocity decomposition As explained in section 3.4.4 the velocity signal needs to be filtered to obtain the average velocity signal. This erases turbulence and high- and low frequency noise. A Fourier series is used, with an amount of Fourier components n , which resembles the lowest root mean square error (RMSE) between the measured signal and Fourier signal. The meaning of RMSE was explained in section 3.4.4.

For wave conditions 1-5 the Fourier analysis was carried out with satisfactory result. More information on the decomposition of the velocity signal can be found in appendix L. The Fourier fit is generated for Vectrino position V1.2 (see figure 3.25). The time series with outlier selection and fit curve can be found in appendix G.

The specifics of the Fourier series can be found in table 4.8.

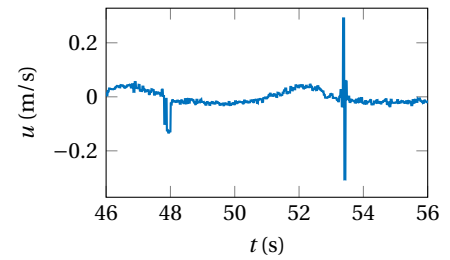


Figure 4.11: Errors in Vectrino measurement (Wave condition 1)

Table 4.8: Specification of Fourier analysis of Vectrino data, u -velocity, position V1.2

	Wave condition				
	1	2	3	4	5
RMSE	0.01098	0.01277	0.01028	0.06466	0.01976
a0	-0.00182	-0.00032	-0.00634	2.34E-14	-0.01093
a1	-0.02716	0.000352	-0.00988	-0.00056	-0.1195
b1	-0.01367	0.000568	-0.0548	-0.0008	-0.1726
a2	0.006278	0.07373	-0.01669	0.1253	0.00387
b2	0.007499	-0.06978	0.01008	0.1217	0.03598
a3	-0.00025	-0.00038	0.004007		0.000556
b3	-0.00345	6.34E-05	0.000703		0.002511
a4	0.000365	-0.00826			
b4	0.001018	-0.03398			
a5		-9.70E-05			
b5		-0.00028			
w	1.154	0.9611	1.536	1.281	3.807
$2\pi/w$	5.445	6.538	4.091	4.905	1.650

Results for wave condition 5 In figure 4.13 the results of the Fourier fit for wave condition 5 are shown, showing the magnitude of deviation from the mean, that the noise resembles. Two lines are drawn at $u=0.05$ m/s and $u=-0.05$ m/s, to show that most of the noise/turbulence stays between these limits. This is approximate 20 percent of the total range.

The fit of the velocity signals in x-direction and z-direction is generated for all 10 Vectrino locations (see figure 3.25 on page 39) using the curve fitting tool in Matlab. The Pearson correlation, explained in section 3.5.3, and coefficient of determination, R^2 (commonly used to express how well modeled data fits the observed data) in this case $R^2 = r^2$, of generated signals with the raw measurements are calculated. Results are given in 4.9. The Pearson correlation is always above 99% for u -velocity, and above 94% for w -velocity. This indicates that the velocity signal defined for further analysis is in very high correlation with the raw measurements. Therefore it is legit to be used as resemblance of flume measured velocity signal. The resulting mean velocity signals that will be taken into the near-field model calibration are illustrated in figure 4.14. The signals that are plotted resemble the highest and lowest correlation of the fit, in x and z direction.

More information on the decomposition of the velocity signal can be found in appendix L.

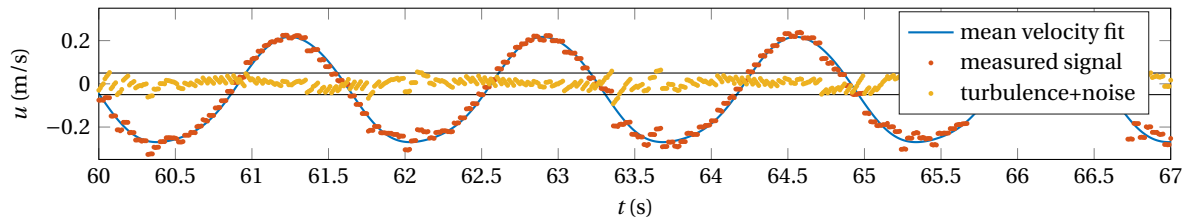


Figure 4.13: Noise obtained by subtracting mean signal from measured time series, wave condition 5. Lines at $u = \pm 0.05$ m/s

Table 4.9: Correlation fit Vectrino u - and w -velocity

Position	u		w	
	r	R^2	r	R^2
V1.1	0.9957	0.9914	0.9942	0.9885
V1.2	0.9952	0.9903	0.9928	0.9857
V2.1	0.9921	0.9843	0.9922	0.9845
V2.2	0.9918	0.9837	0.9841	0.9684
V3.1	0.9937	0.9875	0.9923	0.9847
V3.2	0.9924	0.9849	0.9562	0.9144
V4.1	0.9929	0.9858	0.9914	0.9829
V4.2	0.9826	0.9655	0.9423	0.8879
V5.1	0.9939	0.9879	0.9934	0.9869
V5.2	0.9909	0.9818	0.9797	0.9598

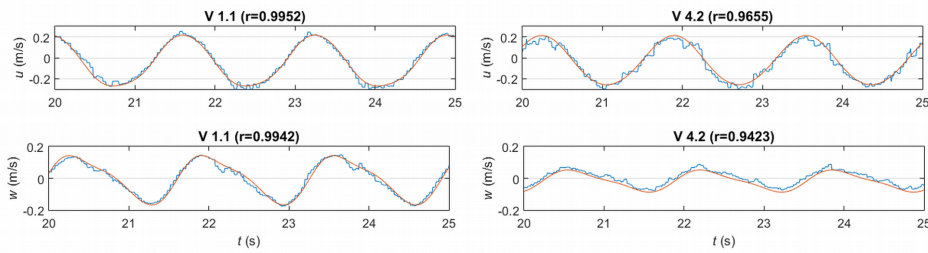


Figure 4.14: Mean velocity signal wave climate 5, highest and lowest correlation for u and w velocity

4.3. Near field modeling

The near field modeling comprehends validation of the SWASH model. Since this implies that the model will work properly, it will soon be clear that instead of validation, calibration of the model is performed. Unfortunately, this means the model is not generally applicable to any situation. First correlation of the model without a structure is calculated for the measured and modeled values. The parameter settings are already discussed in chapter 3. Then the more detailed settings are calibrated with structure, the appointed calibration parameters are set and correlation of the final resulting model will be calculated, for both 2 and 5 layers, as well as model-scale and prototype scale. A diagram of this calibration process is repeated in figure 4.15.

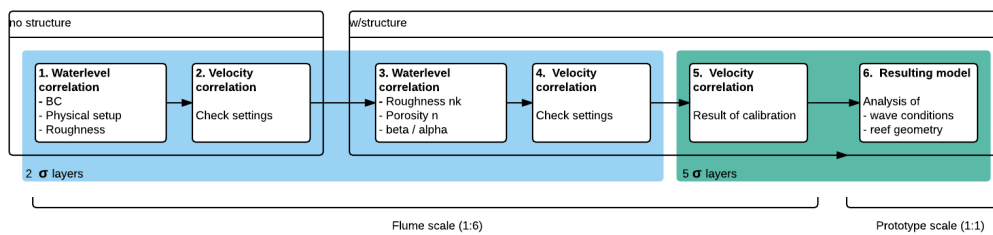


Figure 4.15: Steps in calibration process towards resulting model

4.3.1. Signal processing

The time series for lab measurements and SWASH calculations are not synchronized automatically, there is a phase lag and difference in spin-up time, this can be seen in figure 4.17. An adjustment for phase difference has to be done in order to analyze the correlation of the wave signals. This can be done in two ways. The options are either by means of synchronizing zero-crossings or synchronizing peaks of the signal. When the same method is used in all analysis the results will be comparable and valid, but the correlation per analysis is dependent on the method used. This is illustrated in figure 4.16.

The method used in further analysis is synchronizing the peaks. The synchronized results of the first order calibration, for wave condition 5 is shown in figure 4.18. As additional comparison the theoretical second order Stokes wave with specification of wave condition 5 ($H=0.12$ m, $T=1.63$ s) are plotted. The wave signal is very alike, which indicates that both SWASH and the flume reproduce the theoretical signal with high accuracy.

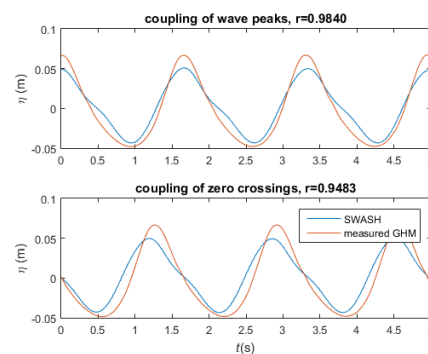


Figure 4.16: Two methods of signal synchronization with Pearson correlation coefficient

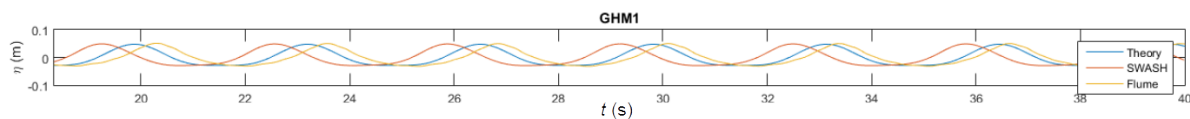


Figure 4.17: Results of validation, not compensated for phase shift (Wave condition 2)

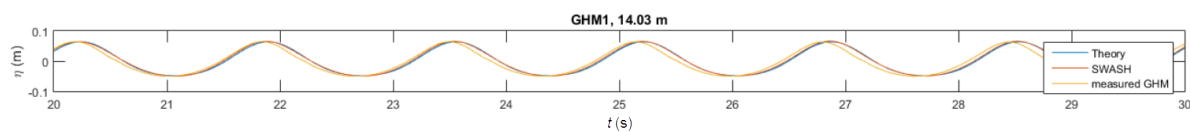


Figure 4.18: Results of validation compensated for phase shift (Wave condition 5)

4.3.2. Validation model scale - no structure

In the first step of the validation process, all SWASH settings are default. The wave condition is imposed by the appropriate boundary condition and the physical properties of the flume are reproduced. The waves are imposed with a velocity signal on each layer, which is explained in appendix I. The nikuradse roughness is set to a standard (rough bottom) value of 7.5×10^{-3} . Finally, the wave damper is resembled with a 'sponge' layer, which dissipates all wave energy, over a length of 6 meters. Additionally, at the end of the domain a weakly reflective boundary condition is applied, to make sure absolutely no reflection occurs in the model. To rule out reflection in the front of the domain, i.e. at the wave paddle, it was attempted to imply a Riemann boundary condition, to allow reflected waves (from the structure) to continue traveling out the domain, instead of being reflected again. Unfortunately the Riemann boundary conditions proved incompatible with the applied wave boundary conditions.

Correlation The values for r and R^2 for the calibration of wave condition 5 are calculated. The correlation of water level lies within the range of $0.98 < r < 1.00$. For these settings of SWASH the velocity correlation is calculated in the same way as water level. For the Vectrino correlation the mean velocity signal, as described in section 4.2.2, is used. The correlation of computed velocity with the measurements lie in the range $0.98 < r < 0.99$.

Note: From here onward the exact and complete set of correlation values and plots can be found in appendix K, for intermediate steps of the calibration leading to the final calibrated model.

Instrumental inaccuracy What became clear after the EMS correlation was assessed, that the difference between measured and computed velocity was due to a shortcoming in the equipment. For higher velocities (under the wave crest) the EMS systematically underestimates the velocity magnitude. This is shown in figure 4.19, where the velocities of SWASH and EMS are set out on the x and y axis. In the positive quadrant (where the wave crest is inducing positive velocities) the EMS measurements are lower than the velocities calculated by SWASH. Therefore this deviation has a physical cause rather than a computational one. This was compared to the deviations for the much milder wave condition 1, where velocities are low and thus the wake effect would have smaller effect. This was indeed the case, for wave condition 1 the deviation was negligible.

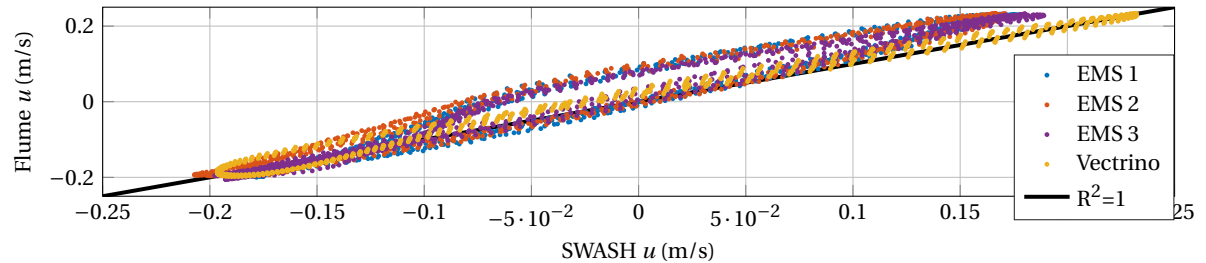


Figure 4.19: Underestimation of velocity under wave crest by EMS

4.3.3. Calibration model scale - with structure

2 layers The model is enhanced with the structure. This induces more uncertainty in the model, since it becomes more complex. Now the physical parameters are calibrated to a sufficiently high correlation without the structure in the last section, the calibration of the structure induced parameters will be done.

Water level As elaborated on in the beginning of section 3.5.2 there are four calibration parameters. For each of the parameters an average, low and high value is used, while other parameters are kept to the 'average' value. Results are given in table 4.10. This calibration is based on the correlation of water levels. Here the amount of sigma layers is kept to 2, in order to limit computational time. It was beforehand checked that using 2 or 5 layers does not have significant influence on the water levels computed by SWASH.

Table 4.10: Correlation of calibration runs

Run	Case	n	n_k	β	α	R^2						avg. R^2
						GHM 1	GHM 2	GHM 3	GHM 4	GHM 5	GHM 6	
0	basecase	38	0.04	2.8	1000	0.988	0.982	0.928	0.820	0.968	0.965	0.942
1	n_{low}	35	0.04	2.8	1000	0.989	0.982	0.926	0.823	0.967	0.974	0.943
2	n_{high}	41	0.04	2.8	1000	0.987	0.982	0.931	0.790	0.970	0.967	0.938
3	nk_{low}	38	0.03	2.8	1000	0.988	0.982	0.928	0.820	0.968	0.965	0.942
4	nk_{high}	38	0.05	2.8	1000	0.988	0.982	0.928	0.820	0.968	0.965	0.942
5	β_{low}	38	0.04	2.5	1000	0.988	0.982	0.930	0.785	0.968	0.970	0.937
6	β_{high}	38	0.04	3.1	1000	0.988	0.982	0.927	0.827	0.966	0.980	0.945
7	β_3	35	0.03	5	1000	0.989	0.982	0.926	0.823	0.967	0.974	0.943
8	β_4	35	0.03	3.5	1000	0.990	0.975	0.940	0.862	0.956	0.981	0.951
9	α_{low}	35	0.03	3.5	500	0.990	0.975	0.940	0.862	0.956	0.981	0.951
10	α_{high}	35	0.03	3.5	1500	0.990	0.975	0.940	0.862	0.956	0.981	0.951

The average correlation is highest for the values that are printed bold in table 4.10. To check the assumption that α is of minor importance this value is also varied considerably in runs 9 and 10, without any noticeable change in the correlation.

The correlation is acceptable, this does however not reflect how well the 'shape' of the wave is resembled. The signals that belong to the highest correlation are plotted in figure 4.20. Also, looking at the spatial result of this calibration, wave damping and reflection is much more significant then in the flume, see table 4.11 and figure 4.23.

Porosity Since the wave climate is monochromatic and it was observed that the structure does not have serious impact on the waves (for example breaking), it is expected that the correlation could be increased.

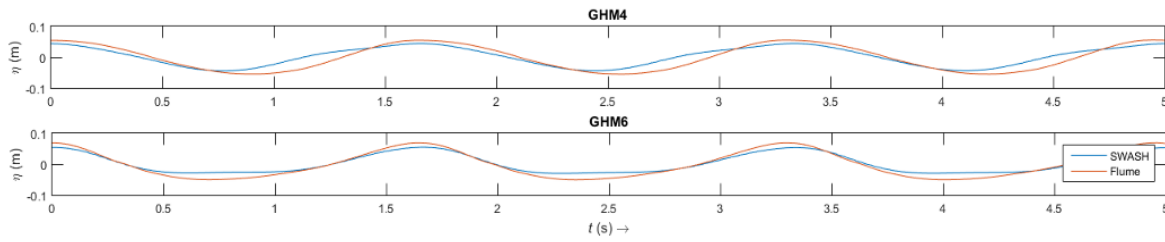


Figure 4.20: Shape of wave signal compared with SWASH and flume, example GHM3 and GHM4

The possibility is explored to look at the calibration parameters outside of their expected range as defined in section 3.5.2. After some rough alterations of Roughness n_k (minor influence) β (limited by SWASH between 1.8 and 3.6, no major changes) and porosity n , it can be concluded that increasing the porosity leads to a better overall correlation between flume and SWASH model. However, increasing the porosity will decrease the influence of β , see equation 3.20. This, together with the increase in correlation for higher porosity, is pictured in graph 4.21. From the calibration table 4.10 it can be concluded that overall correlation for GHM 4 was the worst. Therefore the correlation for this location was also investigated separately, in figure 4.22. This shows the same relations between porosity and β , however it is obvious that correlation is highly improved when applying the higher values for porosity (>0.8).

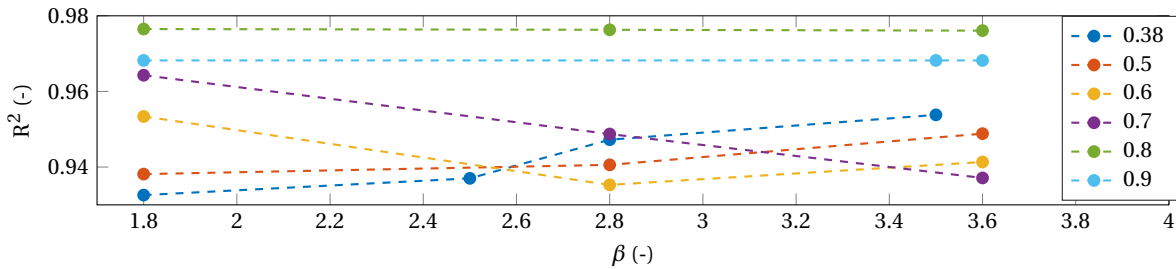


Figure 4.21: Average correlation for various porosity and β

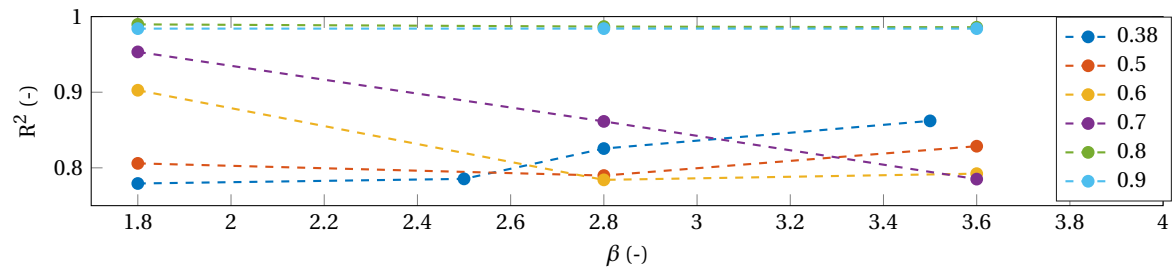


Figure 4.22: correlation for various porosity and β , for GHM 4

Before making the decision that the higher porosity, however physically unrealistic, leads to better results, another comparison is made between the two calibrations. Reflection and transmission is determined for the bold settings in table 4.10, and the same settings but porosity $n=0.8$. These are compared to the measurements in the flume, which have already been determined and printed in tables 4.5 and 4.6. For this the same method of Goda and Suzuki (see appendix F) is used. The results can be found in table 4.11.

Table 4.11: comparison of reflection and transmission for porosities $n=0.38$ and $n=0.8$

Case	GHM 1 (m)	2 (m)	3 (m)	4 (m)	5 (m)	6 (m)	reflection structure	reflection flume	C_t
flume	0.052	0.057	0.057	0.055	0.055	0.055	0.087	0.038	0.963
$n=0.38$	0.048	0.069	0.056	0.042	0.042	0.042	0.220	0.008	0.755
$n=0.8$	0.051	0.065	0.057	0.052	0.052	0.053	0.138	0.007	0.919

The higher porosity gives a better resemblance of the measured reflection and transmission by the structure in the flume. The physically realistic porosity leads to a significant over-estimation of reflection and damping. Spatially, the difference between the two situation looks like figure 4.23. Unfortunately the flume comparison can not be added due to the absence of a full flume-length instantaneous water level measurement. During the experiments it was visually established that the disturbance of the wave shape after passing the structure was minor.

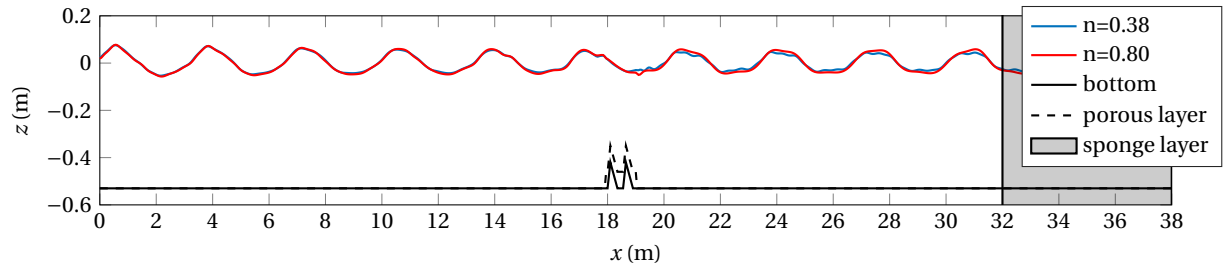


Figure 4.23: spatial result of calibrated settings, for $n=0.38$ and $n=0.8$

Based on these two results it is decided that the high porosity of $n = 0.8$ is used. This is however a drawback in the general applicability of the model, since it can not be assumed that physically realistic input returns accurate results. The correlation for a porosity of $n=0.8$ and $\beta = 1.81$ for water level is $0.96 < r < 1.00$. This is for the two-layered model with structure.

Velocity For the settings resulting from the calibration based on water level correlation the correlation for velocity was determined. However, since the setup here was still 2 layers, a choice was made to compare the measured signal to the velocity in the upper layer. Expectation is that the computed velocity will be higher, since the flume signal was measured halfway in the wave column, while output from swash is in this case at $1/4$ of the water depth from the surface (see figure I.2 in appendix I). Basic wave hydrodynamics say that orbital velocities closer to the surface are higher. The situation and location of output points is sketched in figure 4.24. SWASH 1 and 2 are the output locations for computed velocity, while EMS and the Vectrino are measured depths. The velocity for both layers is visible in figure 4.25, for the location of EMS1. The solid red line resembles the velocity in the upper layer, the dotted line the second layer. The correlation lies between $0.90 < r < 0.97$, but again, should be considered a rough estimate since they are in different locations in the watercolumn. This is visualized in 4.25.

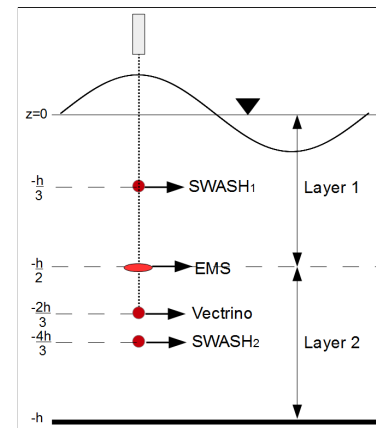


Figure 4.24: Location of measured and calculated velocity (for two σ -layers)

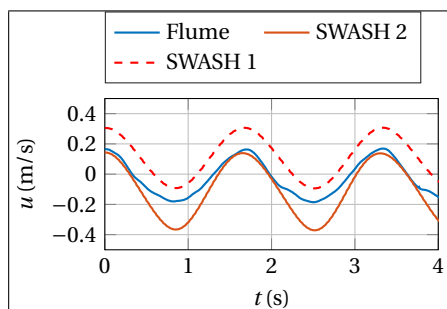


Figure 4.25: Comparison of measured and calculated velocity (for two layers), example for EMS 1

5 layers Next, the model is extended to 5 σ -layers. This was decided to be sufficiently accurate in terms of resolution (see section 3.5.2) while computational time is still acceptable.

Water level Correlation of water level in the GHM locations for the 5 layers is slightly lower than for 2 layers, between $0.95 < r < 0.99$.

Velocity Correlation for the velocity is what is really interesting in this calibration step, since now the velocity output of SWASH will actually correspond to measurement locations in the flume, as indicated in figure 3.30. The calculated correlation for EMS measurements is now $0.96 < r < 0.98$. Again, exact results can be found in appendix K.

Velocity over the structure was measured in 10 locations with a Vectrino I, see figure 3.25. The results of SWASH and flume comparison gives a correlation of $0.94 < r < 0.99$.

4.3.4. Validation prototype scale

The model as defined in the section before is translated to prototype scale. As explained in section 3.4.4, the scaling used is Froude scaling. For the relevant parameters length, time and velocity the scaling rules are repeated:

$$\begin{aligned} \text{Wave height (m)} & n_H = n_L \\ \text{Time (s)} & n_T = n_L^{0.5} \\ \text{Velocity (m/s)} & n_u = n_L^{0.5} \end{aligned}$$

The scale applied is 1:6, so all length scales are multiplied by 6, all timescales multiplied by $\sqrt{6}$. This is done for the water level measurements, which leads to the original wave conditions as defined in section 3.4.2. All input files for SWASH are adjusted by the above scale. Porosity and α and β are kept constant, since these by definition of Froude scaling should be insensitive to scaling.

Water level The upscaled measured signal and upscaled SWASH model's correlation is shown in figure 4.26 and table 4.12. The correlation is now between $0.89 < r < 0.99$. Compared to the flume scale correlation, the lower limit of correlation span has cropped 5 percent. Since no settings are altered, this is ascribed to scaling effects.

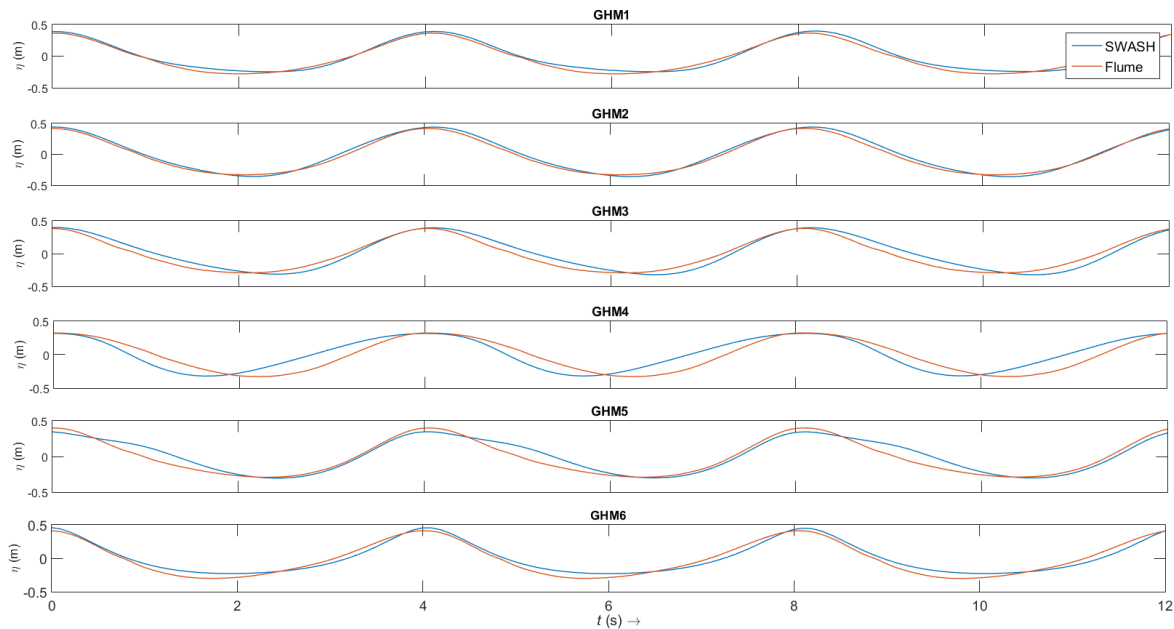


Figure 4.26: comparison water level between upscaled flume measurement and SWASH prototype scale

Velocity The correlation of the velocities is also determined by upscaling the velocity signals measured in the flume following Froude scaling. Correlation is determined in a comparable manner as before. Also an assessment is made of the correlation for velocities in z-direction.

u-velocity For the velocity in x-direction the correlation could be determined like before. These correlations are, for each Vectrino location, above 90 percent. The correlation over all measurement locations has dropped about one percent on average. This is an insignificant decrease, therefore the results of the upscaled velocity and prototype model are considered thrust worthy. To visualize the correlation results the signals of all vectrino measurement locations are plotted in figure 4.27.

Table 4.12: Correlation water level for prototype scale

GHM	r	R^2
1	0.9939	0.9878
2	0.9931	0.9862
3	0.9656	0.9323
4	0.8921	0.7958
5	0.9394	0.8825
6	0.9653	0.9318
average	0.9582	0.9194

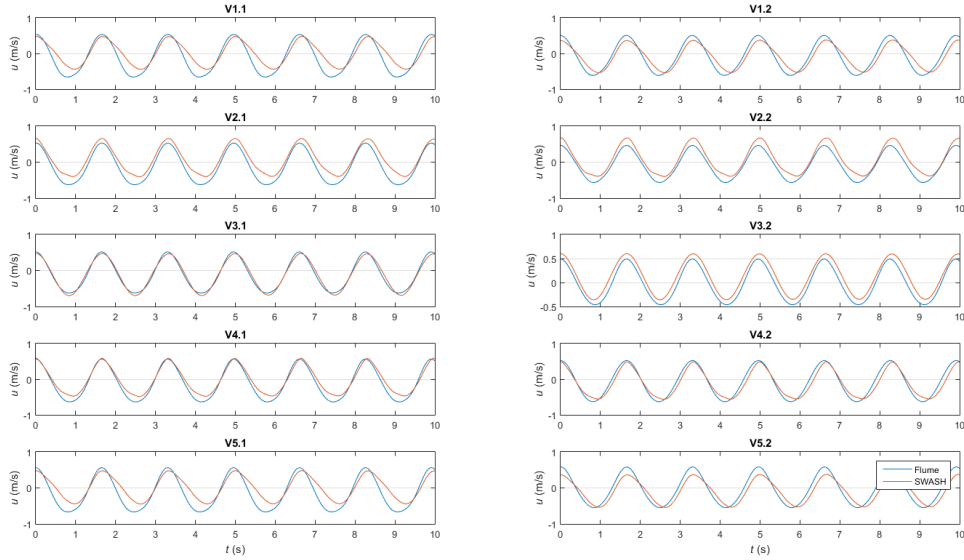


Figure 4.27: Vectrino u -velocities (upscaled) compared to SWASH results - prototype scale

w -velocity error The correlation with the w -velocity is found to be of lesser importance due to the focus on horizontal velocity (see figure 2.6).

When in prototype scale the w -velocity was examined a discontinuity was observed. In SWASH, the velocity in w -direction is calculated to be zero above and in the vicinity of the structure. This is shown in 4.28. It was established that this error was due to the presence of the porous layer, as figure 4.29 shows the velocity patterns without the porous layer.

In consultation with SWASH expert Dr. ir. Zijlema it was concluded this is most probably an error in the SWASH code. The source of the error can be found in the way porosity is accounted for in SWASH. Porosity is included in the momentum equations for u and v velocities (as in equation 3.22). Since SWASH is a shallow water model porosity was not explicitly included in w -momentum equations, assuming w -velocity is small compared to u - and v -velocities. The assumption was that through mass balance the coupling between u -momentum and w -momentum and thus velocity would compensate for the influence of porosity, this seems to be an incorrect assumption.

Table 4.13: Correlation Vectrino u -velocities prototype scale

Position	r	R^2
V1.1	0.9200	0.8464
V1.2	0.9343	0.8729
V2.1	0.9860	0.9721
V2.2	0.9830	0.9663
V3.1	0.9903	0.9806
V3.2	0.9942	0.9885
V4.1	0.9883	0.9767
V4.2	0.9673	0.9356
V5.1	0.9244	0.8545
V5.2	0.9347	0.8737
Average	0.9622	0.9259

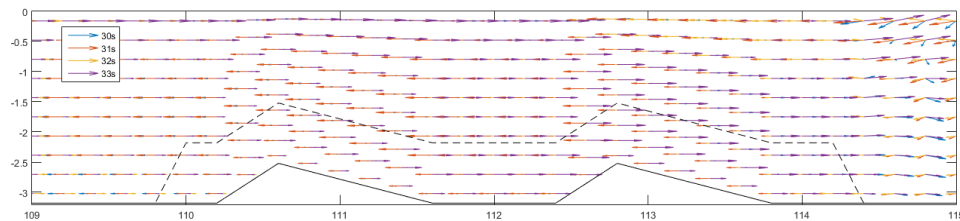


Figure 4.28: Discontinuity in velocity pattern, no w -velocity in vicinity of porous layer

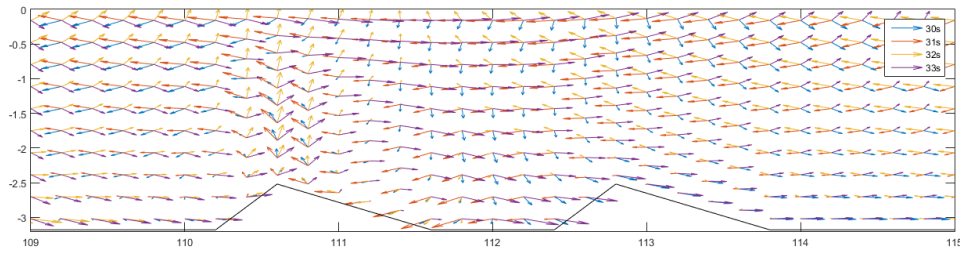


Figure 4.29: Velocity pattern without porous layer, w -velocity is present

Reflection and transmission In table 4.14 the reflection and transmission of the SWASH computations are given. The method of Goda and Suzuki [28] is used.

Table 4.14: Prototype scale reflection and transmission for calibrated SWASH model

Amplitude 1st harmonic (m)						refl. struct (GHM2- GHM3)	refl. flume (GHM4- GHM5)	$C_t \frac{a_{GHM4}}{a_{GHM3}}$
GHM1	GHM2	GHM3	GHM4	GHM5	GHM6			
0.29	0.33	0.33	0.31	0.30	0.29	13.8%	1.1%	93.6%

Compared to the transmission in the flume in table 4.7, which is 97% for wave condition 5, the SWASH model overestimates wave damping by 3 percent, at 94% (see table 4.14). Reflection in the flume is 9 % (see table 4.5). Reflection by swash is higher, 13,3%. This is an overestimation of 5 percent for reflection. This is in accordance with the overestimation of the wave damping; more reflection generally means less transmission.

4.4. Calibrated near-field model

In this section the results of the prototype scale SWASH model, calibrated using one wave condition are stated. Wave condition 5 has the following prototype scale specifications:

- $H = 0.72$ m
- $T = 4$ s
- $h = 3.18$ m

4.4.1. Final settings

The final settings for the model and calibration parameters are repeated in the next table. In particular the high porosity has to be considered with caution in future modeling. This was the governing parameter influencing the correlation of the model, but has also resulted in a physically unrealistic value.

Nikuradse roughness	n_k	0.03
Turbulent friction factor	β	1.80
Laminar friction factor	α	1000
Porosity	n	0.8

4.4.2. Correlation

The correlation (r) of the water level measurements with the prototype SWASH model are between 89 and 99%. For the velocity measurements (u) with the Vectrino this is between 92 and 99%. The correlation of the model is concluded to be sufficiently high so conclusions can be drawn based on this model. However it had to be kept in mind that the model does not solve for w -velocity, and is therefore physically incorrect in its functioning.

4.4.3. Maximum velocities

The amount of sigma layers is 5 for the correlation. However for more detailed velocity patterns a model with 10 layers is used to generate these. The maximum velocities in positive and negative x-direction are plotted in figure 4.30.

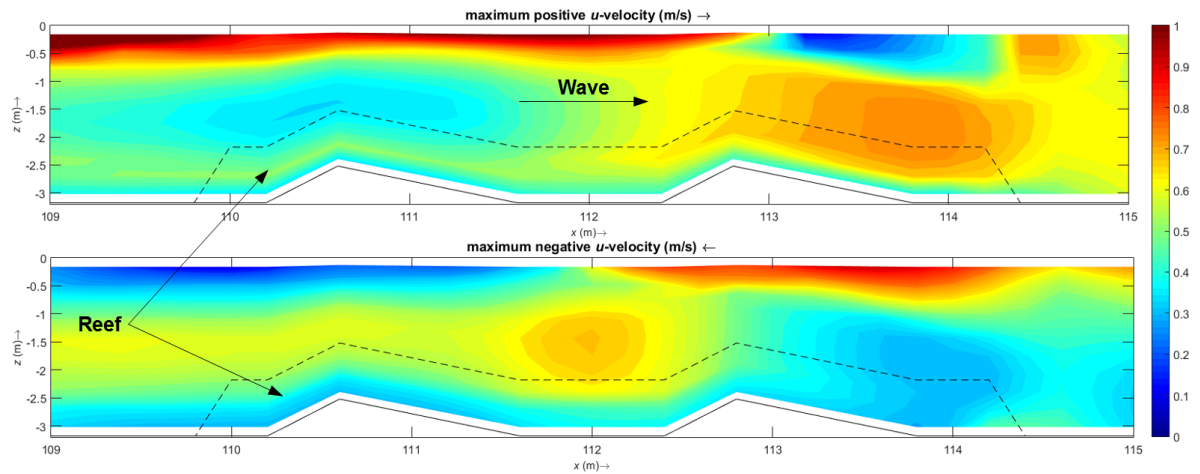


Figure 4.30: Maximum u -velocities in positive and negative direction

4.5. Ecological thresholds

Ecological value is expressed by means of horizontal velocity. This theory is based on a translation from the design requirements of inlet-screens for cooling water, which is explained in chapter 2. Since the wave conditions are monochromatic, the governing velocities used in the analysis is absolute maximum velocity. This is obtained by selection of the maximum value for v -velocity in every grid-point around the structure. Note that therefore the flow structures pictured from here on are not 'snapshots' in time, but composite images. The maximum velocity in positive and negative x -direction is determined in a 10-sigma layer model. These are shown in figure 4.30. Here it is visible that the structure has significant influence on the values of maximum velocity in the horizontal plane.

For the species considered in the case study, Juvenile Sea bream of 20 cm mean length (see section 2.3.2), and the reef implemented in the experiment with an angle of 50deg (see 3.4.3), this leads to a maximum u_+ -velocity of $V_u = V_+ = 0.51$ m/s. The lee side of the structure has an approximate angle of 30 degrees, which gives a maximum negative velocity of $V_- = 0.66$ m/s.

4.6. Synthesis

In this synthesis the analytically derived velocities that limit habitability are combined with the calibrated SWASH model. Furthermore some results of this synthesis are elaborated on, being the 'patchiness' of the velocity pattern and a check of the synthesis without structure.

The ecological threshold is indicated in figure 4.31 by the color change. It can be seen that for the velocities in positive x direction, the threshold is exceeded mostly on the back of the structure. This can be argued to be acceptable, since the specie is forced away from the face of the structure rather than onto it. In the return flow, since the slope of the structure is more gentle, over the full stretch of the units the velocities are below the threshold. Still, the environment as it is is expected to be too energetic for the proposed target species.

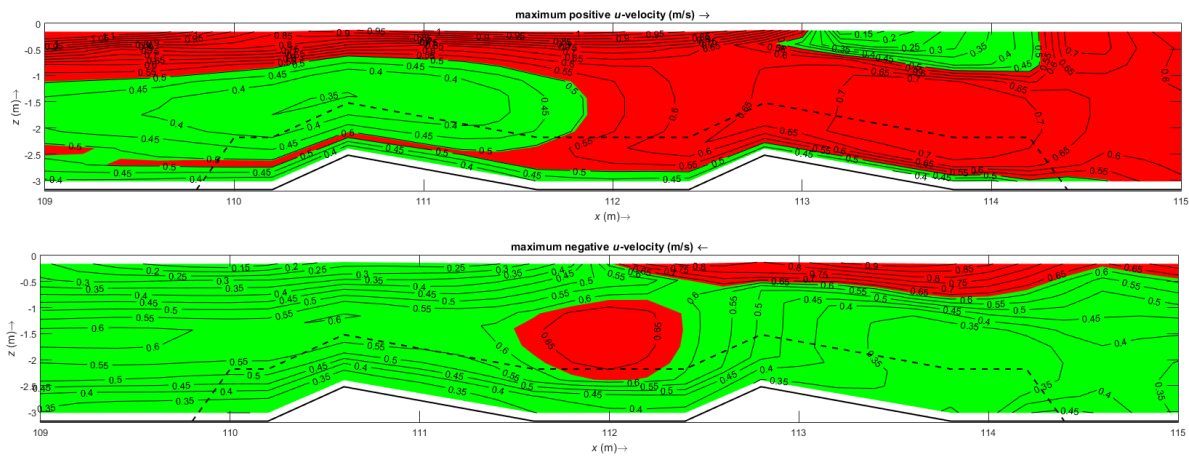


Figure 4.31: Maximum velocities in positive and negative x-direction, threshold for $u_+ = 0.51$ m/s and $u_- = -0.66$ m/s indicated with color scheme

4.6.1. Patchiness

The patchiness of the velocity pattern in figure 4.31 is distinct. Since the patterns cannot be intuitively explained. The model will be validated using two alternative datasets: without reef and the PIV measurements.

No structure For the exact same SWASH model but without the structure and porous layer the velocity fields are created, figure 4.32. These velocities can be compared to theoretical velocity under the imposed second order Stokes wave, plotted in figure 4.33. Looking at the magnitudes over depth for positive and negative velocities, it can be concluded that these are very similar, and the model behaves as desired. It must be mentioned that the thresholds used in this case are not correct: applying equation 2.7 to the situation where there is no structure, i.e. $\alpha=0$, $u_{max} = \infty$.

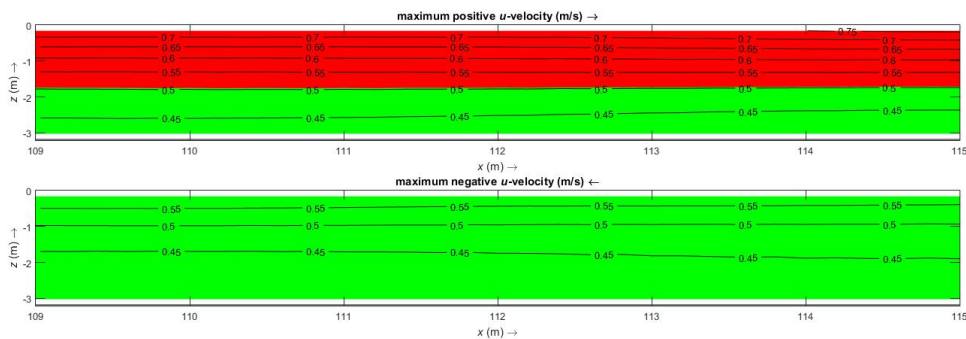


Figure 4.32: Ecological thresholds applied to domain without structure

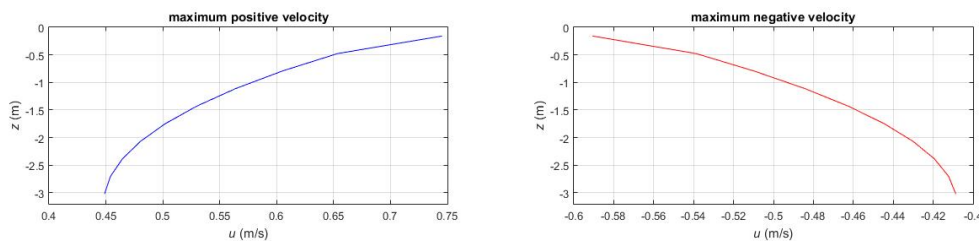


Figure 4.33: Theoretical maximum u -velocity (positive and negative)

PIV measurements More data from the PIV measurements can be found in appendix M. Here discussion of the PIV measurements is limited to the used velocity data. Patchiness over the watercolumn is confirmed by

the PIV measurements. In figure 4.34 it can be seen that above the second reef unit on the left side (the image is mirrored compared to SWASH output) higher velocities are recorded above the structure and on the water surface, with slightly lower velocities in the middle of the water column.

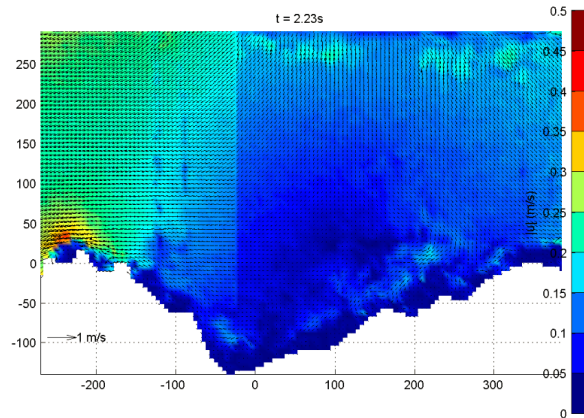


Figure 4.34: Patchiness in PIV measurements (flume scale; does not match SWASH prototype magnitudes)

4.6.2. Ecological value

Figure 4.31 shows distinct velocity patterns within the water column, for which the targeted species are able or not able to swim. The tested setup for these particular wave conditions are unfavorable for providing habitat over the full length of the reef. This is concluded since virtually all locations along the face of the reef are above the threshold at some point. This is visualized in figure 4.35, where the suitability of the reef surface for habitat placement for juvenile Sea Bream with the current wave condition is visualized.

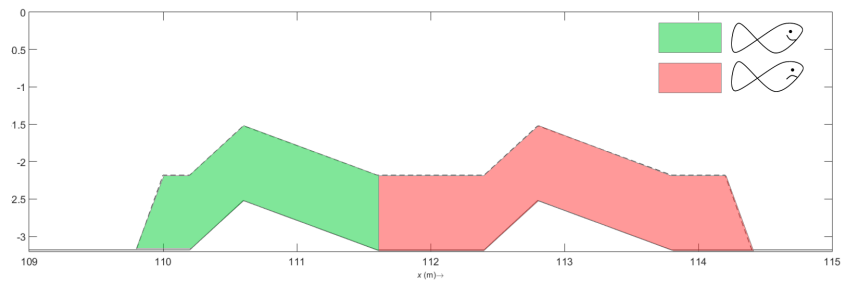


Figure 4.35: Suitability of surface reef for habitat creation

5

Conclusions & Recommendations

In this chapter it is reflected upon if the major objective of this research is met. The goal of this research was to establish a method to integrate ecological and coastal protection functionalities for a 3D printed reef. An additional objective was to define a framework for the product development of 3D printed AR. This framework is defined in section 1.4, and will not be further discussed here. An elaboration on the framework is given in appendix A.

In the first section the conclusions based on the research questions will be elaborated on. Then the results of the method applied to the case study are discussed. Then the restrictions on the developed method will be illustrated. Finally recommendations for future research and application of the tool will be given.

5.1. Conclusions

The main research question was: *"How can an integrated design approach of ecological and coastal protection functionalities, for a 3D printed reef, be established?"* In this research an integrated design method was developed and proven feasible, although with limited applicability. By using a phase-resolving wave model for small scale, detailed computations of hydrodynamics, detailed velocity patterns can be derived over an underwater structure. When this is combined with the geometrically translated empirical formula of Katopodis [41], describing maximum flow velocities for fish, a map can be created that indicates which part of the structure should be equipped with habitat elements. The method can also be used iteratively to design ecologically driven coastal structures, for example 3D printed reef elements. To elaborate on this conclusion, the subquestions that were defined in chapter 1 will be discussed in the following sections.

5.1.1. Parameters

The first subquestion was: *'Which ecological and hydrodynamic parameters should be analyzed?'*

In order to answer this question the literature study was conducted. Since both ecological and hydrodynamic processes can be described over a large range of the spatial and temporal scales, it is important to define the scale at which the research is conducted.

Scale The scale at which this method is focused is in the order of meters, and can be defined in two ways:

- **Hydrodynamic:** The near-field environment, i.e. in close vicinity to the structure. At this scale wave transmission (C_t) can be determined. This rules out far-field processes like longshore currents, sediment transport and tidal influence. It is also suitable to solve flow velocities over a structure, under waves.
- **Ecological:** From a reef perspective it is called meso-scale. At this scale habitat geometry and current patterns are defined, which is appropriate for the used parameter of maximum velocity (u_{max}) in the vicinity of the structure.

An overview was created of functions and contributing parameters of both AR and LCS. From this analysis two parameters were selected that could be analyzed simultaneously. For coastal protection this is the transmission coefficient, or C_t , and as ecological threshold this is u_{max} , maximum horizontal velocity.

5.1.2. Method

The second subquestion was stated as: *'What method should be used to provide insight in both functions simultaneously?'*

The integrated design method for both wave transmission and maximum velocity developed is based on the hydrodynamic numerical model SWASH. The model is phase resolving, so it calculates the full wave motion. It is validated by means of physical tests, with a resulting accuracy of >90% for waterlevel and >85% for velocities. By using the defined ecological thresholds, a visual interpretation of the ecological value of the structure by means of velocity limitations is at hand.

5.1.3. 3D printed AR

The last subquestion that was answered is: *'How can this method be used to contribute to the design of 3D printed reefs?'*

The way this method can be used in the design of 3D printed artificial reef units in the nearshore environment, is twofold.

Design on reef-unit scale The method can be used to analyze the influence of the shape of a reef-unit on wave attenuation and ecological habitability on the surface of the structure. This is what is done in this research. This can be extended by applying the method iteratively; alter shape until it fulfills both wave attenuating and maximum velocity requirements.

Also the velocity patterns can be interpreted as limits to which species can be facilitated. When multiple target species of deviating length are defined, within the same cross section different locations can be equipped with specie-specific habitat elements.

Integration of 3D printed elements in conventional breakwater Another approach that can be taken with this method, is to analyze velocity patterns around conventional low crested breakwaters. When a hybrid structure is considered (elaborated on in recommendations), with this tool the location of 3D printed elements in the breakwater can be determined, by looking where favorable velocity conditions occur.

5.2. Case study Sant'Agostino

From the application of this method to the case study of Sant d'Agostino, it is concluded that the current design is not optimal (see figure 5.1) when juvenile Sea Bream is targeted, with these wave conditions and the given geometry of the structure. Also, the wave transmission of the two reef units is 96 percent, which implies that wave damping by the current design is minor.

For the current design, as it is concluded to be insufficient in both coastal protection and habitat creation, it is advised to apply an iterative design approach. In this way the shape of the unit could be optimized looking at the velocity patterns and the maximum velocity patterns, while the desired wave attenuation can be reached by increasing the amount of units. Looking at the formula of Briganti (2.2) in chapter 2, an increase in structure width B will definitely lead to an increase wave damping. Of course the choice to model two units was a simplification of the actual vision how these structures should be applied, in a staggered field (see figure 2.8 on page 19). So when installing multiple reef units in the cross shore direction, it is expected wave damping can be increased to its desired value.

An inaccuracy in SWASH that should be kept in mind is that it overestimates damping of the waves. In this case it overestimates the damping by about 200 percent. This is in this case only 3 percent of the total wave height, but it is unknown if this overestimation will linearly increase when damping increases, or that it will remain a small percentage of the wave height. Therefore it is recommended to evaluate this when further analysis is done.

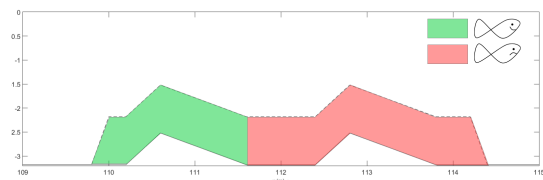


Figure 5.1: Suitability of surface reef for habitat creation

5.3. Method restrictions

The method developed to assess the integrated ecological and coastal performance of this artificial reef breakwater has been found to be suitable because it was possible to prove that the designed structure is unfavorable for the selected species, under the design wave condition. However, this method has limitations to its applicability and accuracy. Discussion of these limitations and their implications on the applicability of the method is necessary. These limitations are split into three categories: self-imposed, tool-induced and knowledge gap.

5.3.1. Self imposed

The first self imposed limitation is that the model is set up in 2DV, which does not account for the full complexity of the system in 3D. The extra dimension can introduce change in the velocity patterns, as on the orientation of the habitat towards the flow direction. Also, when the units are installed in a staggered grid, contraction of the flow in between the units can lead to large velocity gradients, which can not be predicted in 2DV. This tool can therefore robustly be used to assess the along-channel flow fields for structures that are approximately alongshore uniform, like underwater breakwaters. For the application of staggered structures, it is advised to expand the hydrodynamic model to 3D.

A second limitation is that the analysis is carried out for monochromatic waves only. This assumption is not unusual in engineering design modeling. For example, it is common practice for an extreme wave condition to be defined as the governing design criteria in order to determine the limit state of a structure, e.g. the reef should be able to withstand an 1/1000 years wave. However, this is too simplified looking at the ecological functioning. The species considered have a certain lifespan, while of that lifespan they also spend only their juvenile period in the vicinity of reefs. Also, the occurrence of one limit state wave will probably have totally different ecological effects than a continuous wave signal. Therefore it can be said that the approach of looking at the maximum velocity under this monochromatic (extreme) wave condition is too simplified and results in an unnecessarily strict limitation on habitat suitability of the structure. For habitat considerations it could therefore be considered to come up with an alternative 'significant wave' definition. For example a once per year wave, or include the duration of the wave condition (extreme wave condition duration < 1 hour) by means of ecological statistics.

For coastal protection purposes it is important to realize that using a natural wave spectrum, waves will interact different with the structure. For example long waves might travel over the structure undisturbed, which increases the risk of erosion compared to the regular waves.

Third self induced limitation is the robustness of the SWASH model calibration. It is calibrated using one wave conditions. There is no information on how these setting will perform with different boundary conditions. From the physical model data on additional wave climates is available, which can be used to make an assessment of the robustness of the model as it is. This is not done due to time constraints.

5.3.2. Tool-induced

Tool-induced limitations are two-fold. The most significant is that an error was identified in the code where SWASH accounts for porosity. In the vicinity of the porous layer, calculated vertical velocity is zero. Porosity in SWASH is included in the momentum balance in x- and y- directions, but not in z-direction. Assumption here was that this would be corrected automatically through the mass balance, which in this case turned out to be a wrongful assumption. Therefore conservation of mass and momentum is not guaranteed.

Secondly an inaccuracy was found in the physical measurements, when using the Electro Magnetic Sensors to measure horizontal velocity. The disk-shaped instruments showed increasing underestimation of the velocity under the wave crest for higher waves. This was established to be due to the wake effect of the shape of the device. In future wave-measurements it is advised to use either sphere-shaped EMS instruments or 'sideways looking' disk-shaped instruments.

5.3.3. Knowledge gap

The last limitation is the knowledge gap. In this research ecological value is determined using an 'engineering' approach; simplifying the system to a simplified scenario and by looking at this basic system expect that it is to an extent representative for the full system. Unfortunately, this is not how ecological systems work. It is stressed that evaluating a design for one target species does not warrant ecological success. However, alternative design tools for the integration of ecological and coastal protection functions in the marine environment that capture ecological complexity are virtually non-existing.

An example for the engineering approach that a single target species is chosen. In ecological terms this

is very limited, since an ecosystem can not be simplified to one certain species. The factors that contribute to success or failure of an habitat are very extensive, and can not be extrapolated. However, here an effort is made to add to the very limited availability of engineering tools that are also indicative for ecological functioning. Up until now the modeling of ecosystems has proven impossible. Ecologists who come across this tool might therefore be skeptic. The tool might be considered useful for design of the structure to prevent it from failing for this particular parameter, but it is not a measure of added ecological value of the reef.

The main knowledge restriction is that ecological value can not be accurately caught in an hydrodynamic model. Tools are available that allow for high physical complexity to be analyzed. However, ecological complexity is not possible to be included with these tools. This is in essence a limitation in terms of knowledge and understanding.

So, in the light of these limitations, which way can this tool be considered useful? The value in this tool lies in providing a bridge between ecological and engineering approach to submerged structures. It can function as a conversation-starter between engineers and ecologists about the incorporation of habitat in a design. Furthermore, although (because of uncertainties) absolute values might not be correct, the method gives a good understanding of where in a cross-section of the structure less energetic conditions can be found. This can be useful as decision support tool when placing habitat-elements within a given structure design.

5.4. Recommendations

5.4.1. Ecological design

Current design guidelines for ecological influence of LCS are focused on mitigation and minimizing negative effects. This tool, when further developed, could contribute towards a more pro-active approach in the design phase, where the ecological effects of the structure might eventually be considered positive and an asset to the existing ecosystem. In order to get there, a couple of ecologically driven recommendations are defined.

Ecological complexity Tools are available that allow for high physical complexity to be analyzed. However, ecological complexity can not be modeled at a quantitative level just yet. In order to correctly judge the ecological implications of a structure it is therefore very important to incorporate ecological engineers in the design process.

Habitat geometry For now the roughness and porosity of the structures surface has been simplified to a known rock grading class in the physical model. This resulted in a homogeneous cover of the whole reef, in terms of habitat elements (interstitial space). As elaborated on in [53], habitat complexity, so geometrical variance over the AR, is a very important driver for ecological complexity. This is something that in the design could be combined with the varying hydrodynamic conditions along the face of the structure, in order to optimally use its surface for various types of habitat creation. The method can thus be used to determine the placement of certain ecological design elements. It would be interesting to investigate if for other habitat elements (for example overhangs or spikes) other physical parameters than velocity are governing.

5.4.2. Improvement of modeling

Robustness of model It would be worth testing how well the upscaled SWASH model correlates to the other 6 wave conditions that have been generated in the flume. In that way it becomes clear if the settings of the prototype near-field model are characteristic for this type of structure. If this is the case, the model can safely be used for other cases.

SWASH w -velocity It is recommended that research is done on the exact cause of the discrepancy in the calculation of w -velocity in SWASH. Since this problem seems to be caused by an error in the code concerning porosity, it might also serve as an opportunity to see if there is an explanation for the physically unrealistic value for porosity ($n=0.8$).

EMS measurements in waves When assessing the correlation of velocities measured by the EMS meters, it was found that the EMS are underestimating the peak velocities under wave crests. This is caused by a wake effect of the disk-shaped measurement probe. Therefore it is advised for future wave measurements in the flume to use 'sideway' looking EMS meters.

5.4.3. Recommendations for the industry

Economic implications As mentioned in chapter 1, the third pillar of sustainable innovation (see figure 1.2) is economic. This has not been taken into account during this research, but important to be valued upon giving a fully integrated advice on the applicability of this technique. Also it could be interesting to look at alternative applications of the 3D printed technique in coastal engineering. An example is the integration of 3D printed units in a hybrid structure, like a more conventional rubble mound breakwater.

Alternative construction methods If the ecologically enhanced structures proof viable, it is not practical to 3D print on a large scale, since it is not cost and time effective. Therefore other construction methods should be considered. The indispensable characteristics of the 3D printed reefs (if any) should be identified. The material, dredged sediment and an environmentally neutral binder can be utilized by alternative construction methods, like extrusion or molding.

List of Figures

1	Methodology	vii
2	Geometrical translation of ecologically induced velocity threshold (Left image copied from Katopodis [41])	viii
3	Maximum horizontal velocity for positive and negative x-direction	ix
4	Maximum horizontal velocity for positive and negative x-direction, ecological threshold for $u_+=0.51$ m/s and $u_-=-0.66$ m/s indicated with color scheme (green = below threshold)	ix
1.1	General product development framework for Artificial Reefs	2
1.2	Three pillars of sustainable development, source: www.exhibitseed.org	3
1.3	Case study site Sant'Agostino, Italy	4
1.4	Framework for coastline defense AR product development	6
1.5	Methodology of this research	6
1.6	Differentiation of the domains of the four used models. Colors coincide with figure 1.5	7
1.7	Structure of report	8
2.1	Reef balls, source www.reefball.org	11
2.2	Ecological infrastructure (copied from Schiereck [67])	12
2.3	Food chain (as defined in Kolijn [44])	13
2.4	Sea bream, source: www.fishdb.co.uk	13
2.5	Low crested structure dimensions [62]	16
2.6	Geometrical translation of ecologically induced velocity threshold, left image copied from Katopodis [41].	18
2.7	3D printed unit for Monaco pilot project (deep water)	19
2.8	impression of staggered application of monolithic reef units	19
2.9	Ecological and hydrodynamic scales	20
2.10	Focus in analyzing reef design during this study	20
2.11	Spatial distribution of models used	21
3.1	Place of modeling within research (red)	23
3.2	Location of wave data from met/ocean database, <i>caption from Boskalis.world at 06/08/2015</i>	24
3.3	Bathymetry in the vicinity of the case site [40]	24
3.4	Bathymetry in vicinity of the case site, the red circle is the location of the case study site and colors indicate depth. Length of coastline is approx. 400 km	25
3.5	SWAN output point for nearshore wave data	25
3.6	Bottom profile based on case study S't Agostino	26
3.7	Interpolated grid spacing and depth, number of grid cells = 597	26
3.8	10 reef envelopes analyzed in XBeach	27
3.9	Concept of 'structure envelope' with relevant dimensions	27
3.10	Example of points for which wave height is analyzed (zoom of structure envelopes 1-4)	28
3.11	XBeach and SWASH domains	29
3.12	Zoom of domain considered in SWASH and physical tests	29
3.13	4 structures analyzed for varying angle of structure face	30
3.14	Influence on structures 1-4 on water level is negligible	31
3.15	Maximum velocity profile for 4 structures, in 5 sigma layers	31
3.16	Change in wave conditions plotted against wave theories (Le Mehaute ([23]))	33
3.17	Pore and rock size distribution, with a median pore size of 20 cm	35
3.18	Rock sample handling	35
3.19	Characteristics of rock sample (N=156)	36
3.20	Pore size distribution prototype scale	36

3.21	Geometry of steel frame (dimensions in cm)	37
3.22	Flume dimensions (Picture[44])	37
3.23	Overview of test setup	38
3.24	Reef structures in flume	38
3.25	Overview of Vectrino measurements setup	39
3.26	Vectrino (W Uijttewaal, 2013)	39
3.27	Calibration of GHM 1-6, linear conversion coefficient	40
3.28	EMS (W. Uijttewaal, 2013)	41
3.29	Steps in calibration process towards resulting model	41
3.30	location of output locations v_n for SWASH, with the position of vectrino measurements in dotted line	42
3.31	Arrangement of unknowns in a staggered grid: (a) standard layout (central difference scheme) and (b) Keller-box scheme. u is horizontal velocity, w is vertical velocity and q is non-hydrostatic pressure. Copied from Zijlema [77]	44
3.32	Maximum u -velocity for various fish length L and angle of structure α	45
4.1	Place of results and discussion within research (red)	47
4.2	Bottom profile	48
4.3	H_{rms} for 6 scenarios	48
4.4	10 reef envelopes analyzed in XBeach	49
4.5	Wave-height decrease over structure envelopes 1-10	49
4.6	Transmission of waves per square meter cross sectional area of structures 1-10 (wave scenario 4)	49
4.7	Measured wave signal of wave climates 1 to 5	50
4.8	Comparison of theoretical Stokes wave vs. measured signal for wave condition 5	50
4.9	Example maximum and mean wave heights in GHM 1 to 6	52
4.10	Maximum wave height for wave conditions 1-5, along the flume, with (solid) and without (dotted) structure	52
4.12	Outlier cancellation: manual selection (example for wave condition 1)	53
4.11	Errors in Vectrino measurement (Wave condition 1)	53
4.13	Noise obtained by subtracting mean signal from measured time series, wave condition 5. Lines at $u = \pm 0.05$ m/s	54
4.14	Mean velocity signal wave climate 5, highest and lowest correlation for u and w velocity	54
4.15	Steps in calibration process towards resulting model	54
4.16	Two methods of signal synchronization with Pearson correlation coefficient	55
4.17	Results of validation, not compensated for phase shift (Wave condition 2)	55
4.18	Results of validation compensated for phase shift (Wave condition 5)	55
4.19	Underestimation of velocity under wave crest by EMS	56
4.20	Shape of wave signal compared with SWASH and flume, example GHM3 and GHM4	57
4.21	Average correlation for various porosity and β	57
4.22	correlation for various porosity and β , for GHM 4	57
4.23	spatial result of calibrated settings, for $n=0.38$ and $n=0.8$	58
4.24	Location of measured and calculated velocity (for two σ -layers)	58
4.25	Comparison of measured and calculated velocity (for two layers), example for EMS 1	58
4.26	comparison water level between upscaled flume measurement and SWASH prototype scale	59
4.27	Vectrino u -velocities (upscaled) compared to SWASH results - prototype scale	60
4.28	Discontinuity in velocity pattern, no w -velocity in vicinity of porous layer	60
4.29	Velocity pattern without porous layer, w -velocity is present	61
4.30	Maximum u -velocities in positive and negative direction	62
4.31	Maximum velocities in positive and negative x-direction, threshold for $u_+=0.51$ m/s and $u_-=-0.66$ m/s indicated with color scheme	63
4.32	Ecological thresholds applied to domain without structure	63
4.33	Theoretical maximum u -velocity (positive and negative)	63
4.34	Patchiness in PIV measurements (flume scale; does not match SWASH prototype magnitudes)	64
4.35	Suitability of surface reef for habitat creation	64
5.1	Suitability of surface reef for habitat creation	66

B.1	Offshore wave climate	84
B.2	Grids for worldwaves wave calculations	85
B.3	worldwaves output point	85
B.4	Scatter plots and extrapolation of results EVA	87
C.1	Count of food sources required by Level 1 species	90
D.1	Building method reef structure for flume testing (2DV)	95
E.1	Flume testing matrix	101
G.1	Wave condition 1 - Fourier	107
G.2	Wave condition 2 - Fourier	108
G.3	Wave condition 3 - Fourier	108
G.4	Wave condition 4 - Fourier	108
G.5	Wave condition 5 - Fourier	109
H.1	Short wave signal	111
H.2	Short wave height (H_{rms}) at $x=1887$ m	111
H.3	Transformation long wave influence on beginning of SWASH domain	112
H.4	Measured wave signal of wave climates 6 and 7	113
H.5	result of a 8-term Fourier analysis on wave condition 6	113
H.6	Wave condition 6 - Sum of sine	114
H.7	Wave condition 7 - Sum of sine	114
I.1	higher harmonic disturbances in SWASH due to water level boundary condition	115
I.2	Equidistant layers for velocity boundary conditions	116
K.1	Water level correlation, 2 layers, no structure	120
K.2	Water level correlation, 5 layers	121
K.3	U -velocity correlation (EMS), 5 layers	121
K.4	U -velocity correlation (Vectrino), 5 layers	121
L.1	Power spectrum for vectrino measurements in u -direction	123
M.2	Tracks of the laser sheet and synchronization points	125
M.1	Principle of setup PIV	125
M.3	Coordinates of PIV time series	126
M.4	overlay of vectrino and PIV measurements in x and z directions for location V2.2 and V2.3	127

List of Tables

1.1	Problem description	4
3.1	Peak over Threshold results for location 6	25
3.2	Wave condition scenarios in deep water	27
3.3	Dimensions of 10 reef envelopes	28
3.4	Values for factors in Mannings roughness coefficient	30
3.5	Froude scaling laws	32
3.6	Monochromatic wave conditions used in this physical measurement campaign	32
3.7	New wave conditions	33
3.8	Rock grading in accordance to a median pore-size of 0.2 meter	35
3.9	Scaled rock grading characteristics	35
3.10	Rock grading characteristics	36
3.11	Rock grading according to grading test - Prototype scale	36
3.12	Distance between probes, following Lin & Huang theory	40
3.13	Values for turbulent friction factor β from literature	43
3.14	Specifications of SWASH setup	43
4.1	Deep water wave climates and their shallow water conditions at $z = -2.0$ m	48
4.2	Analysis of wave transmission for structure envelopes 1-10	49
4.3	Wave conditions for physical model	50
4.4	Reflection of wave conditions	51
4.5	Reflection with and without reef, before structure (GHM3)	51
4.6	Reflection with and without reef, after structure (GHM4)	51
4.7	Transmission coefficient $C_t (H_{out}/H_{in})$	52
4.8	Specification of Fourier analysis of Vectrino data, u -velocity, position V1.2	53
4.9	Correlation fit Vectrino u - and w -velocity	54
4.10	Correlation of calibration runs	56
4.11	comparison of reflection and transmission for porosities $n=0.38$ and $n=0.8$	57
4.12	Correlation water level for prototype scale	59
4.13	Correlation Vectrino u -velocities prototype scale	60
4.14	Prototype scale reflection and transmission for calibrated SWASH model	61
B.1	Results of EVA location 6	86
B.2	Results of EVA for corresponding peak period location 6	86
C.1	Primary and secondary consumers common in Mediterranean, reef associated shallow waters	89
G.1	Specification of Fourier analysis of Vectrino data, u -velocity, position V1.2	107
H.1	Analysis of wave transmission for structure envelopes 1-10 - surf beat mode	112
H.2	Bi-chromatic wave conditions	113
H.3	Results of sum of sine analysis Vectrino data	113
I.1	Values for z_1 and z_2 for 2 equidistant layers	116
K.1	Correlation, 2 layers, no structure	119
K.2	Water level correlation, 2 layers	119
K.3	Water level correlation, 5 layers	120

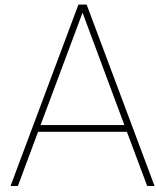
Bibliography

- [1]
- [2]
- [3] HD Armono and KR Hall. Wave transmission on submerged breakwaters made of hollow hemispherical shape artificial reefs. In *Canadian Coastal Conference*, pages 313–322, 2003.
- [4] Mark Baine. Artificial reefs: a review of their design, application, management and performance. *Ocean and Coastal Management*, 44(3):241–259, 2001.
- [5] JA Bohnsack. Habitat structure and the design of artificial reefs. In *Habitat Structure*, pages 412–426. Springer, 1991.
- [6] James A Bohnsack and David L Sutherland. Artificial reef research: a review with recommendations for future priorities. *Bulletin of Marine Science*, 37(1):11–39, 1985.
- [7] Bas W Borsje, Bregje K van Wesenbeeck, Frank Dekker, Peter Paalvast, Tjeerd J Bouma, Marieke M van Katwijk, and Mindert B de Vries. How ecological engineering can serve in coastal protection. *Ecological Engineering*, 37(2):113–122, 2011.
- [8] Stephen A Bortone. A perspective of artificial reef research: the past, present, and future. *Bulletin of Marine Science*, 78(1):1–8, 2006.
- [9] Stephen A Bortone, Tony Martin, and Charles M Bundrick. Factors affecting fish assemblage development on a modular artificial reef in a northern gulf of mexico estuary. *Bulletin of Marine Science*, 55(2-3): 319–332, 1994.
- [10] Richard E Brock and James E Norris. An analysis of the efficacy of four artificial reef designs in tropical waters. *Bulletin of Marine Science*, 44(2):934–941, 1989.
- [11] Mark Buckley, Ryan Lowe, and Jeff Hansen. Evaluation of nearshore wave models in steep reef environments. *Ocean Dynamics*, 64(6):847–862, 2014.
- [12] KW Buijs. *Ecology-based bed protection of offshore wind turbines*. PhD thesis, TU Delft, Delft University of Technology, 2015.
- [13] HF Burcharth and OK Andersen. On the one-dimensional steady and unsteady porous flow equations. *Coastal engineering*, 24(3):233–257, 1995.
- [14] Yong-gang Cao, Chang-bo Jiang, and Yu-chuan Bai. Numerical study on flow structure near two impermeable trapezoid submerged breakwaters on slop bottoms. *Journal of Hydrodynamics, Ser. B*, 22(5): 190–196, 2010.
- [15] L Cavaleri. The wind and wave atlas of the mediterranean sea-the calibration phase. *Advances in Geosciences*, 2(2):255–257, 2005.
- [16] Kun-Hsiung Chang. Review of artificial reefs in taiwan: emphasizing site selection and effectiveness. *Bulletin of Marine Science*, 37(1):143–150, 1985.
- [17] Eric Charbonnel, Christophe Serre, Sandrine Ruitton, Jean-Georges Harmelin, and Antony Jensen. Effects of increased habitat complexity on fish assemblages associated with large artificial reef units (french mediterranean coast). *ICES Journal of Marine Science: Journal du Conseil*, 59(suppl):S208–S213, 2002.

- [18] Adrien Cheminee, Enric Sala, Jeremy Pastor, Pascaline Bodilis, Pierre Thiriet, Luisa Mangialajo, Jean-Michel Cottalorda, and Patrice Francour. Nursery value of cystoseira forests for mediterranean rocky reef fishes. *Journal of experimental marine biology and ecology*, 442:70–79, 2013.
- [19] Kees d'Angremond and F Van Roode. *Breakwaters and closure dams*. CRC Press, 2004.
- [20] Robert George Dean and Robert A Dalrymple. *Water wave mechanics for engineers and scientists*. Advanced Series on Ocean Engineering. World Scientific Publishing, Singapore, 1991.
- [21] Stichting Deltares. Xbeach open source community, 2016.
- [22] Gianna Fabi, Alessandra Spagnolo, Denise Bellan-Santini, Eric Charbonnel, Burak Ali Çiçek, Juan J Goutayer García, Antony C Jensen, Argiris Kallianiotis, and Miguel Neves dos Santos. Overview on artificial reefs in europe. *Brazilian Journal of Oceanography*, 59(SPE1):155–166, 2011.
- [23] JD Fenton. Nonlinear wave theories. *the Sea*, 9(1):3–25, 1990.
- [24] Carlos EL Ferreira, Jose EA Gonççaves, and Ricardo Coutinho. Community structure of fishes and habitat complexity on a tropical rocky shore. *Environmental Biology of Fishes*, 61(4):353–369, 2001.
- [25] Alan Friedlander, James Beets, and William Tobias. Effects of fish aggregating device design and location on fishing success in the us virgin islands. *Bulletin of Marine Science*, 55(2-3):592–601, 1994.
- [26] Lynne E Frostick, Stuart J McLelland, and Theresa G Mercer. *Users Guide to Physical Modelling and Experimentation: Experience of the HYDRALAB Network*. CRC Press, 2011.
- [27] N Garcia, JL Lara, and IJ Losada. 2-d numerical analysis of near-field flow at low-crested permeable breakwaters. *Coastal Engineering*, 51(10):991–1020, 2004.
- [28] Yoshimi Goda and Tasumasa Suzuki. Estimation of incident and reflected waves in random wave experiments. *Coastal engineering proceedings*, 1(15), 1976.
- [29] Michael R Gourlay and Gildas Colleter. Wave-generated flow on coral reefs—an analysis for two-dimensional horizontal reef-tops with steep faces. *Coastal Engineering*, 52(4):353–387, 2005.
- [30] MR Gourlay. Wave transformation on a coral reef. *Coastal Engineering*, 23(1):17–42, 1994.
- [31] Lee E Harris. Artificial reefs for ecosystem restoration and coastal erosion protection with aquaculture and recreational amenities. *Reef Journal*, 1(1):235–246, 2009.
- [32] Lee E Harris and Lee E Harris. Artificial reef structures for shoreline stabilization and habitat enhancement. In *Proceedings of the 3rd International Surfing Reef Symposium*, pages 176–178, 2003.
- [33] Stephen J Hawkins, Hans Falk Burcharth, Barbara Zanuttigh, and Alberto Lamberti. *Environmental design guidelines for low crested coastal structures*. Elsevier, 2010.
- [34] Clifford J Hearn. Perspectives in coral reef hydrodynamics. *Coral Reefs*, 30(1):1–9, 2011.
- [35] R. Hill, H. Vissers. 3d printed reefs. *Boskalis Magazine*, (3), 11/2015 2015.
- [36] Bas Hoonhout. Xbeach documentation. 2015.
- [37] Michael Isaacson. Measurement of regular wave reflection. *Journal of Waterway, Port, Coastal, and Ocean Engineering*, 117(6):553–569, 1991.
- [38] Leslie Angus Jackson and Bobbie B Corbett. Review of existing multi-functional artificial reefs. In *Australasian Conference on Coasts and Ports, Melbourne, Australia*, pages 1–6, 2007.
- [39] Anes Jakupovic. Large scale additive manufacturing, d-shape: Material characterization and optimization. Technical report, University of Trieste, 2013.
- [40] Jeppesen. Jeppesen c-map charts in high detail, 2015.
- [41] Chris Katopodis. Fish screening guide for water intakes. *Working Document, Freshwater Institute, Fisheries and Oceans Canada, Winnipeg, Man*, page 5, 1992.

- [42] Evamaria W Koch. Beyond light: physical, geological, and geochemical parameters as possible submersed aquatic vegetation habitat requirements. *Estuaries*, 24(1):1–17, 2001.
- [43] MRA Koehl. Mini review: hydrodynamics of larval settlement into fouling communities. *Biofouling*, 23(5):357–368, 2007.
- [44] Danker J Kolijn. *Effectiveness of a multipurpose artificial underwater structure as a coral reef canopy: hydrodynamic and ecological connectivity*. PhD thesis, TU Delft, Delft University of Technology, 2014.
- [45] RJ Leewis, Ies de Vries, and Hermien Busschbach. Lessons from a controversial experiment. In *The responses of marine organisms to their environments. Proceedings of the 30th European Marine Biology Symposium*, pages 327–36, 1995.
- [46] Jamie Lescinski. Environmental impact assessment. Technical report, FPA2, 12-03 2015.
- [47] Inigo J Losada, Javier L Lara, Erik D Christensen, and Nicolas Garcia. Modelling of velocity and turbulence fields around and within low-crested rubble-mound breakwaters. *Coastal Engineering*, 52(10):887–913, 2005.
- [48] Ryan J Lowe, James L Falter, Marion D Bandet, Geno Pawlak, Marlin J Atkinson, Stephen G Monismith, and Jeffrey R Koseff. Spectral wave dissipation over a barrier reef. *Journal of Geophysical Research: Oceans (1978-2012)*, 110(C4), 2005.
- [49] Ryan J Lowe, James L Falter, Jeffrey R Koseff, Stephen G Monismith, and Marlin J Atkinson. Spectral wave flow attenuation within submerged canopies: Implications for wave energy dissipation. *Journal of Geophysical Research: Oceans (1978-2012)*, 112(C5), 2007.
- [50] S Mead. Multiple-use options for coastal structures: Unifying amenity, coastal protection and marine ecology. *Reef Journal*, 1(1):291–311, 2009.
- [51] BA Mellink. *Numerical and experimental research of wave interaction with a porous breakwater*. PhD thesis, TU Delft, Delft University of Technology, 2012.
- [52] Stephen G Monismith. Hydrodynamics of coral reefs. *Annu. Rev. Fluid Mech.*, 39:37–55, 2007.
- [53] PS Moschella, M Abbiati, Per Aberg, L Airoidi, JM Anderson, F Bacchiocchi, F Bulleri, Grete E Dinesen, M Frost, and E Gacia. Low-crested coastal defence structures as artificial habitats for marine life: using ecological criteria in design. *Coastal Engineering*, 52(10):1053–1071, 2005.
- [54] Olivier Musard, Laurence Le Du-Blayo, Patrice Francour, Jean-Pierre Beurier, Eric Feunteun, and Luc Talassinos. *Underwater Seascapes: From geographical to ecological perspectives*. Springer Science & Business Media, 2014.
- [55] Makoto Nakamura. Evolution of artificial fishing reef concepts in japan. *Bulletin of Marine Science*, 37(1):271–278, 1985.
- [56] Robert J Nicholls, Frank MJ Hoozemans, and Marcel Marchand. Increasing flood risk and wetland losses due to global sea-level rise: regional and global analyses. *Global Environmental Change*, 9:S69–S87, 1999.
- [57] AS Nortek. Vectrino velocimeter user guide. *Nortek AS, Vangkroken, Norway*, 2009.
- [58] Helen Pickering, David Whitmarsh, and Antony Jensen. Artificial reefs as a tool to aid rehabilitation of coastal ecosystems: investigating the potential. *Marine Pollution Bulletin*, 37(8):505–514, 1999.
- [59] Nigel Pontee. Defining coastal squeeze: a discussion. *Ocean & coastal management*, 84:204–207, 2013.
- [60] V; Bailey M Price, B; Fay. Guidelines for siting, construction, development, and assessment of artificial reefs. Technical report, US Dept. of Commerce, National Oceanic and Atmospheric Administration, 2007.
- [61] AJHM Reniers, EB Thornton, TP Stanton, and JA Roelvink. Vertical flow structure during sandy duck: observations and modeling. *Coastal Engineering*, 51(3):237–260, 2004.

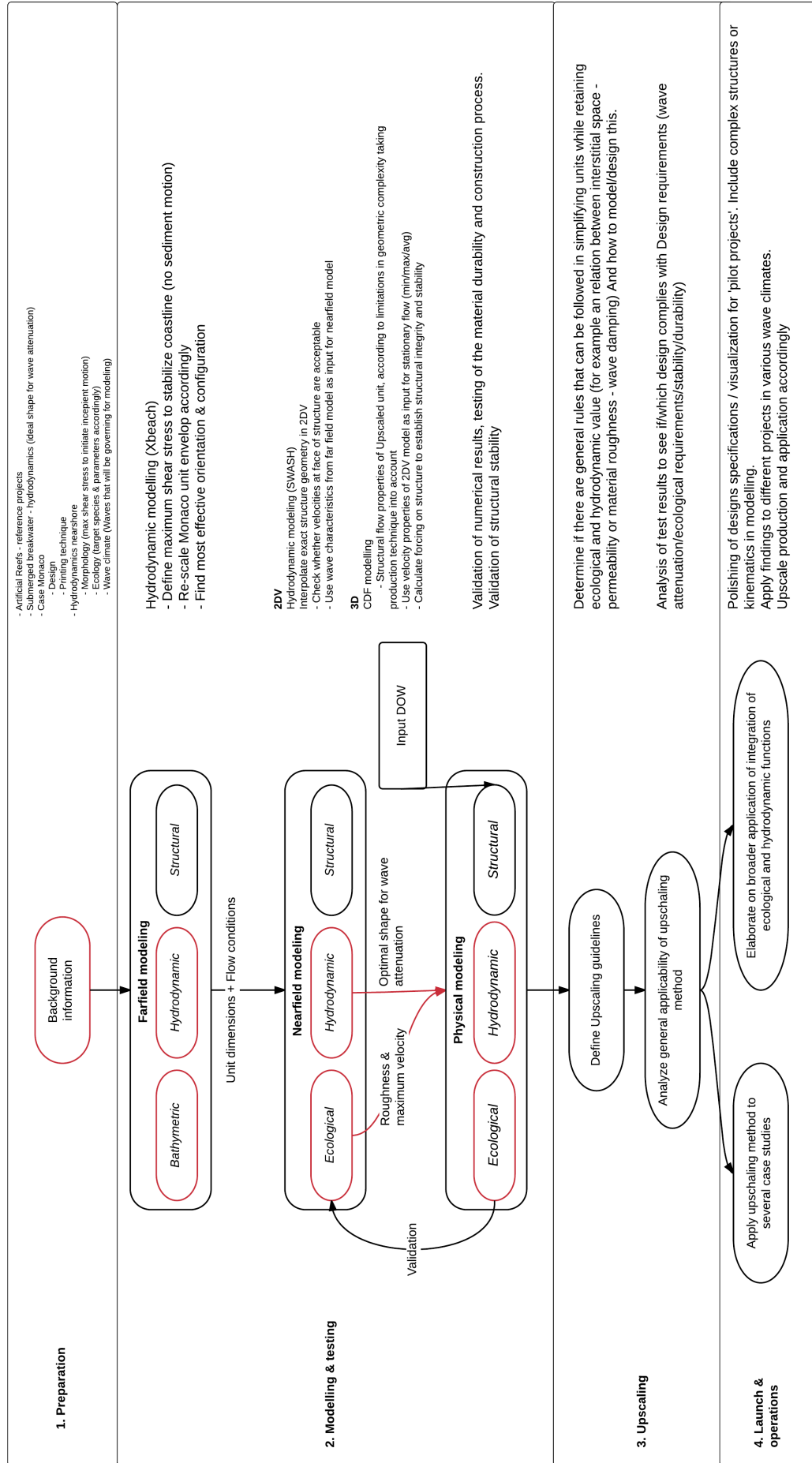
- [62] Construction Industry Research, Information Association, Civieltechnisch Centrum Uitvoering Research en Regelgeving, and Centre d'études maritimes et fluviales. *The Rock Manual: The use of rock in hydraulic engineering*, volume 683. Ciria, 2007.
- [63] George Stephen Ritchie. The admiralty chart. *Military Engineer (US Army)*, 9:389–180, 1967.
- [64] Emma Rochelle-Newall, Richard JT Klein, Robert J Nicholls, Kevin Barrett, Horst Behrendt, Ton HM Bresser, Andrzej Cieslak, Erwin FLM de Bruin, Tony Edwards, Peter MJ Herman, et al. Group report: global change and the european coast—climate change and economic development. In *Managing European Coasts*, pages 239–254. Springer, 2005.
- [65] Enric Sala, Enric Ballesteros, Panagiotis Dendrinou, Antonio Di Franco, Francesco Ferretti, David Foley, Simonetta Frascchetti, Alan Friedlander, Joaquim Garrabou, and Harun Guçlusoy. The structure of mediterranean rocky reef ecosystems across environmental and human gradients, and conservation implications. *PloS one*, 7(2):e32742, 2012.
- [66] Sarah Sangster. *A design study of nature friendly banks made of residual material to enhance biodiversity in a port*. PhD thesis, Delft University of Technology, 2015.
- [67] Gerrit J Schiereck. *Introduction to bed, bank and shore protection*. CRC Press, 2003.
- [68] Robin L Sherman, David S Gilliam, and Richard E Spieler. Artificial reef design: void space, complexity, and attractants. *ICES Journal of Marine Science: Journal du Conseil*, 59(suppl):S196–S200, 2002.
- [69] Richard E Spieler, David S Gilliam, and Robin L Sherman. Artificial substrate and coral reef restoration: what do we need to know to know what we need. *Bulletin of Marine Science*, 69(2):1013–1030, 2001.
- [70] MJF Stive and J Bosboom. Coastal dynamics i: lectures notes cie4305. 2012.
- [71] Graham Symonds, Kerry P Black, and Ian R Young. Wave-driven flow over shallow reefs. *Journal of Geophysical Research: Oceans (1978-2012)*, 100(C2):2639–2648, 1995.
- [72] Pierre Thiriet, Adrien Cheminee, Luisa Mangialajo, and Patrice Francour. How 3d complexity of macrophyte-formed habitats affect the processes structuring fish assemblages within coastal temperate seascapes? In *Underwater Seascapes*, pages 185–199. Springer, 2014.
- [73] RIO TINTO. A practical guide to the construction and management of artificial reefs in northwestern australia.
- [74] I Verdegaal. *The influence of core permeability on the stability of interlocking, single layer armour units*. PhD thesis, TU Delft, Delft University of Technology, 2013.
- [75] IK Workman and JW Watson. Artificial reefs as refuge for juvenile red snappers (*lutjanus campechanus*) on shrimp fishing grounds in the gulf of mexico. In *Proceedings of the International Conference on Ecological System Enhancement Technology for Aquatic Environments*, volume 2, pages 663–666, 1995.
- [76] Ben Chie Yen. Open channel flow resistance. *Journal of hydraulic engineering*, 128(1):20–39, 2002.
- [77] Marcel Zijlema. Swash user manual, 22/02/2016 2015.



Product development framework

The complete product development framework, as touched upon in section 1.4 is visualized again, with the proposed actions that are involved in the step that they are adjacent to. This is shown in the schedule on the next page.

Product Development Framework



B

SWAN input & Extreme value analysis

The detailed wave climate from the offshore wave buoy from MET-ocean, near the case site of Bay Bagni Sant'Agostino is pictured in B.1. The location of the wave data is indicated in 3.2.

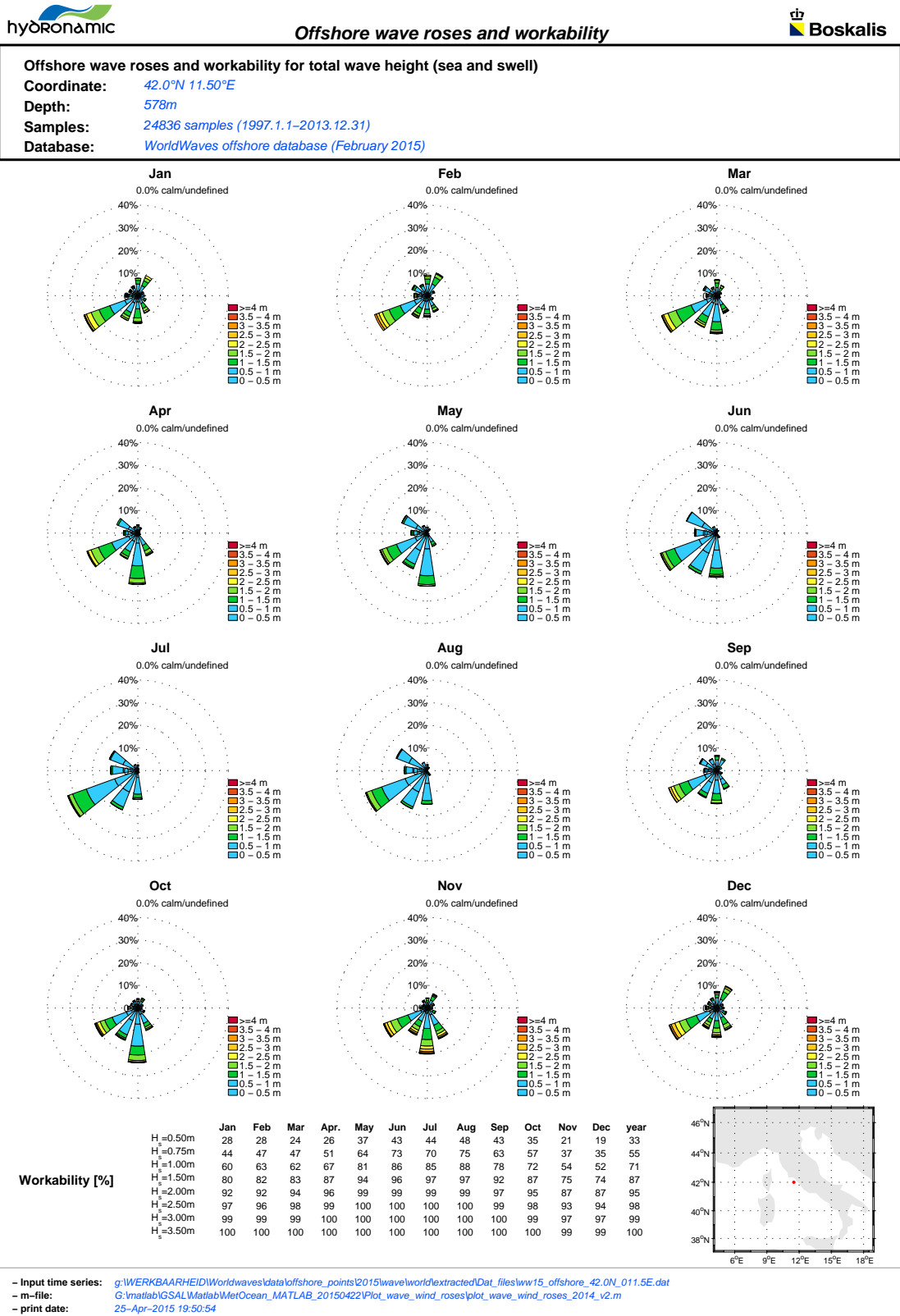


Figure B.1: Offshore wave climate

Wave modeling

The grid used in SWAN / Worldwaves, an in-house tool at Boskalis that makes use of the SWAN wave modeling code, is indicated in B.2. The larger grid has a grid cell spacing of 1000 m, for the nested detailed grid the cell size is 100 m.

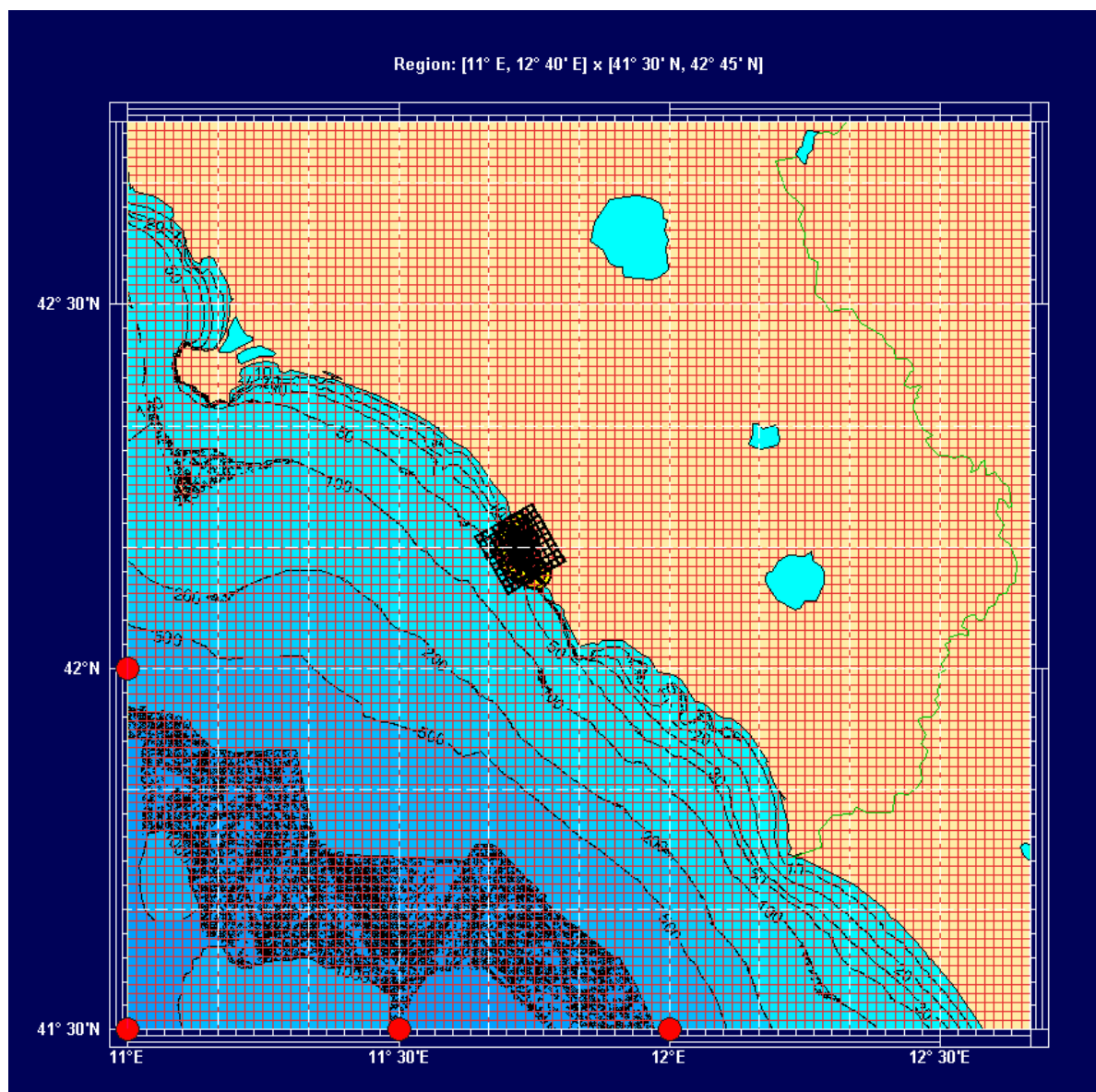


Figure B.2: Grids for worldwaves wave calculations

Extreme Value Analysis

After the offshore data from MET-ocean is translated by SWAN, an extreme value analysis is done to determine the governing wave condition. This wave condition will be used in further analysis, in order to limit complexity. An EVA is done to estimate the probability of an unusually large storm event, based on a dataset which might not cover a long period of time. The EVA is carried out on the output of SWAN, pictures in B.3.

There are two approaches for an EVA. It can either be based on a series of annual maxima (AMS) or a certain threshold above



Figure B.3: worldwaves output point

Table B.1: Results of EVA location 6

Directional design values for the Wave Height Hsig [m] (All waves)								
Coordinates: 42°9.8'N, 11°42.3'E								
Period: January-December								
Directional Sector		Design Value Hss (m)					RSQ	No. of Samples
Lbounds	Ubounds	Return Period (Years)						
		1	10	50	100	1000		
345	15							0
15	165							0
165	195	2.3	3.1	3.7	3.9	4.5	0.989	107
195	225	3.1	4.2	4.7	4.9	5.5	0.985	88
225	255	3.7	5.0	5.9	6.2	7.4	0.993	303
255	285	2.3	4.1	4.7	5.0	5.7	0.986	31
285	315							3
315	345							1
0	360	3.9	5.0	5.7	5.9	6.8	0.994	533
Omni		3.9	5.0	5.7	5.9	6.8	0.994	533

Table B.2: Results of EVA for corresponding peak period location 6

Associated Peak wave period [s] (All waves)							
Directional Sector		Return Period (Years)					
Lbounds	Ubounds	1	10	50	100	1000	
345	15						
15	165						
165	195	8.1	9.5	10.3	10.6	11.4	
195	225	8.6	9.9	10.5	10.7	11.4	
225	255	9.4	11.0	11.9	12.2	13.3	
255	285	7.2	9.5	10.2	10.5	11.2	
285	315						
315	345						
0	360	9.8	11.1	11.8	12.1	12.9	
Omni		9.8	11.1	11.8	12.1	12.9	

which conditions are considered storm. This method is called Peak over Threshold (POT) and is used in this EVA. The threshold has to be manually determined. In this case after an iterative proces the threshold of 1.5 m is chosen.

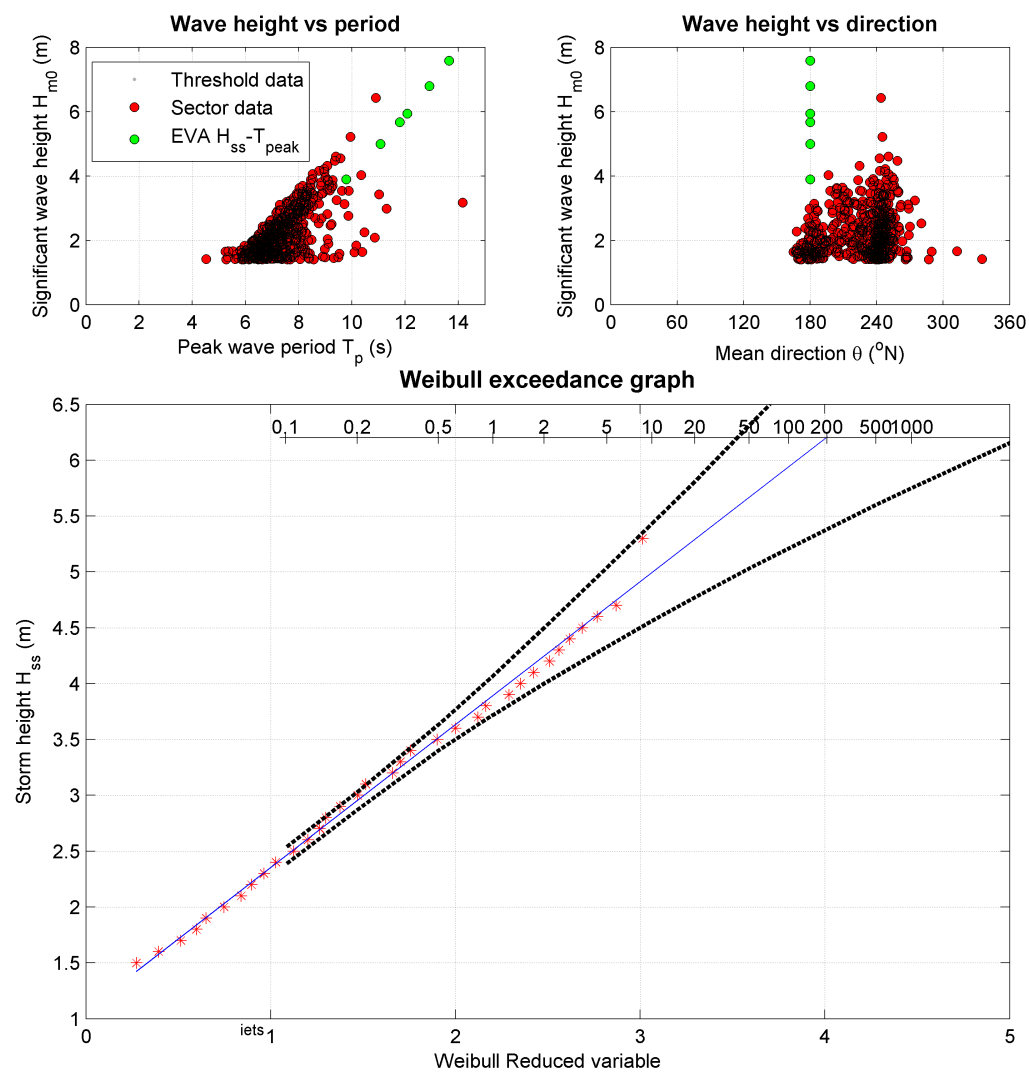


Figure B.4: Scatter plots and extrapolation of results EVA

C

Target species

An attempt was made to do an ecological analysis, in order to arrive at a target species that will have positive influence in the whole ecosystem. By using the species database www.fishbase.org (freely accessible database, established, modified and checked by over 500 collaborators worldwide).

- A first selection of reef associated, Mediterranean, native species was made.
- This list was narrowed down by looking at the depth preferences and habitat definitions.

Table C.1: Primary and secondary consumers common in Mediterranean, reef associated shallow waters

specie	Scientific name	English name	Habitat
1. Juvenile grouper	<i>Epinephelus marginatus</i>	Dusky Grouper	rocky bottoms
2. Wrasse	<i>Ctenolabrus rupestris</i>	Goldsinny-wrasse	On rocky weed-covered shores
	<i>Labrus merula</i>	Brown wrasse	around rocks and seaweeds
	<i>Labrus mixtus</i>	Cuckoo wrasse	algal zone of rocky shores
	<i>Labrus viridis</i>	Green Wrasse	littoral zone near rocks and eel-grass beds
	<i>Symphodus melanocercus</i>		in rocky areas and seagrass beds
	<i>Symphodus melops</i>	Corkwing wrasse	near rocks and eel-grass bed lagoons
	<i>Symphodus ocellatus</i>		near rocks and eel-grass beds.
	<i>Symphodus roissali</i>	Five-spotted wrasse	near rocks mainly in eel-grass beds
	<i>Symphodus rostratus</i>		near rocks mainly in eel-grass beds
	<i>Symphodus tinca</i>	East Atlantic peacock wrasse	near rocks mainly in eel-grass beds sometimes in salty lagoons
	<i>Thalassoma pavo</i>	Ornate wrasse	coastal waters near rocks and eel-grass beds
	<i>Coris julis</i>	Mediterranean rainbow wrasse	littoral zone near rocks and eelgrass bed
3. Damselfish	<i>Chromis chromis</i>	Damselfish	in midwater above or near rocky reefs or above seagrass meadows
4. Cardinal Fish	<i>Apogon imberbis</i>	Cardinal fish	Inhabits muddy or rocky bottoms and cave
5. Flying gurnard	<i>Dactylopterus volitans</i>	Flying gurnard	sand mud or over rocks in sandy areas
	<i>Grammonus ater</i>		shallow rocky areas hides in caves during the day
6. Bermuda sea chub	<i>Kyphosus sectatrix</i>	Bermuda sea chub	shallow waters over turtle grass and or rocky bottom and around coral reefs
7. Mediterranean moray	<i>Muraena helena</i>	Mediterranean moray	under rocks or corals.
8. Molly miller	<i>Scartella cristata</i>	Molly miller	shallow rocky areas and tide pools
9. Nursehound	<i>Scyliorhinus stellaris</i>	Nursehound	rough even rocky or coralline ground and algal-covered bottoms
10. Marbled electric ray	<i>Torpedo marmorata</i>	Marbled electric ray	seagrass areas rocky reefs and adjacent soft bottoms
11. Flatfish (general)	<i>Pleuronectiformes</i>	Flounder, Sole, Tarbot	Near shore, sheltered sandy bottoms
12. Juvenile sea bream	<i>Pagrus auratus</i>	Sea bream / Dorada	rocky reefs

Foodsource

The food source of the species was examined, leading to the rough estimation of the count in C.1. Multiple food sources per species were found so the count does not add up to a significant number.

The red counts are the sum of that class. This is to create a rough overview of food source for Level 1 target species, the classes are not verified to be ecologically correct. The food sources with a black lining are most important, since they act as a food source to the most level 1 species. This level is no further taken into account for this research, since it is assumed that geometric variability and physical properties on meso-scale are governed by the primary and secondary consumer species.

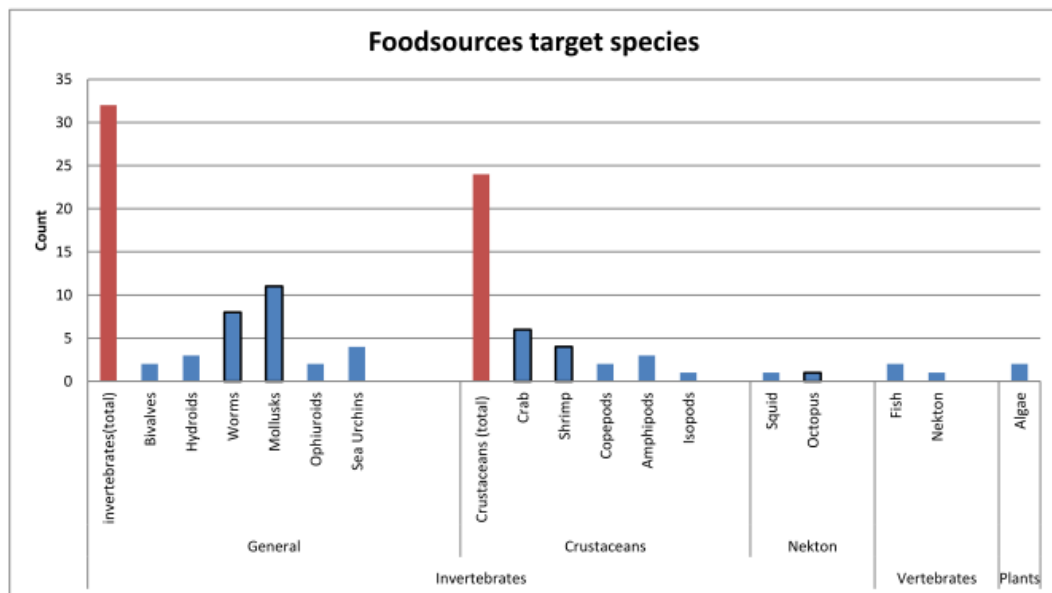


Figure C.1: Count of food sources required by Level 1 species



Rock grading & construction reef

In this appendix the data on the rock grading that was performed on the sample showed in figure 3.18b on page 35 is summed up. After this the construction method of the reef is described by means of pictures.

Rock grading

The rock sample weight measurements and calculated diameters as well as probability distribution are documented in the following table.

sample #	Cumulative weight [g]	$P_c = R_i / (N + 1)$	D_{n50} [m]	D_{50} [m]
1	25	0.0064	0.0200	0.0238
2	64	0.0127	0.0232	0.0276
3	103	0.0191	0.0232	0.0276
4	144	0.0255	0.0236	0.0281
5	186	0.0318	0.0238	0.0283
6	229	0.0382	0.0240	0.0285
7	272	0.0446	0.0240	0.0285
8	315	0.0510	0.0240	0.0285
9	361	0.0573	0.0245	0.0292
10	408	0.0637	0.0247	0.0294
11	457	0.0701	0.0250	0.0298
12	507	0.0764	0.0252	0.0300
13	557	0.0828	0.0252	0.0300
14	608	0.0892	0.0254	0.0302
15	659	0.0955	0.0254	0.0302
16	710	0.1019	0.0254	0.0302
17	762	0.1083	0.0255	0.0304
18	814	0.1146	0.0255	0.0304
19	867	0.1210	0.0257	0.0306
20	920	0.1274	0.0257	0.0306
21	973	0.1338	0.0257	0.0306
22	1027	0.1401	0.0259	0.0308
23	1081	0.1465	0.0259	0.0308
24	1136	0.1529	0.0260	0.0310
25	1192	0.1592	0.0262	0.0312
26	1249	0.1656	0.0263	0.0314
27	1306	0.1720	0.0263	0.0314
28	1363	0.1783	0.0263	0.0314
29	1421	0.1847	0.0265	0.0315
30	1480	0.1911	0.0266	0.0317

sample #	Cumulative weight [g]	$P_c = R_i / (N + 1)$	D_{n50} [m]	D_{50} [m]
31	1540	0.1975	0.0268	0.0319
32	1600	0.2038	0.0268	0.0319
33	1662	0.2102	0.0271	0.0322
34	1724	0.2166	0.0271	0.0322
35	1786	0.2229	0.0271	0.0322
36	1848	0.2293	0.0271	0.0322
37	1910	0.2357	0.0271	0.0322
38	1973	0.2420	0.0272	0.0324
39	2037	0.2484	0.0274	0.0326
40	2102	0.2548	0.0275	0.0328
41	2167	0.2611	0.0275	0.0328
42	2232	0.2675	0.0275	0.0328
43	2298	0.2739	0.0277	0.0329
44	2364	0.2803	0.0277	0.0329
45	2431	0.2866	0.0278	0.0331
46	2498	0.2930	0.0278	0.0331
47	2566	0.2994	0.0279	0.0333
48	2635	0.3057	0.0281	0.0334
49	2704	0.3121	0.0281	0.0334
50	2774	0.3185	0.0282	0.0336
51	2847	0.3248	0.0286	0.0341
52	2921	0.3312	0.0287	0.0342
53	2996	0.3376	0.0289	0.0344
54	3071	0.3439	0.0289	0.0344
55	3148	0.3503	0.0291	0.0347
56	3226	0.3567	0.0292	0.0348
57	3304	0.3631	0.0292	0.0348
58	3384	0.3694	0.0295	0.0351
59	3464	0.3758	0.0295	0.0351
60	3546	0.3822	0.0297	0.0354
61	3629	0.3885	0.0299	0.0355
62	3712	0.3949	0.0299	0.0355
63	3795	0.4013	0.0299	0.0355
64	3878	0.4076	0.0299	0.0355
65	3962	0.4140	0.0300	0.0357
66	4047	0.4204	0.0301	0.0358
67	4132	0.4268	0.0301	0.0358
68	4218	0.4331	0.0302	0.0360
69	4304	0.4395	0.0302	0.0360
70	4393	0.4459	0.0306	0.0364
71	4482	0.4522	0.0306	0.0364
72	4571	0.4586	0.0306	0.0364
73	4660	0.4650	0.0306	0.0364
74	4752	0.4713	0.0309	0.0368
75	4845	0.4777	0.0310	0.0369
76	4939	0.4841	0.0311	0.0370
77	5034	0.4904	0.0312	0.0372
78	5130	0.4968	0.0313	0.0373
79	5227	0.5032	0.0314	0.0374
80	5324	0.5096	0.0314	0.0374
81	5423	0.5159	0.0317	0.0377
82	5523	0.5223	0.0318	0.0378
83	5624	0.5287	0.0319	0.0379

sample #	Cumulative weight [g]	$P_c = R_i / (N + 1)$	D_{n50} [m]	D_{50} [m]
84	5726	0.5350	0.0320	0.0381
85	5828	0.5414	0.0320	0.0381
86	5931	0.5478	0.0321	0.0382
87	6035	0.5541	0.0322	0.0383
88	6140	0.5605	0.0323	0.0384
89	6247	0.5669	0.0325	0.0387
90	6355	0.5732	0.0326	0.0388
91	6463	0.5796	0.0326	0.0388
92	6573	0.5860	0.0328	0.0390
93	6683	0.5924	0.0328	0.0390
94	6794	0.5987	0.0329	0.0392
95	6907	0.6051	0.0331	0.0394
96	7021	0.6115	0.0332	0.0395
97	7138	0.6178	0.0335	0.0398
98	7255	0.6242	0.0335	0.0398
99	7375	0.6306	0.0338	0.0402
100	7498	0.6369	0.0340	0.0405
101	7622	0.6433	0.0341	0.0406
102	7747	0.6497	0.0342	0.0407
103	7874	0.6561	0.0344	0.0410
104	8003	0.6624	0.0346	0.0412
105	8133	0.6688	0.0347	0.0413
106	8265	0.6752	0.0348	0.0415
107	8397	0.6815	0.0348	0.0415
108	8530	0.6879	0.0349	0.0416
109	8669	0.6943	0.0355	0.0422
110	8810	0.7006	0.0356	0.0424
111	8952	0.7070	0.0357	0.0425
112	9096	0.7134	0.0359	0.0427
113	9244	0.7197	0.0362	0.0431
114	9395	0.7261	0.0364	0.0434
115	9548	0.7325	0.0366	0.0436
116	9702	0.7389	0.0367	0.0437
117	9859	0.7452	0.0369	0.0440
118	10027	0.7516	0.0378	0.0450
119	10198	0.7580	0.0380	0.0452
120	10371	0.7643	0.0381	0.0454
121	10550	0.7707	0.0386	0.0459
122	10732	0.7771	0.0388	0.0462
123	10915	0.7834	0.0389	0.0463
124	11103	0.7898	0.0392	0.0467
125	11291	0.7962	0.0392	0.0467
126	11480	0.8025	0.0393	0.0468
127	11674	0.8089	0.0396	0.0472
128	11880	0.8153	0.0404	0.0481
129	12086	0.8217	0.0404	0.0481
130	12298	0.8280	0.0408	0.0486
131	12517	0.8344	0.0413	0.0491
132	12739	0.8408	0.0414	0.0493
133	12967	0.8471	0.0418	0.0498
134	13200	0.8535	0.0421	0.0501
135	13435	0.8599	0.0422	0.0503
136	13671	0.8662	0.0423	0.0503

sample #	Cumulative weight [g]	$P_c = R_i / (N + 1)$	D_{n50} [m]	D_{50} [m]
137	13916	0.8726	0.0428	0.0510
138	14161	0.8790	0.0428	0.0510
139	14410	0.8854	0.0431	0.0513
140	14665	0.8917	0.0434	0.0517
141	14928	0.8981	0.0438	0.0522
142	15201	0.9045	0.0444	0.0529
143	15475	0.9108	0.0445	0.0529
144	15767	0.9172	0.0454	0.0541
145	16063	0.9236	0.0456	0.0543
146	16374	0.9299	0.0464	0.0552
147	16685	0.9363	0.0464	0.0552
148	16998	0.9427	0.0465	0.0553
149	17316	0.9490	0.0467	0.0556
150	17636	0.9554	0.0468	0.0557
151	17973	0.9618	0.0476	0.0567
152	18312	0.9682	0.0477	0.0568
153	18670	0.9745	0.0486	0.0579
154	19040	0.9809	0.0491	0.0585
155	19435	0.9873	0.0502	0.0598
156	19837	0.9936	0.0505	0.0601

Building method reef

		
Casted metal frame	Washing rock	Drying of the rock
		
Epoxy-primer	Removing small rocks	Sample for analysis
		
Weighing sample (156 pcs)	Samples for density	Determining volume
		
Coating with epoxy	Hardening of rock layer	Reef structures (1:6)

Figure D.1: Building method reef structure for flume testing (2DV)

E

Planning

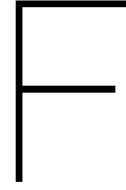
week	date	day	Test ID	Structure	Wave climate	# of waves	Duration (s)	Parameters to be measured		Position vectrino	Comments / FILENAME.ASC
								measured	measured		
3	15-Dec		11.4 S0	WC4	50	271	Hs (GHM), Flow (EMS), Velocity (ADV), WL	V1.2	0-WC4_V1_2.ASC		
			11.5 S0	WC5	50	271	Hs (GHM), Flow (EMS), Velocity (ADV), WL	V1.2	0-WC5_V1_2.ASC		
	16-Dec	13		13.1 S1	WC1	50	271	Hs (GHM), Flow (EMS), Velocity (ADV), WL	V1.1	1-WC1_V1_1.ASC	
				13.2 S1	WC1	50	271	Hs (GHM), Flow (EMS), Velocity (ADV), WL	V1.2	1-WC1_V1_2.ASC	
				13.3 S1	WC1	50	271	Hs (GHM), Flow (EMS), Velocity (ADV), WL	V2.1	1-WC1_V2_1.ASC	
				13.4 S1	WC1	50	271	Hs (GHM), Flow (EMS), Velocity (ADV), WL	V2.2	1-WC1_V2_2.ASC	
				13.5 S1	WC1	50	271	Hs (GHM), Flow (EMS), Velocity (ADV), WL	V3.1	1-WC1_V3_1.ASC	
				13.6 S1	WC1	50	271	Hs (GHM), Flow (EMS), Velocity (ADV), WL	V3.2	1-WC1_V3_2.ASC	
				13.7 S1	WC1	50	271	Hs (GHM), Flow (EMS), Velocity (ADV), WL	V4.1	1-WC1_V4_1.ASC	
				13.8 S1	WC1	50	271	Hs (GHM), Flow (EMS), Velocity (ADV), WL	V4.2	1-WC1_V4_2.ASC	
				13.9 S1	WC1	50	271	Hs (GHM), Flow (EMS), Velocity (ADV), WL	V5.1	1-WC1_V5_1.ASC	
				14.1 S1	WC1	50	271	Hs (GHM), Flow (EMS), Velocity (ADV), WL	V5.2	1-WC1_V5_2.ASC	
	17-Dec	14		14.2 S1	WC2	50	163	Hs (GHM), Flow (EMS), Velocity (ADV), WL	V1.1	1-WC2_V1_1.ASC	
				14.3 S1	WC2	50	163	Hs (GHM), Flow (EMS), Velocity (ADV), WL	V1.2	1-WC2_V1_2.ASC	
				14.4 S1	WC2	50	163	Hs (GHM), Flow (EMS), Velocity (ADV), WL	V2.1	1-WC2_V2_1.ASC	
				14.5 S1	WC2	50	163	Hs (GHM), Flow (EMS), Velocity (ADV), WL	V2.2	1-WC2_V2_2.ASC	
				14.6 S1	WC2	50	163	Hs (GHM), Flow (EMS), Velocity (ADV), WL	V3.1	1-WC2_V3_1.ASC	
				14.7 S1	WC2	50	163	Hs (GHM), Flow (EMS), Velocity (ADV), WL	V3.2	1-WC2_V3_2.ASC	
			14.8 S1	WC2	50	163	Hs (GHM), Flow (EMS), Velocity (ADV), WL	V4.1	1-WC2_V4_1.ASC		
			14.9 S1	WC2	50	163	Hs (GHM), Flow (EMS), Velocity (ADV), WL	V4.2	1-WC2_V4_2.ASC		
21-Dec	15		15.1 S1	WC2	50	163	Hs (GHM), Flow (EMS), Velocity (ADV), WL	V5.1	1-WC2_V5_1.ASC		
			15.2 S1	WC2	50	163	Hs (GHM), Flow (EMS), Velocity (ADV), WL	V5.2	1-WC2_V5_2.ASC		
			15.3 S1	WC3	50	204	Hs (GHM), Flow (EMS), Velocity (ADV), WL	V1.1	1-WC3_V1_1.ASC		
			15.4 S1	WC3	50	204	Hs (GHM), Flow (EMS), Velocity (ADV), WL	V1.2	1-WC3_V1_2.ASC		
			15.5 S1	WC3	50	204	Hs (GHM), Flow (EMS), Velocity (ADV), WL	V2.1	1-WC3_V2_1.ASC		
			15.6 S1	WC3	50	204	Hs (GHM), Flow (EMS), Velocity (ADV), WL	V2.2	1-WC3_V2_2.ASC		
			15.7 S1	WC3	50	204	Hs (GHM), Flow (EMS), Velocity (ADV), WL	V3.1	1-WC3_V3_1.ASC		
			15.8 S1	WC3	50	204	Hs (GHM), Flow (EMS), Velocity (ADV), WL	V3.2	1-WC3_V3_2.ASC		
			15.9 S1	WC3	50	204	Hs (GHM), Flow (EMS), Velocity (ADV), WL	V4.1	1-WC3_V4_1.ASC		
			16.1 S1	WC3	50	204	Hs (GHM), Flow (EMS), Velocity (ADV), WL	V4.2	1-WC3_V4_2.ASC		
			16.2 S1	WC3	50	204	Hs (GHM), Flow (EMS), Velocity (ADV), WL	V5.1	1-WC3_V5_1.ASC		
			16.3 S1	WC3	50	204	Hs (GHM), Flow (EMS), Velocity (ADV), WL	V5.2	1-WC3_V5_2.ASC		
			16.4 S1	WC4	50	122	Hs (GHM), Flow (EMS), Velocity (ADV), WL	V1.1	1-WC4_V1_1.ASC		
			16.5 S1	WC4	50	122	Hs (GHM), Flow (EMS), Velocity (ADV), WL	V1.2	1-WC4_V1_2.ASC		
		22-Dec	16		16.1 S1	WC3	50	204	Hs (GHM), Flow (EMS), Velocity (ADV), WL	V4.2	1-WC3_V4_2.ASC
					16.2 S1	WC3	50	204	Hs (GHM), Flow (EMS), Velocity (ADV), WL	V5.1	1-WC3_V5_1.ASC
					16.3 S1	WC3	50	204	Hs (GHM), Flow (EMS), Velocity (ADV), WL	V5.2	1-WC3_V5_2.ASC
					16.4 S1	WC4	50	122	Hs (GHM), Flow (EMS), Velocity (ADV), WL	V1.1	1-WC4_V1_1.ASC
	16.5 S1			WC4	50	122	Hs (GHM), Flow (EMS), Velocity (ADV), WL	V1.2	1-WC4_V1_2.ASC		

NOT IN THE LAB

week	date	day	Test ID	Structure	Wave climate	# of waves	Duration (s)	Parameters to be measured		Position vectrino	Comments / FILENAME.ASC		
								Hs (GHM), Flow (EMS), Velocity (ADV), WL	Hs (GHM), Flow (EMS), Velocity (ADV), WL				
4	23-Dec		16.6 S1	WC4	WC4	50	122	Hs (GHM), Flow (EMS), Velocity (ADV), WL	V2.1	1-WC4_V2_1.ASC			
			16.7 S1	WC4	WC4	50	122	Hs (GHM), Flow (EMS), Velocity (ADV), WL	V2.2	1-WC4_V2_2.ASC			
			16.8 S1	WC4	WC4	50	122	Hs (GHM), Flow (EMS), Velocity (ADV), WL	V3.1	1-WC4_V3_1.ASC			
			16.9 S1	WC4	WC4	50	122	Hs (GHM), Flow (EMS), Velocity (ADV), WL	V3.2	1-WC4_V3_2.ASC			
			17.1 S1	WC4	WC4	50	122	Hs (GHM), Flow (EMS), Velocity (ADV), WL	V4.1	1-WC4_V4_1.ASC			
			17.2 S1	WC4	WC4	50	122	Hs (GHM), Flow (EMS), Velocity (ADV), WL	V4.2	1-WC4_V4_2.ASC			
			17.3 S1	WC4	WC4	50	122	Hs (GHM), Flow (EMS), Velocity (ADV), WL	V5.1	1-WC4_V5_1.ASC			
			17.4 S1	WC4	WC4	50	122	Hs (GHM), Flow (EMS), Velocity (ADV), WL	V5.2	1-WC4_V5_2.ASC			
			17.5 S1	WC5	WC5	50	82	Hs (GHM), Flow (EMS), Velocity (ADV), WL	V1.1	1-WC5_V1_1.ASC			
			17.6 S1	WC5	WC5	50	82	Hs (GHM), Flow (EMS), Velocity (ADV), WL	V1.2	1-WC5_V1_2.ASC			
			17.7 S1	WC5	WC5	50	82	Hs (GHM), Flow (EMS), Velocity (ADV), WL	V2.1	1-WC5_V2_1.ASC			
			17.8 S1	WC5	WC5	50	82	Hs (GHM), Flow (EMS), Velocity (ADV), WL	V2.2	1-WC5_V2_2.ASC			
			17.9 S1	WC5	WC5	50	82	Hs (GHM), Flow (EMS), Velocity (ADV), WL	V3.1	1-WC5_V3_1.ASC			
			18.1 S1	WC5	WC5	50	82	Hs (GHM), Flow (EMS), Velocity (ADV), WL	V3.2	1-WC5_V3_2.ASC			
			18.2 S1	WC5	WC5	50	82	Hs (GHM), Flow (EMS), Velocity (ADV), WL	V4.1	1-WC5_V4_1.ASC			
			18.3 S1	WC5	WC5	50	82	Hs (GHM), Flow (EMS), Velocity (ADV), WL	V4.2	1-WC5_V4_2.ASC			
18	24-Dec		18.4 S1	WC5	WC5	50	82	Hs (GHM), Flow (EMS), Velocity (ADV), WL	V5.1	1-WC5_V5_1.ASC			
			18.5 S1	WC5	WC5	50	82	Hs (GHM), Flow (EMS), Velocity (ADV), WL	V5.2	1-WC5_V5_2.ASC			
			18.6 S1	WC6	WC6	50	163	Hs (GHM), Flow (EMS), Velocity (ADV), WL	V1.1	1-WC6_V1_1.ASC			
			18.7 S1	WC6	WC6	50	163	Hs (GHM), Flow (EMS), Velocity (ADV), WL	V1.2	1-WC6_V1_2.ASC			
			18.8 S1	WC6	WC6	50	163	Hs (GHM), Flow (EMS), Velocity (ADV), WL	V2.1	1-WC6_V2_1.ASC			
			18.9 S1	WC6	WC6	50	163	Hs (GHM), Flow (EMS), Velocity (ADV), WL	V2.2	1-WC6_V2_2.ASC			
			19.1 S1	WC6	WC6	50	163	Hs (GHM), Flow (EMS), Velocity (ADV), WL	V3.1	1-WC6_V3_1.ASC			
			19.2 S1	WC6	WC6	50	163	Hs (GHM), Flow (EMS), Velocity (ADV), WL	V3.2	1-WC6_V3_2.ASC			
			19.3 S1	WC6	WC6	50	163	Hs (GHM), Flow (EMS), Velocity (ADV), WL	V4.1	1-WC6_V4_1.ASC			
			19.4 S1	WC6	WC6	50	163	Hs (GHM), Flow (EMS), Velocity (ADV), WL	V4.2	1-WC6_V4_2.ASC			
19	28-Dec		19.5 S1	WC6	WC6	50	163	Hs (GHM), Flow (EMS), Velocity (ADV), WL	V5.1	1-WC6_V5_1.ASC			
			19.6 S1	WC6	WC6	50	163	Hs (GHM), Flow (EMS), Velocity (ADV), WL	V5.2	1-WC6_V5_2.ASC			
			20.1 S1	WC7	WC7	50	122	Hs (GHM), Flow (EMS), Velocity (ADV), WL	V1.1	1-WC7_V1_1.ASC			
			20.2 S1	WC7	WC7	50	122	Hs (GHM), Flow (EMS), Velocity (ADV), WL	V1.2	1-WC7_V1_2.ASC			
			20.3 S1	WC7	WC7	50	122	Hs (GHM), Flow (EMS), Velocity (ADV), WL	V2.1	1-WC7_V2_1.ASC			
			20.4 S1	WC7	WC7	50	122	Hs (GHM), Flow (EMS), Velocity (ADV), WL	V2.2	1-WC7_V2_2.ASC			
20	29-Dec		20.5 S1	WC7	WC7	50	122	Hs (GHM), Flow (EMS), Velocity (ADV), WL	V3.1	1-WC7_V3_1.ASC			
			20.6 S1	WC7	WC7	50	122	Hs (GHM), Flow (EMS), Velocity (ADV), WL	V3.2	1-WC7_V3_2.ASC			
			Process data & analysis of interesting wave conditions										
			20.1 S1	WC7	WC7	50	122	Hs (GHM), Flow (EMS), Velocity (ADV), WL	V1.1	1-WC7_V1_1.ASC			
20.2 S1	WC7	WC7	50	122	Hs (GHM), Flow (EMS), Velocity (ADV), WL	V1.2	1-WC7_V1_2.ASC						
20.3 S1	WC7	WC7	50	122	Hs (GHM), Flow (EMS), Velocity (ADV), WL	V2.1	1-WC7_V2_1.ASC						
20.4 S1	WC7	WC7	50	122	Hs (GHM), Flow (EMS), Velocity (ADV), WL	V2.2	1-WC7_V2_2.ASC						
20.5 S1	WC7	WC7	50	122	Hs (GHM), Flow (EMS), Velocity (ADV), WL	V3.1	1-WC7_V3_1.ASC						
20.6 S1	WC7	WC7	50	122	Hs (GHM), Flow (EMS), Velocity (ADV), WL	V3.2	1-WC7_V3_2.ASC						

week	date	day	Test ID	Structure	Wave climate	# of waves	Duration (s)	Parameters to be measured		Position vetricino	Comments / FILENAME.ASC
								Hs (GHM), Flow (EMS), Velocity (ADV), WL	Hs (GHM), Flow (EMS), Velocity (GHM), Flow (EMS), Velocity (GHM), Flow (EMS), Velocity (ADV), WL		
			20.8 S1		WC7	50	122	Hs (GHM), Flow (EMS), Velocity (ADV), WL	V4.2	1-WC7_V4_2.ASC	
			20.9 S1		WC7	50	122	Hs (GHM), Flow (EMS), Velocity (ADV), WL	V5.1	1-WC7_V5_1.ASC	
	30-Dec	21	21.1 S1		WC7	50	122	Hs (GHM), Flow (EMS), Velocity (ADV), WL	V5.2	1-WC7_V5_2.ASC	
6	4-Jan	22						Remove structure from wave flume			
	5-Jan	23	23.1 S0		WC6	50	163	Hs (GHM), Flow (EMS), Velocity (ADV), WL	V1.2	0-WC6_V1_2.ASC	
	6-Jan	24	24.1 S0		WC7	50	122	Hs (GHM), Flow (EMS), Velocity (ADV), WL	V1.2	0-WC7_V1_2.ASC	
	7-Jan							Painting structures for PIV measurements			
7	8-Jan	25	S1			50	81.64965809	Velocity ZDV			
	11-Jan	26	S1			50	81.64965809	Velocity ZDV			
	12-Jan	27	S1		WC5	50	81.64965809	Velocity ZDV	-	PIV measurements	
	13-Jan	28	S1			50	81.64965809	Velocity ZDV			
	14-Jan	29	S1			50	81.64965809	Velocity ZDV			
	15-Jan	30						Cleaning of laboratory setup			

Figure E.1: Flume testing matrix



Wave reflection

This shortened description of the method of Suzuki and Goda Goda and Suzuki [28] is based on the documents from the Fluid mechanics lab at TU Delft. These are written and revised by H. Klaasman in 2005.

To establish the reflection of a regular wave the method of Goda and Suzuki [28] is used, which is also described in Goda(1985). Two wave gauges are used which are approximately one fourth of a wavelength apart.

The basic equations for a regular wave with wave gauges located at $x = x_1$ and $x = x_2$ are:

$$\eta(x_1, t) = \sum_{n=1}^N a_{i,n} \cos(k_n x_1 - \omega_n t + \theta_{i,n}) + \sum_{n=1}^N a_{r,n} \cos(k_n x_1 + \omega_n t + \theta_{r,n}) \quad (E1)$$

$$\eta(x_2, t) = \sum_{n=1}^N a_{i,n} \cos(k_n x_2 - \omega_n t + \theta_{i,n}) + \sum_{n=1}^N a_{r,n} \cos(k_n x_2 + \omega_n t + \theta_{r,n}) \quad (E2)$$

With:

- η is the waterlevel elevation relative to the mean waterlevel
- t time
- $a_{i,n}, a_{r,n}$ amplitude of the n -harmonic of the incoming / reflected wave
- k_n The wave number of the n^{th} harmonic
- ω_n radial frequency of the n^{th} harmonic, from dispersion relationship $\omega = \sqrt{gk \tanh(kh)}$
- $\theta_{i,n}, \theta_{r,n}$ phase of the n^{th} harmonic of the incoming / reflected wave

When the reflected wave is determined only the first harmonic is considered. Higher harmonics, free or bound harmonics are not taken into account.

For the first harmonic equations E1 and E2 transform to

$$\eta(x_1, t) = a_i \cos(kx_1 - \omega t + \theta_i) + a_r \cos(kx_1 + \omega t + \theta_r) \quad (E3)$$

$$\eta(x_2, t) = a_i \cos(kx_2 - \omega t + \theta_i) + a_r \cos(kx_2 + \omega t + \theta_r) \quad (E4)$$

Equation E3 can be rewritten as:

$$\eta(x_1, t) = a_i \{ \cos(kx_1 + \theta_i) \cos(\omega t) + \sin(kx_1 + \theta_i) \sin(\omega t) \} + a_r \{ \cos(kx_1 + \theta_r) \cos(\omega t) - \sin(kx_1 + \theta_r) \sin(\omega t) \} \quad (E5)$$

or

$$\eta(x_1, t) = A_1 \cos(\omega t) + B_1 \sin(\omega t) \quad (E6)$$

This can be repeated for equation E4, leading to:

$$\eta(x_2, t) = A_2 \cos(\omega t) + B_2 \sin(\omega t) \quad (E7)$$

From this the following system of equations can be derived:

$$A_1 = a_i \cos(kx_1 + \theta_i) + a_r \cos(kx_1 + \theta_r) \quad (\text{E8})$$

$$B_1 = a_i \sin(kx_1 + \theta_i) - a_r \sin(kx_1 + \theta_r) \quad (\text{E9})$$

$$A_2 = a_i \cos(kx_2 + \theta_i) + a_r \cos(kx_2 + \theta_r) \quad (\text{E10})$$

$$B_2 = a_i \sin(kx_2 + \theta_i) - a_r \sin(kx_2 + \theta_r) \quad (\text{E11})$$

Equations E8 to E11 lead to the complex equations:

$$A_1 + iB_1 = a_i e^{ikx_1} e^{i\theta_i} + a_r e^{-ikx_1} e^{-i\theta_r} \quad (\text{E12})$$

$$A_2 + iB_2 = a_i e^{ikx_2} e^{i\theta_i} + a_r e^{-ikx_2} e^{-i\theta_r} \quad (\text{E13})$$

with $i = \sqrt{-1}$.

In matrix notation:

$$\begin{pmatrix} e^{ikx_1} & e^{-ikx_1} \\ e^{ikx_2} & e^{-ikx_2} \end{pmatrix} \begin{pmatrix} a_i e^{i\theta_i} \\ a_r e^{-i\theta_r} \end{pmatrix} = \begin{pmatrix} A_1 + iB_1 \\ A_2 + iB_2 \end{pmatrix} \quad (\text{E14})$$

A's and B's on the right hand side of E14 can be found from harmonic analysis of $\eta(x_1, t)$ and $\eta(x_2, t)$ from E6 and E7, by means of a Fast Fourier Transformation (FFT). In Refreg two zero crossings with the same sign change are determined, one at the beginning and one at the end of the measured signal from the first gauge ($x = x_1$). This determines the length of the signal to be analyzed. The signal is in this case considered to be cyclic. The cut off error caused by the wave period not being a multitude of the timestep is ignored. Hereafter the FFT function of Matlab is applied to the two signals coming from wave gauges at $x = x_1$ and $x = x_2$, with the amount of measurements that corresponds to the timeslot between the earlier mentioned zero-crossings. The period that corresponds to the FFT-coefficient with the highest absolute value will be used as the base-period.

An example of the result of this analysis, carried out by the Refreg.m program, is printed below.

```
Program Refreg ver 19, refl of regular wave, substr. moving average
16-Feb-2016 14:47:27
```

```
*****Input values*****
```

```
Input file: WC1_5refreg
```

```
Time step in input file:      0.0100 s
```

```
Time interval asked:          50.0000,    80.0000
```

```
Time interval used:           50.0000,    80.0000
```

```
Time step used:                0.0100 s
```

```
Number of samples used:       2805
```

```
Channels used:
```

```
cols:                          1          2
```

```
pos (m):                        0.00      0.80
```

```
scale to m:                     1.0000    1.0000
```

```
average waterdepth (m):        0.5300
```

```
*****
```

```
Results of SFN_harm9:
```

number of samples: 2805

position 1

i	f	a	b	c	phi
1	0.606061	-0.048651	-0.017288	0.051631	2.800155
2	1.212121	0.006199	0.005848	0.008522	-0.756285

position 2

i	f	a	b	c	phi
1	0.606061	0.019377	-0.058768	0.061880	1.252302
2	1.212121	-0.007939	-0.004217	0.008989	2.653329

reflection coefficient calculated with velocity 0:

distance of wave gauges : 0.800 m

position 1

Position : 0.000 m
 period of 1st harmonic : 1.6500 s
 wave length : 3.2698 m
 A-component of harmonic : -0.0487
 B-component of harmonic : -0.0173
 amplitude of harmonic : 0.0516 m

position 2

Position : 0.800 m
 period of 1st harmonic : 1.6500 s
 wave length : 3.2698 m
 A-component of harmonic : 0.0194
 B-component of harmonic : -0.0588
 amplitude of harmonic : 0.0619 m

amplitude of incoming wave : 0.0568 m
 amplitude of reflected wave : 0.0051 m
 reflection coefficient : 0.0905

phase of incoming wave : -7.15 deg
 phase of reflected wave : -86.35 deg

determinant : 1.9989

Phases have been calculated with respect to a position halfway the two wave gauges;
 t=0 at the first sample of the measurements

* Warning:

* if a trend is found in the measurements,
 * the wave number k will change with the time,
 * and the equations used in this program are no
 * no longer valid.

G

Fourier series of Vectrino signal

The velocity signals measured with the Vectrino are decomposed using Fourier series. The values of the fourier terms can be found in table 4.8 in chapter 4. The table is repeated below.

The resulting mean velocity signals are plotted in this chapter, and serve as illustration to proof the validity of this method used to determine the mean velocity.

Table G.1: Specification of Fourier analysis of Vectrino data, u -velocity, position V1.2

	Wave condition				
	1	2	3	4	5
RMSE	0.01098	0.01277	0.01028	0.06466	0.01976
a0	-0.00182	-0.00032	-0.00634	2.34E-14	-0.01093
a1	-0.02716	0.000352	-0.00988	-0.00056	-0.1195
b1	-0.01367	0.000568	-0.0548	-0.0008	-0.1726
a2	0.006278	0.07373	-0.01669	0.1253	0.00387
b2	0.007499	-0.06978	0.01008	0.1217	0.03598
a3	-0.00025	-0.00038	0.004007		0.000556
b3	-0.00345	6.34E-05	0.000703		0.002511
a4	0.000365	-0.00826			
b4	0.001018	-0.03398			
a5		-9.70E-05			
b5		-0.00028			
w	1.154	0.9611	1.536	1.281	3.807
$2\pi/w$	5.445	6.538	4.091	4.905	1.650

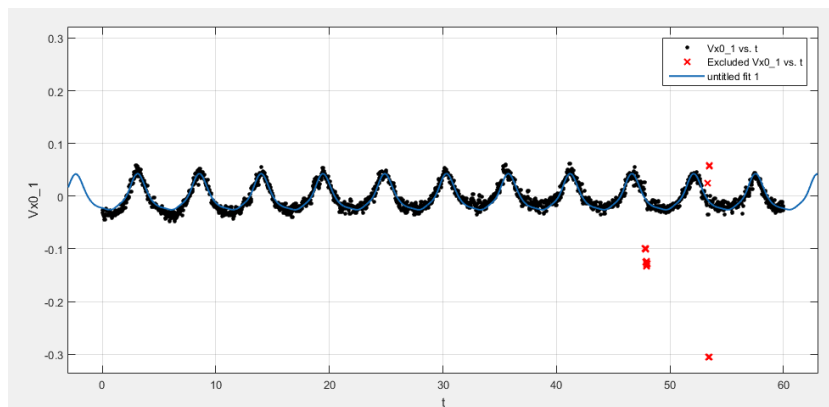


Figure G.1: Wave condition 1 - Fourier

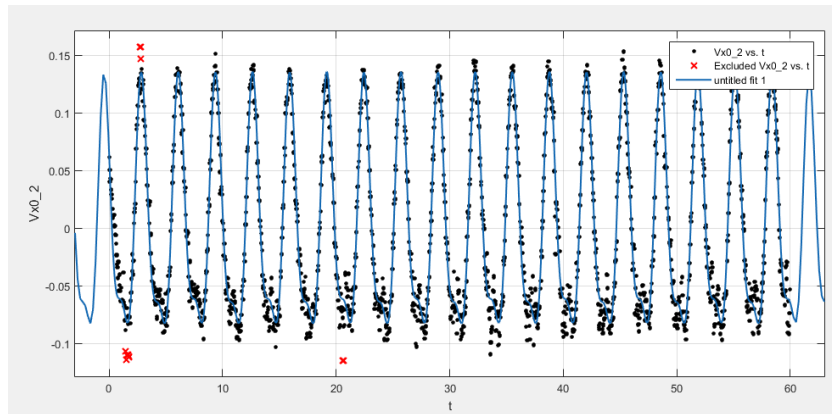


Figure G.2: Wave condition 2 - Fourier

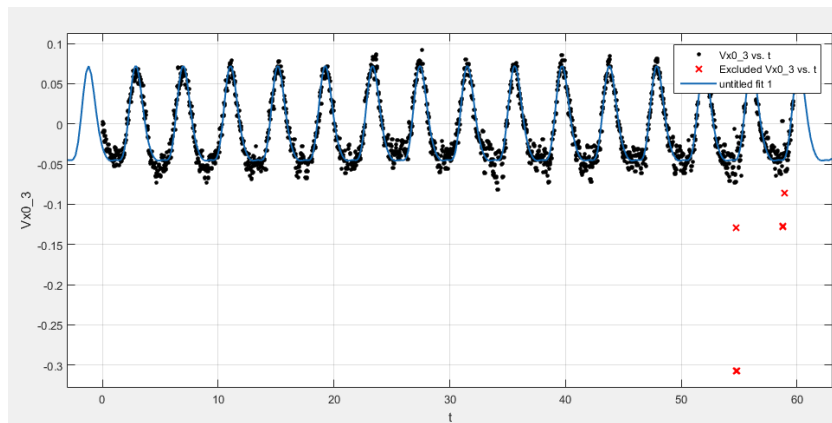


Figure G.3: Wave condition 3 - Fourier

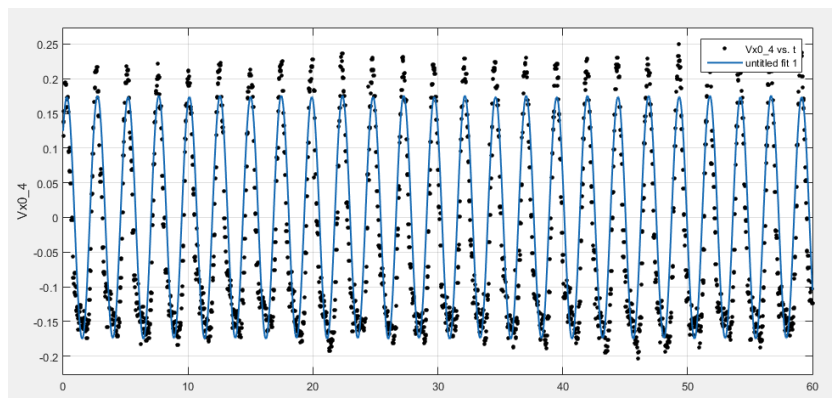


Figure G.4: Wave condition 4 - Fourier

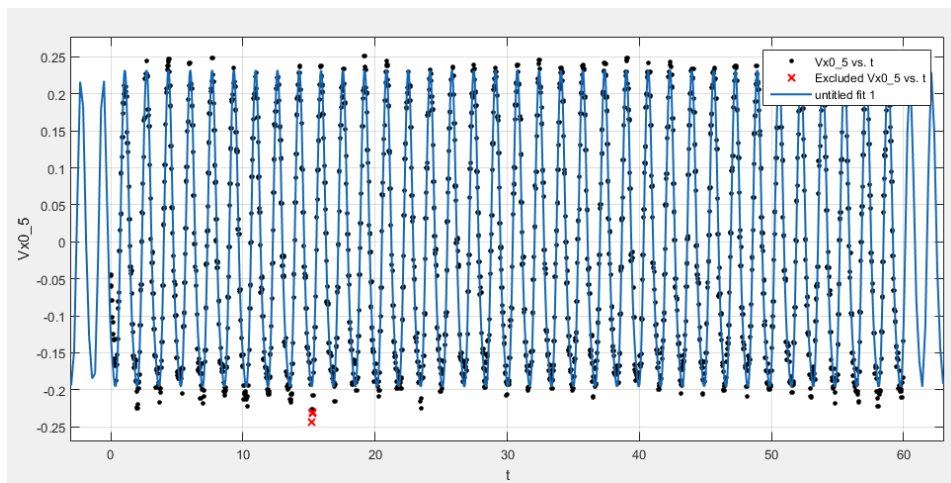
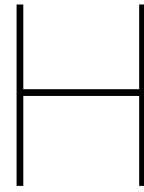


Figure G.5: Wave condition 5 - Fourier



Bichromatic waves

In the vicinity of the breaking zone, short waves are largely destroyed by breaking and frictional effects, while bound long waves propagate through the breaker zone where they are 'released'. Long waves can become edge waves that travel along the shoreline, increasing long shore transport, and also produce variation in the set-up and run-up in the surf zone of the primary waves, causing a broader reach of the wave attack. The oscillating movement in the near shore environment is called surfbeat. This is also the name of the second mode of XBeach, which does solve for the bound long waves. Although in this research wave attenuation and thus erosion protection is only qualitatively analyzed, since long waves are an important factor they should in a later stage be taken into account in far-field modeling.

Long waves are naturally present in a wave spectrum. In this appendix a more simplified signal is explored, namely a bi-chromatic signal, with a long wave signal superimposed on the short wave signal. This is the most simplified form of a spectrum, with just two frequencies.

XBeach

The long wave period is defined as $4 * T_{m0}$. XBeach then calculates the long wave signal following the theory of Longuet-Higgins and Steward (1964) [36]. The wave signal that occurs when the long wave is imposed on the short wave signal is shown in H.1. How this influences the wave height can be deduced from the plot in H.2.

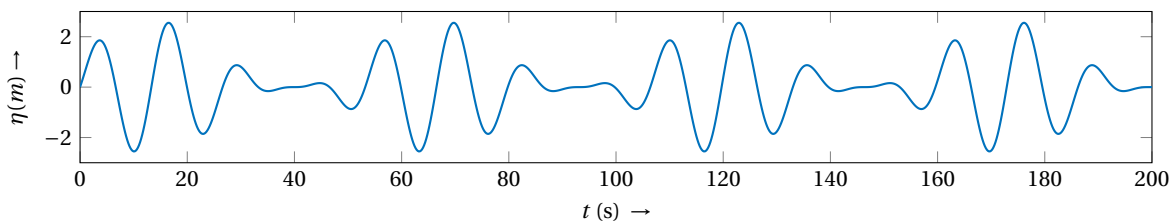


Figure H.1: Short wave signal

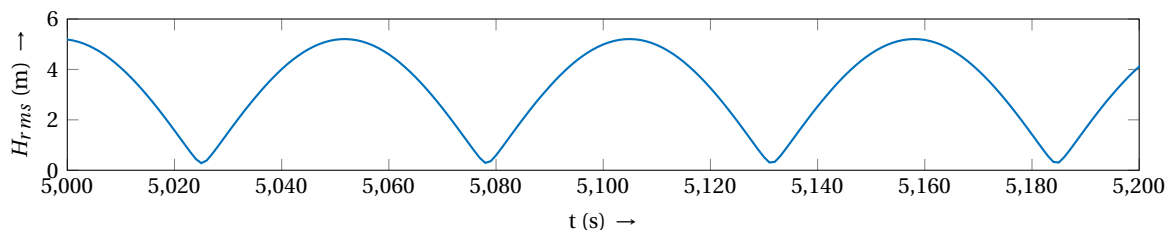


Figure H.2: Short wave height (H_{rms}) at $x=1887$ m

It is important to realize that the high frequency and low frequency (short and long) waves are expressed

in different parameters of the output of XBeach. Short waves are expressed in 'H', the H_{rms} wave height based on instantaneous wave energy. Long waves are solved in the shallow water equations, expressed as water level fluctuation in z_s . In order to be able to take both oscillations in account for the wave transmission, some data analysis is necessary.

$$H_{highfreq.} = \sqrt{\langle H_{rms}^2 \rangle} \quad (H.1)$$

$$H_{lowfreq.} = \sqrt{8} \sqrt{\sigma_{z_s}} = \sqrt{8} * var(z_s) \quad (H.2)$$

$$H_{total} = \sqrt{H_{highfreq.}^2 + H_{lowfreq.}^2} \quad (H.3)$$

The H_{total} can be calculated for the incoming (H_i) and transmitted signal (H_t), and serve as input for equation 3.3. In order to rule out the reflection of the structure, h_i was extracted from the base runs, without structure. The result of this analysis is shown in table H.1 below. The result that structure 9 performs best concerning effectivity per squared meter cross section, is in accordance with the monochromatic wave analysis results (table 4.2) in chapter 4.

Table H.1: Analysis of wave transmission for structure envelopes 1-10 - surf beat mode

#	H	L	D	A (m^2)	Wave height H [m] (short/long waves)						Kt (-)	$\frac{1-K_t}{A} (m^{-2})$
					short _{in}	long _{in}	tot _{in}	short _{out}	long _{out}	tot _{out}		
0	0	0	0	0	0.844	0.131	0.854	-	-	-	-	-
1	1	10	-4	10	0.844	0.131	0.854	0.756	0.132	0.768	0.899	0.010
2	2	10	-4	20	0.844	0.131	0.854	0.695	0.117	0.768	0.825	0.009
3	1	20	-4	20	0.844	0.131	0.854	0.733	0.130	0.768	0.871	0.006
4	2	20	-4	40	0.844	0.131	0.854	0.644	0.111	0.654	0.765	0.006
5	1	10	-3	10	0.491	0.101	0.501	0.437	0.086	0.446	0.889	0.011
6	2	10	-3	20	0.491	0.101	0.501	0.346	0.055	0.768	0.698	0.015
7	1	20	-3	20	0.491	0.101	0.501	0.412	0.082	0.420	0.839	0.008
8	2	20	-3	40	0.491	0.101	0.501	0.290	0.048	0.294	0.586	0.010
9	1	10	-2	10	0.280	0.065	0.287	0.237	0.045	0.241	0.841	0.016
10	1	20	-2	20	0.280	0.065	0.287	0.212	0.039	0.216	0.752	0.012

Long wave

In figure H.3 the change in wave height (influenced by long wave motion) from the beginning of XBeach domain to the start of SWASH domain is plotted. From this graph it can be seen that in the beginning, long waves have a large influence on the wave height in time. When looking at the shallow water wave height however, this influence has largely disappeared.

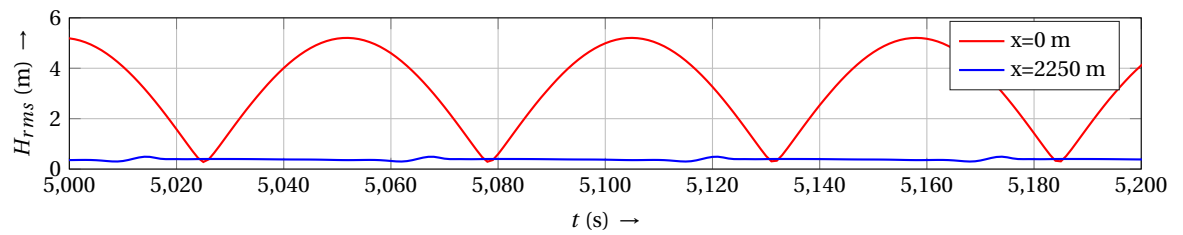


Figure H.3: Transformation long wave influence on beginning of SWASH domain

Physical model

For wave conditions 6 and 7 (the bi-chromatic signals) the Fourier analysis could not be finished with accurate results, see figure H.5.

Therefore another approach was used, namely a fit with a sum of sine algorithm, see equation H.4.

$$y = \sum a_i \sin(b_i x + c_i) \quad (H.4)$$

The equation is closely related to the Fourier series, main difference is that this sum of sine equation includes the phase constant, and it does not include a constant term, a_0 in equation 3.15.

Table H.2: Bi-chromatic wave conditions

	Actual conditions			Scaled conditions			Comments
WC6	0.48	7.0 / 9.0	3.50	0.08	2.86 / 3.67	0.58	Bichromatic
WC7	0.72	5.0 / 7.0	3.18	0.12	2.45	0.53	Bichromatic

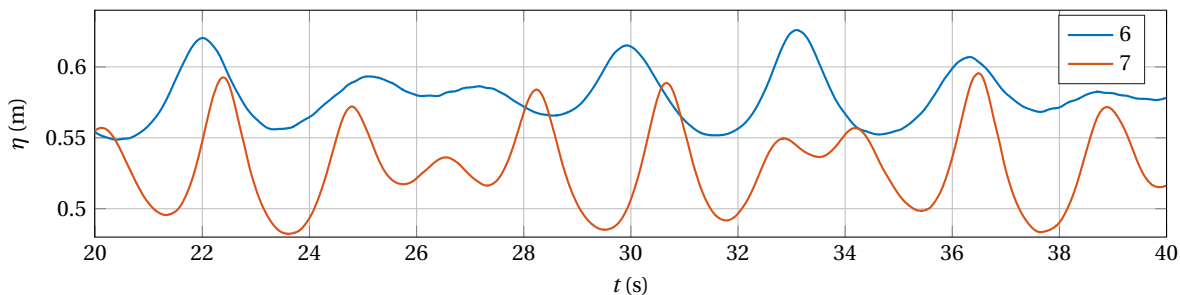


Figure H.4: Measured wave signal of wave climates 6 and 7

For this approach the fit was much better, see figure H.6.

The sum-of-sine fits are given in table H.3, the resulting signals in figures H.6 and H.7.

Table H.3: Results of sum of sine analysis Vectrino data

	Wave condition	
	6	7
RMSE	0.02017	0.03759
a1	0.07438	0.1269
b1	1.731	2.231
c1	-2.387	4.036
a2	0.07231	0.09818
b2	2.226	3.123
c2	-0.7824	0.4371

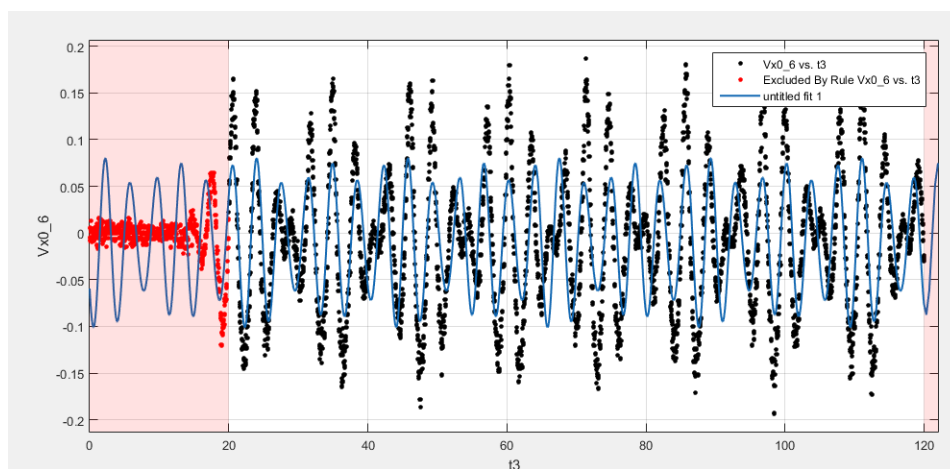


Figure H.5: result of a 8-term Fourier analysis on wave condition 6

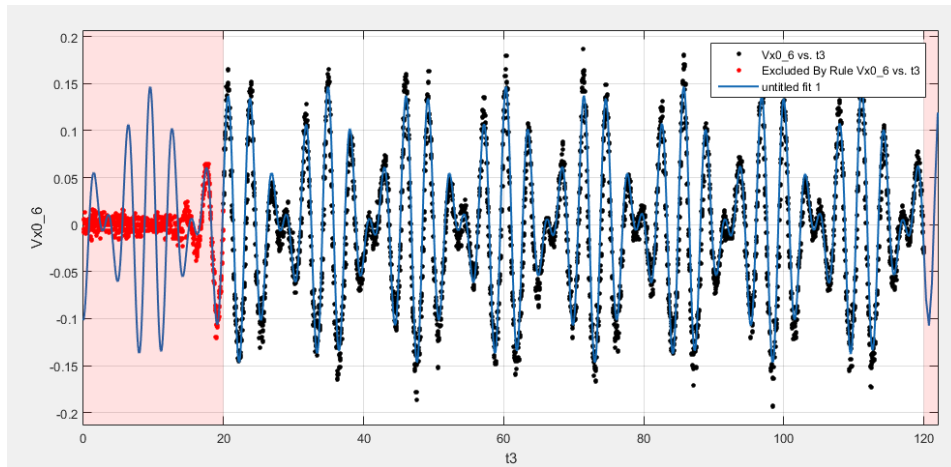


Figure H.6: Wave condition 6 - Sum of sine

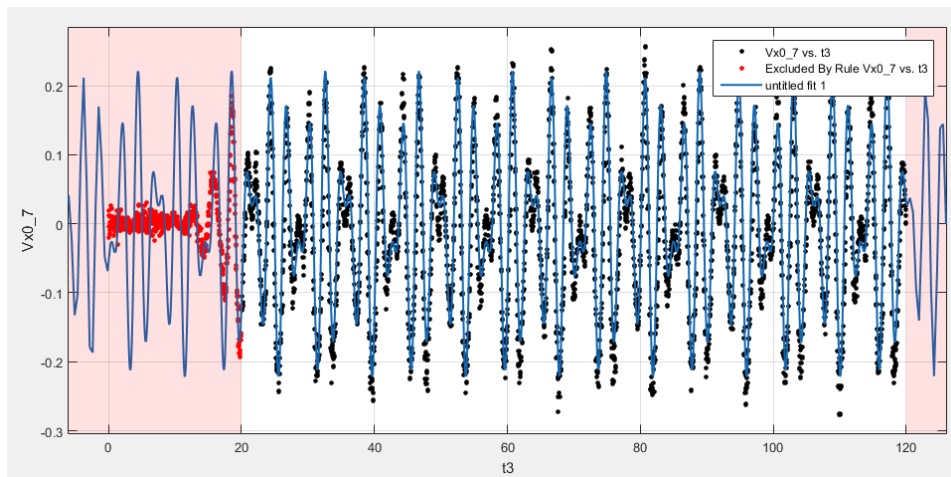


Figure H.7: Wave condition 7 - Sum of sine

Derivation stokes wave BC for SWASH

The first batch of SWASH modeling, before physical testing, was done by applying a water level boundary condition. This was defined with linear wave theory, and gave reliable and clean results as for wave propagation through the domain.

During physical testing the transition was made from linear to Second order Stokes theory. This non-linear wave theory is used in the steering software for the wave paddle.

The SWASH model setup for calibration did not give sufficient results for a water-level boundary condition with Second order Stokes theory. This was generating spurious harmonics in the water-level all through the domain, not resembling the results of the physical test, see I.1.

SWASH is validated for fifth order stokes waves with an $a/h = 0.1$. Since this is the same order magnitude as the wave condition that is aimed to model, namely condition 5, see 3.7. This condition enholds $a=0.056$ m, $T=1.650$ s and $h=0.53$, which gives $a/h = 0.101$.

From the validated 5th order model as a starting point each alteration was backtracked to arrive at the required, stable second order stokes wave condition.

Boundary condition

Since for the 5th order stokes model the wave condition applied is a velocity boundary condition rather than a waterlevel boundary condition, first second order stokes theory had to be derived in order to program the boundary conditions for two equidistant layers. Starting point is the u velocity found in Dean and Dalrymple [20], I.1.

$$u = \frac{-\delta\phi}{\delta x} = \frac{H}{2} \frac{gk}{\sigma} \frac{\cosh(k(h+z))}{\cosh(kh)} \cos(kx - \sigma t) + \frac{3}{16} \frac{H^2 \sigma k \cosh(2k(h+z))}{\sinh^4(kh)} \cos 2(kx - \sigma t) \quad (I.1)$$

With:

- ϕ = velocity potential (see Dean and Dalrymple [20])
- k = wavenumber
- σ = dispersion relation = $\sqrt{gk \tanh(kh)}$

The wave number k is implicit, but approximated by following the theory of Fenton & Mckee, described in Fenton [23]. This gives the explicit value for k in equation I.2, which has a maximum error of 1.5%.

$$k = \frac{\omega^2 h}{g} \frac{\coth(w \sqrt{\frac{h}{g}})^{\frac{3}{2}}}{h} \quad (I.2)$$

Since the boundary condition will be applied as a timeseries at the beginning of the domain, $x=0$.

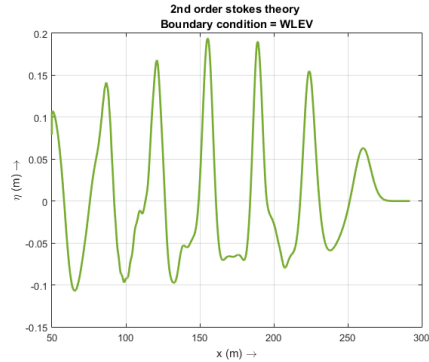


Figure I.1: higher harmonic disturbances in SWASH due to water level boundary condition

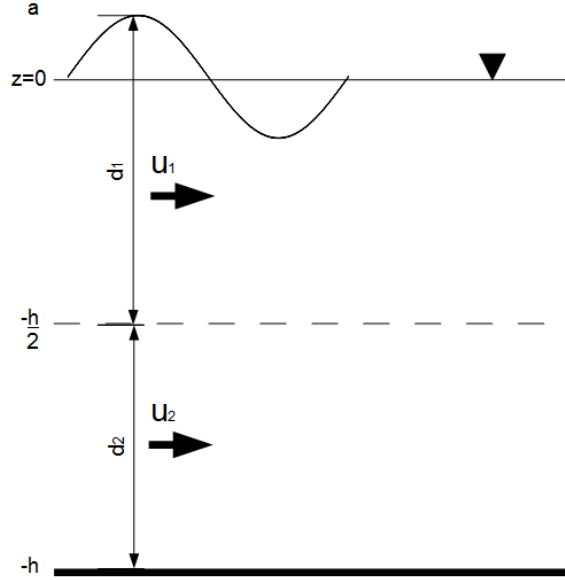


Figure I.2: Equidistant layers for velocity boundary conditions

Table I.1: Values for z_1 and z_2 for 2 equidistant layers

Velocity	z_1	z_2
u_1	a	-h/2
u_2	-h/2	-h

Equation I.1 is integrated over two equidistant depths, and divided by these depth intervals to arrive at the required boundary conditions, which are the average velocity over that depth.

$$\int_{z_1}^{z_2} u(z, t) dz = \int_{z_1}^{z_2} A_1 \cosh(k(h+z)) + A_2 \cosh(2k(h+z)) dz = \frac{1}{k} A_1 [\sinh(k(h+z))]_{z_1}^{z_2} + \frac{1}{2k} A_2 [\sinh(2k(h+z))]_{z_1}^{z_2} \quad (I.3)$$

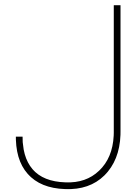
with:

$$A_1 = \frac{H g k \cos(-\sigma t)}{2 \sigma \cosh(kh)}, A_2 = \frac{3 H^2 \sigma k \cos(-2\sigma t)}{16 \sinh^4(kh)} \quad (I.4)$$

The situation is sketched in figure I.2. The values for z_1 and z_2 in equation I.3 are given in table I.1

This derivation is implemented in matlab, in order to create two timeseries of velocities in location u_1 and u_2 , indicated in figure I.2. Additionally the theoretical water level is generated to compare SWASH results to. Water level for second order stokes waves is defined in equation I.5.

$$\eta = \frac{H_1}{2} \cos(kx - \sigma t) + \frac{H_1^2 k}{16} \frac{\cosh(kh)}{\sinh^3(kh)} (2 + \cosh(2kh)) \cos(2(kx - \sigma t)) \quad (I.5)$$



SWASH model setup

One of the used SWASH input files is printed below.

```
*****HEADING*****
$
PROJ 'Merel_Kroon_flumescale'
$
$ Second order Stokes wave in a flume
$
*****MODEL INPUT*****
$
MODE NONST ONED
$
CGRID 0. 0. 0. 38. 0. 760 0
$
VERT 5

$ input bottom including impermeable structure core
INPGRID BOTTOM 0. 0. 0. 760 0 .05 .53
READINP BOTTOM 1. 'botWC5_struct.bot' 1 0 FREE

$ input structure porous layer
INPGRID HSTRUCTURE 0. 0. 0. 760 0 .05 .53
READINP HSTRUCTURE 1. 'hstruct.bot' 1 0 FREE
INPGRID POROSITY 0. 0. 0. 760 0 .05 .53
READINP POROSITY 1. 'porosity.bot' 1 0 FREE
INPGRID FRICTION 0. 0. 0. 760 0 0.05 .53
READINP FRICTION 1. 'nikuradse.bot' 1 0 FREE
$
INIT zero
$
BOU SIDE W CCW BTYPE VEL LAY 1 SM00 0.5 SEC CON SERIES 'WC5a.bnd'
BOU SIDE W CCW BTYPE VEL LAY 2 SM00 0.5 SEC CON SERIES 'WC5b.bnd'
BOU SIDE W CCW BTYPE VEL LAY 3 SM00 0.5 SEC CON SERIES 'WC5c.bnd'
BOU SIDE W CCW BTYPE VEL LAY 4 SM00 0.5 SEC CON SERIES 'WC5d.bnd'
BOU SIDE W CCW BTYPE VEL LAY 5 SM00 0.5 SEC CON SERIES 'WC5e.bnd'

BOU SIDE E CCW BTYPE RADIATION
SPON RI 6.
POROSITY 0.035 0.07 1000 1.81
$
```

```
FRICtion LOGLaw ROUGHNESS 7.5e-3
VISCOsity Vertical KEPS 0.07 0.16
NONHYD BOX PREC ILU
$
DISCRET UPW UMOM V NONE
DISCRET CORRDEP NONE
$
TIMEI 0.2 0.5
$
$***** OUTPUT REQUESTS *****
$
POINTS 'GAUGE' FILE 'GHMs'
TABLE 'GAUGE' NOHEAD 'WC5.tbl' TSEC WATL OUTPUT 000000.000 0.01 SEC
TABLE 'COMPGRID' NOHEAD 'dWC5.tbl' XP WATL
POINTS 'EMS' FILE 'EMS'
TABLE 'EMS' NOHEAD 'EMS.tbl' TSEC VKSIK OUTPUT 000000.000 0.0001 SEC

TEST 1,0
COMPUTE 000000.000 0.0001 SEC 000080.000
STOP
```



Results calibration SWASH

In this appendix the calibration results are given for the intermediate calibration steps taken to reach the prototype calibrated model, discussed in section 4.3.4.

Model scale - no structure

2 layers

Table K.1: Correlation, 2 layers, no structure

	r	R^2
GHM 1	0.9975	0.9950
GHM 2	0.9990	0.9980
GHM 3	0.9973	0.9947
GHM 4	0.9923	0.9846
GHM 5	0.9817	0.9638
GHM 6	0.9933	0.9867
EMS 1	0.9831	0.9150
EMS 2	0.9810	0.9438
Vectrino	0.9942	0.9738
EMS 3	0.9906	0.8956

Model scale - structure

2 layers

Table K.2: Water level correlation, 2 layers

	r	R^2
GHM 1	0.9949	0.9898
GHM 2	0.9944	0.9888
GHM 3	0.9614	0.9242
GHM 4	0.9948	0.9897
GHM 5	0.9877	0.9755
GHM 6	0.9955	0.9910
EMS 1	0.9758	0.9521
EMS 2	0.9705	0.9418
Vectrino	0.9790	0.9585
EMS 3	0.8951	0.8011

5 layers

The corresponding graphs can be found in K.2, K.3 and K.4.

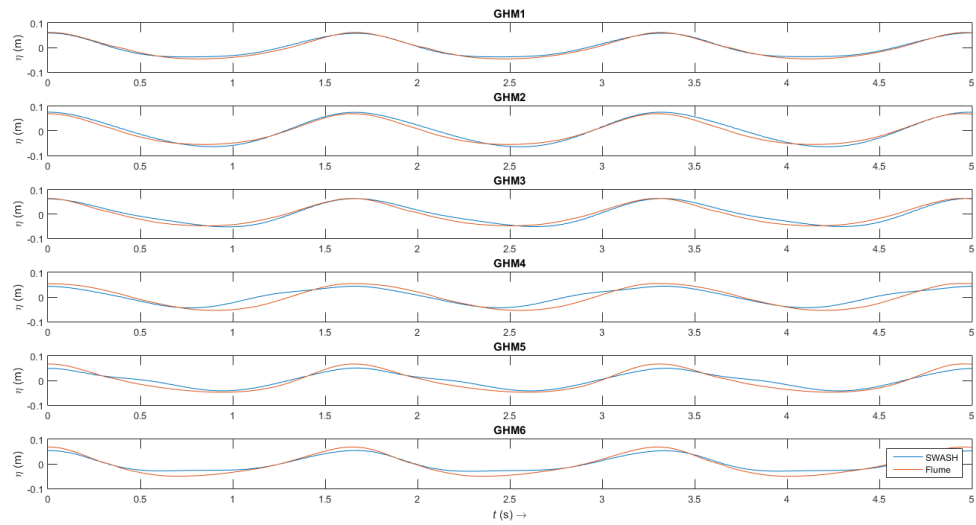


Figure K.1: Water level correlation, 2 layers, no structure

Table K.3: Water level correlation, 5 layers

	r	R^2
GHM 1	0.9901	0.9802
GHM 2	0.9863	0.9729
GHM 3	0.9889	0.9780
GHM 4	0.9496	0.9017
GHM 5	0.9816	0.9635
GHM 6	0.9761	0.9527
EMS 1	0.9826	0.9655
EMS 2	0.9566	0.9152
EMS 3	0.9735	0.9476
V1.1	0.9535	0.9091
V1.2	0.9475	0.8977
V2.1	0.9871	0.9744
V2.2	0.9902	0.9805
V3.1	0.9913	0.9826
V3.2	0.9951	0.9901
V4.1	0.9969	0.9938
v4.2	0.9900	0.9801
V5.1	0.9478	0.8983
V5.2	0.9609	0.9234
average	0.9760	0.9530

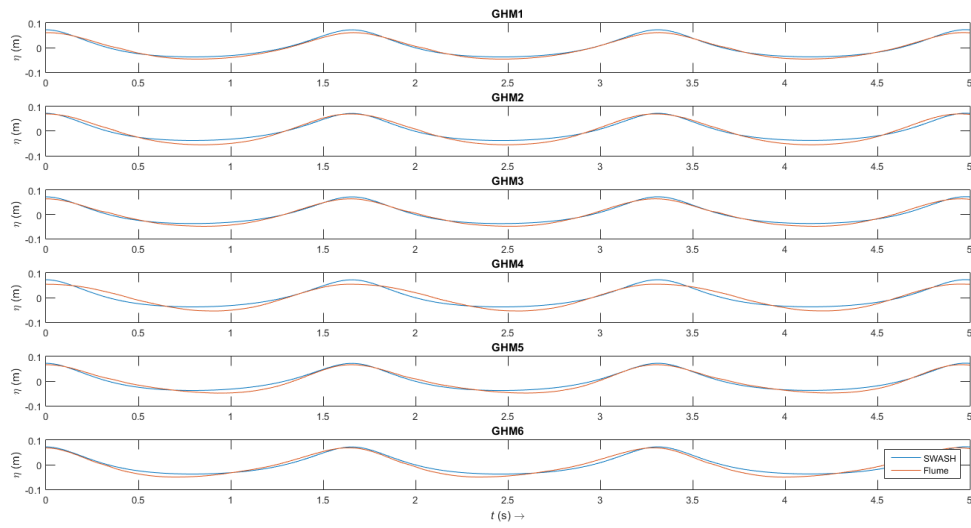
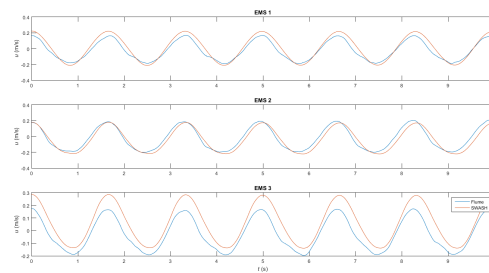
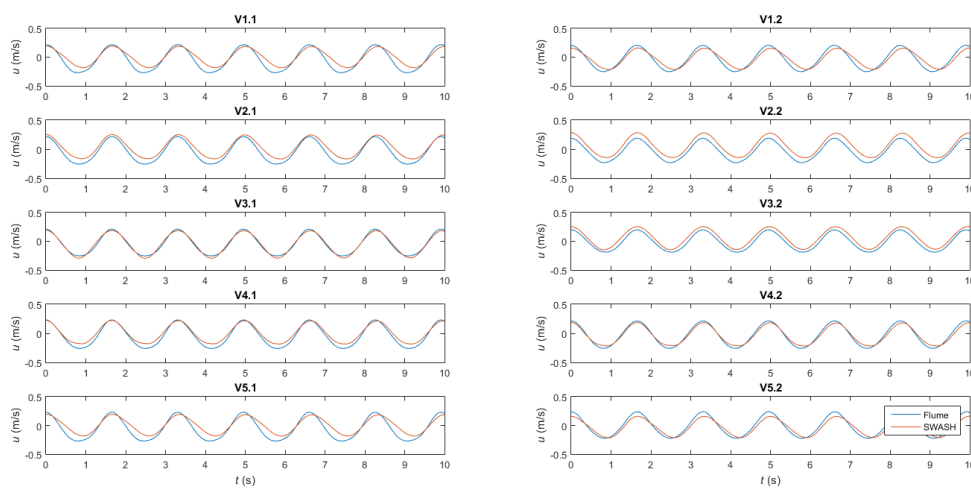


Figure K.2: Water level correlation, 5 layers

Figure K.3: U -velocity correlation (EMS), 5 layersFigure K.4: U -velocity correlation (Vectrino), 5 layers



Velocity decomposition

Turbulence has been identified as a key parameter that can contribute to ecological and hydrodynamic processes that are not fully explained yet. However, turbulence falls out of the scope of this research due to the scale-restrictions set to limit complexity.

Since the vectrino measurements consist of mean velocity, turbulence and high/low-frequency noise, it is interesting to look at the spectrum of the measured velocity signal. Looking at the shape of the spectrum can help in determining if the velocity measurements are trustworthy. When the spectrum shows peaks in locations you do not expect, this can point at higher harmonics not accounted for in computations, or a frequency disturbance caused by for example electrical equipment.

In figure L.1 the power - frequency spectrum for all 10 vectrino measurement locations (for u -velocity) are plotted. Indicated are the typical slope for turbulence ($-5/3$) and the frequency of the monochromatic wave, which corresponds with the energy peak in the spectrum. Higher harmonics of the wave frequency are also indicated.

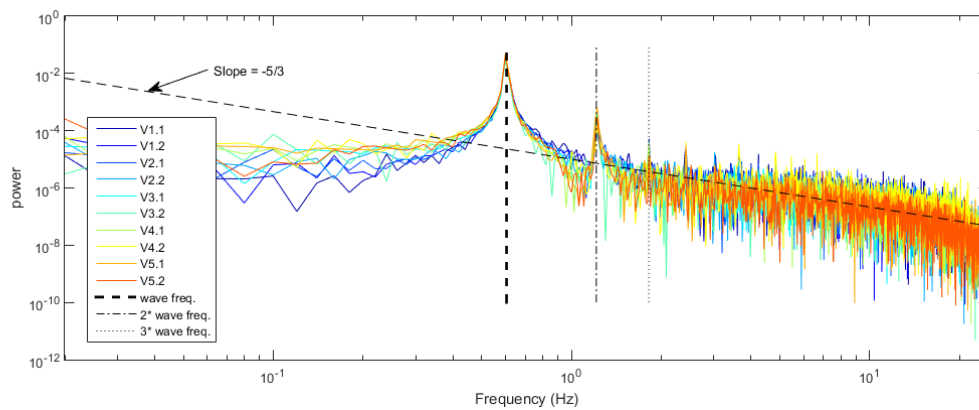
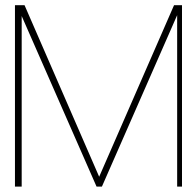


Figure L.1: Power spectrum for vectrino measurements in u -direction



PIV measurements

During the length of the physical measurement campaign it was decided it could be interesting to expand the gathered dataset with Particle Image Velocimetry (PIV) measurements. This state-of-the-art technique allows for very detailed velocity measurements. This is reached by making use of a laser beam that is lead through a prism to create a light-sheet. This sheet of light reflects on particles that are fed into the water column. The reflection is picked up by two very sensitive cameras, of which the shutter time is out of phase. In this way the track of a particle can be traced. Software analysis of the images identifies the particles and calculates the velocity. Setup of the PIV measurements is pictured in M.1. The complete setup has to be covered, to prevent light penetration.

This technique is able to track velocities very close to the surface of a structure and very turbulent conditions, without disturbing the flow by inserting an instrument. The PIV measurements were done over the full length of the depression between the two reef units, by moving the laser beam 2 times. The three tracks of the laser beam can be found in the merged image M.2. The results were merged by Bas Hofland (TU Delft).

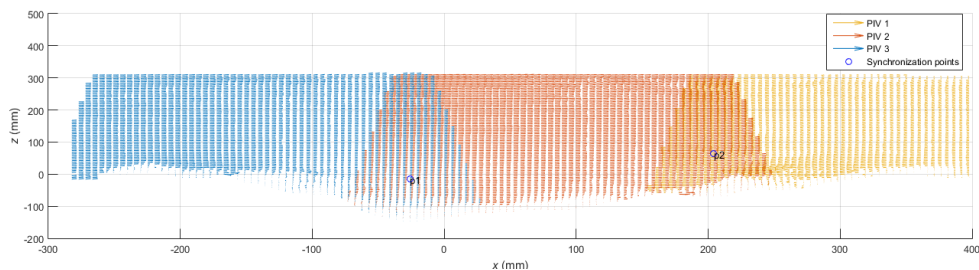


Figure M.2: Tracks of the laser sheet and synchronization points

In chapter 4 a snapshot of the PIV data is used to add to the discussion that the patchy velocity pattern can be explained. To determine if the PIV measurements are in accordance to the Vectrino measurements, a comparison is made. In order to do so, the vectrino measurement locations are translated to the PIV reference system. At these locations, pictured in figure M.3 the velocity signal is extracted from the PIV dataset. A qualitative comparison is made by looking at the plotted results in M.4. The results are satisfactory, the vectrino and PIV measurements correlate very well and therefore the results are inter-comparable, as is done for the patchiness in 4.

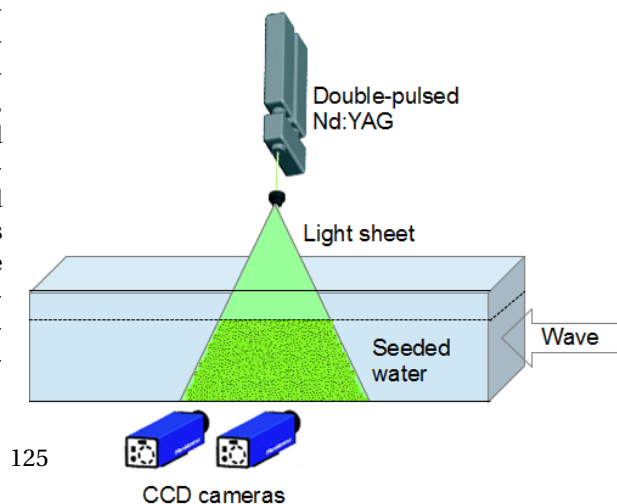


Figure M.1: Principle of setup PIV

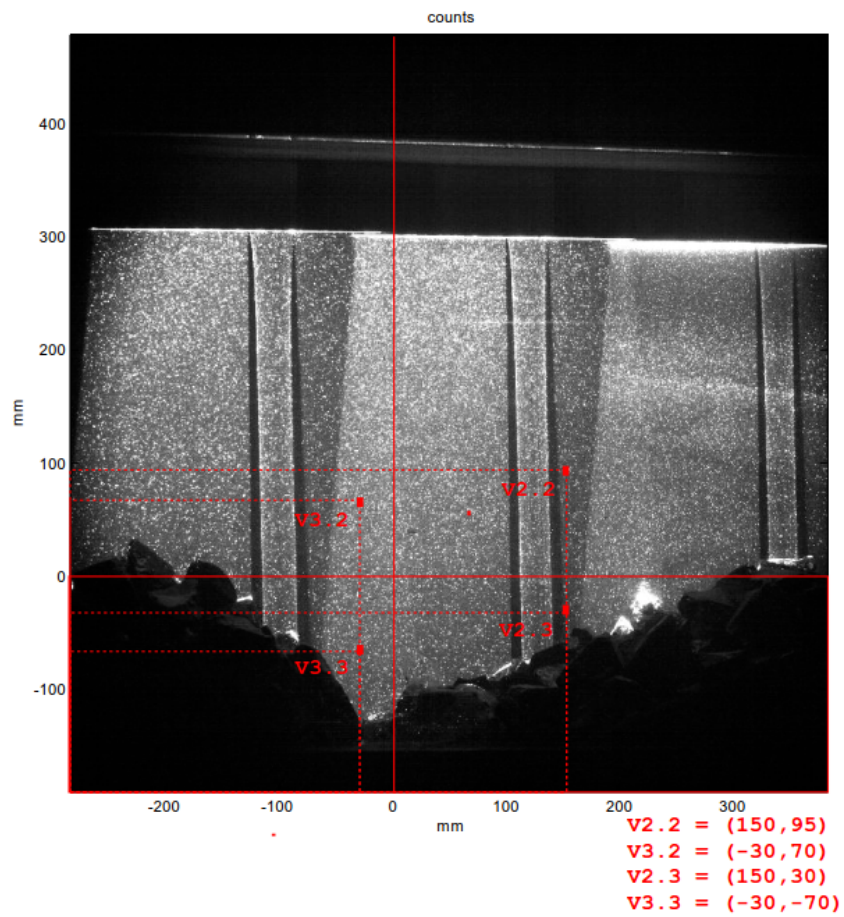


Figure M.3: Coordinates of PIV time series

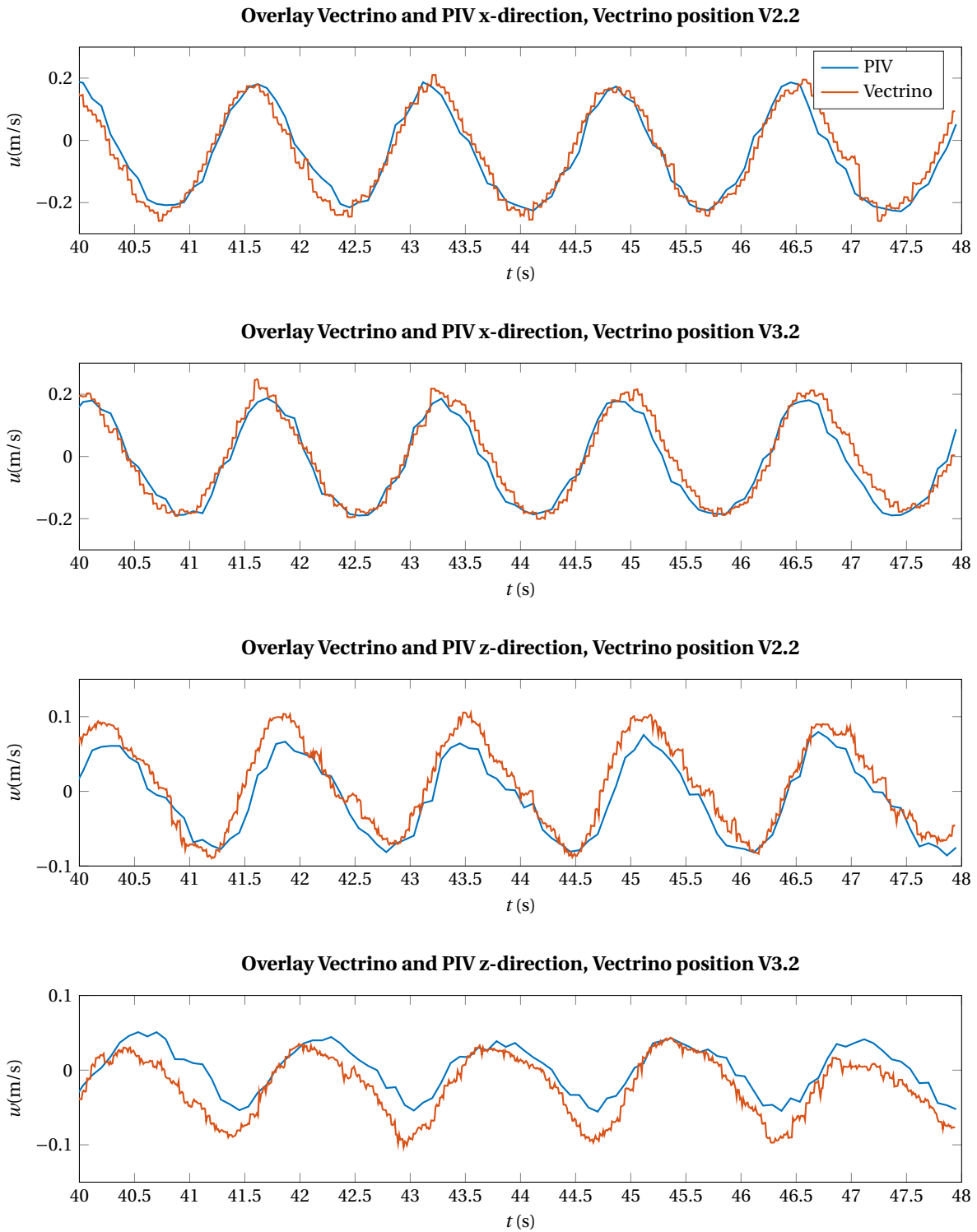


Figure M.4: overlay of vectrino and PIV measurements in x and z directions for location V2.2 and V2.3